1995-03

Small satellite attitude control for sun-oriented operations utilizing a momentum bias with magnetic actuators

Wolfe, Scott Michael

Monterey, California. Naval Postgraduate School

NAVAL POSTGRADUATE SCHOOL
Monterey, California

THESIS

SMALL SATELLITE ATTITUDE CONTROL FOR SUN-ORIENTED OPERATIONS UTILIZING A MOMENTUM BIAS WITH MAGNETIC ACTUATORS

by

Scott Michael Wolfe

March 1995

Thesis Co-Advisors: Harold A. Titus
K. T. Alfriend

REPORT DOCUMENTATION PAGE

Form Approved OMB No. 0704

1. AGENCY USE ONLY *(Leave blank)*	2. REPORT DATE March 1995	3. REPORT TYPE AND DATES COVERED Master's Thesis

4. TITLE AND SUBTITLE : SMALL SATELLITE ATTITUDE CONTROL FOR SUN-ORIENTED OPERATIONS UTILIZING A MOMENTUM BIAS WITH MAGNETIC ACTUATORS

5. FUNDING NUMBERS

6. AUTHOR(S) Wolfe, Scott M.

7. PERFORMING ORGANIZATION NAME(S) AND ADDRESS(ES)
Naval Postgraduate School
Monterey CA 93943-5000

8. PERFORMING ORGANIZATION REPORT NUMBER

9. SPONSORING/MONITORING AGENCY NAME(S) AND ADDRESS(ES)

10. SPONSORING/MONITORING AGENCY REPORT NUMBER

11. SUPPLEMENTARY NOTES The views expressed in this thesis are those of the author and do not reflect the official policy or position of the Department of Defense or the U.S. Government. This thesis contains computer simulation code which has not been tested under all possible conditions. Its validity for every possible scenario is not guaranteed.

12a. DISTRIBUTION/AVAILABILITY STATEMENT Approved for public release; distribution unlimited

12b. DISTRIBUTION CODE

13. ABSTRACT *(maximum 200 words)* The feasibility of using a three axis control, momentum bias system with magnetic actuators for sun-oriented operations is explored. Relevant equations of motion are developed for a sun-oriented coordinate system and control laws are developed for: initial spacecraft capture after launch vehicle separation; reorientation from Earth-oriented to a sun-oriented operations mode; sun-oriented attitude control; and momentum wheel control.

Simulations demonstrating the stability and time responsiveness of the system are performed. Sensor noise input tests are performed to investigate the systems susceptibility to imperfect conditions. Cross product of inertia effects are also input to test for system instability.

14. SUBJECT TERMS Magnetic torque rod attitude control, Small satellite Sun-oriented attitude control, Spacecraft disturbance torque analysis and generation, Beta angle.

15. NUMBER OF PAGES
119

16. PRICE CODE

17. SECURITY CLASSIFICATION OF REPORT	18. SECURITY CLASSIFICATION OF THIS PAGE	19. SECURITY CLASSIFICATION OF ABSTRACT	20. LIMITATION OF ABSTRACT
Unclassified	Unclassified	Unclassified	UL

NSN 7540-01-280-5500

Standard Form 298 (Rev. 2-89)
Prescribed by ANSI Std. 239-18

Approved for public release; distribution is unlimited.

SMALL SATELLITE ATTITUDE CONTROL FOR SUN-ORIENTED OPERATIONS UTILIZING A MOMENTUM BIAS WITH MAGNETIC ACTUATORS

Scott M. Wolfe
Lieutenant, United States Navy
B.S., United States Naval Academy, 1987

Submitted in partial fulfillment
of the requirements for the degrees of

MASTER OF SCIENCE IN ELECTRICAL ENGINEERING
MASTER OF SCIENCE IN ENGINEERING SCIENCE (ASTRONAUTICS)

from the

NAVAL POSTGRADUATE SCHOOL
March 1995

Author: [redacted]
Scott M. Wolfe

Approved by: [redacted]
Harold A. Titus, Co-Advisor

[redacted]
K. T. Alfriend, Co-Advisor

[redacted]
Michael A. Morgan, Chairman
Department of Electrical and Computer Engineering

[redacted]
Daniel J. Collins, Chairman
Department of Aeronautics and Astronautics

ABSTRACT

The feasibility of using a three axis control, momentum bias system with magnetic actuators for sun-oriented operations is explored. Relevant equations of motion are developed for a sun-oriented coordinate system and control laws are developed for: initial spacecraft capture after launch vehicle separation; reorientation from Earth-oriented to a sun-oriented operations mode; sun-oriented attitude control; and momentum wheel control.

Simulations demonstrating the stability and time responsiveness of the system are performed. Sensor noise input tests are performed to investigate the systems susceptibility to imperfect conditions. Cross product of inertia effects are also input to test for system instability.

DISCLAIMER

"This thesis contains computer simulation code which has not been tested under all possible conditions. Its validity for every possible scenario is not guaranteed."

TABLE OF CONTENTS

I. INTRODUCTION 1

A. BACKGROUND 1

B. HISTORY 2

C. PURPOSE 2

II. SPACECRAFT CONFIGURATION AND MISSION ASSUMPTIONS 5

A. ORBIT 7

B. BETA ANGLE DEVELOPMENT 7

C. REFERENCE FRAMES 12

1. Earth-oriented Orbital Reference Frame 12

2. Sun-oriented Orbital Reference Frame 12

3. Body-fixed Reference Frame 13

D. SPACECRAFT BUS DESCRIPTION 13

E. ATTITUDE DETERMINATION AND CONTROL COMPONENTS 14

1. Sensors 14

a. Earth Sensor 14

b. Sun Sensors 17

c. Magnetometers 17

2. Actuators 19

a. Momentum Wheel 19

b. Magnetic Torque Rods 21

c. Thrusters 23

F. SYSTEM PERFORMANCE 23

G. SIMULATION 24

III. SPACE ENVIRONMENT AND ITS EFFECT ON THE SPACECRAFT 25

A. EARTH'S MAGNETIC FIELD DEVELOPMENT 25

B. TORQUES WHICH AFFECT THE SPACECRAFT 27

1. Disturbance Torques 27
a. Aerodynamic 28
b. Solar Pressure 29
c. Gravity Gradient 32
d. Residual Magnetic Torque 34
e. Total Torque 35
IV. EQUATIONS OF MOTION AND ATTITUDE CONTROL LAWS 37
A. EQUATIONS OF MOTION 37
B. CONTROL FLOW 39
C. ATTITUDE CONTROL LAWS 40
1. Satellite Capture After Booster Separation 40
2. Momentum Wheel Control 44
3. Momentum Wheel Desaturation Control 47
4. Control for Transition from Earth-oriented to Sun-oriented Attitude 48
5. Sun-oriented Attitude Control 49
V. CONCLUSIONS AND RECOMMENDATIONS 63
A. CONCLUSIONS 63
B. RECOMMENDATIONS 64
APPENDIX: SIMULATION BLOCKS AND MATLAB CODE 65
LIST OF REFERENCES 103
INITIAL DISTRIBUTION LIST 105

ACKNOWLEDGMENTS

I would like to thank Professor Terry Alfriend and Professor Harold Titus for the time and effort they expended to help me finish this document. Their pursuit of academic excellence is commendable. I would also like to thank Professor Leonard of the Aeronautics Department for his tolerance of me when I popped into his office for answers to difficult questions. The staff of the Servo/Controls Lab at NPS also has my utmost thanks for putting up with me for the last three months and reserving me a powerful computer (if only they could get Costello out of there). Special thanks goes to Chester who felt free to provide his literary expertise every time he got near the computer. Finally, I would like to thank my loving wife, Mary, who kept me motivated and put up with her grumpy husband who came home late every day.

I. INTRODUCTION

A. BACKGROUND

Recently, a National Research Council study group recommended the U. S. government develop and launch several satellites to monitor the sun and the effect of solar radiation on the Earth's climate. The council's board on global change wants a series of orbiters to provide long term, uninterrupted and overlapping observations of the sun. Earth-based sensors are unable to detect precise fluctuations in solar emissions because the atmosphere absorbs much of the energy. [Ref. 1]

A sun-watching program spread over many decades may be precluded by a limited access to space due to rising costs and limited launch capabilities. Therefore, the group advocated the possible use of civilian or military environmental satellites to help survey the sun. Satellites under the control of the National Oceanic and Atmospheric Administration and the U. S. Air Force Defense Meteorological Satellite Program could possibly be brought into service for this purpose, but the study states that satellites dedicated solely for this program are needed to avoid interruption in the data being taken. [Ref. 1]

Candidate satellites for this program would have to have long endurance, a relatively high altitude to avoid any atmospheric interference, and a precision sun-pointing accuracy of at least one half degree for measuring instrument requirements. A momentum bias system with magnetic control actuators appears to be a good, relatively low cost choice to satisfy the first and last requirements.

The popularity of momentum bias spacecraft is due primarily to their ability to provide reasonably good attitude accuracy (better than 0.5 degree) with relatively lightweight and inexpensive attitude control hardware. Gyroscopic stiffness provided by the momentum wheel is a key feature of this system, especially if the momentum bias vector can be oriented toward or away from the sun for safe mode recovery. The use of magnetic attitude control for satellite applications has become quite popular due to its light weight, relatively low power consumption, and long life expectancy. Additionally, magnetic attitude control systems provide a smoother torque output as opposed to the

magnetic attitude control systems provide a smoother torque output as opposed to the impulsive output of mass expulsion systems and also avoid catastrophic failure due to the lack of moving parts. [Ref. 2] Although magnetic control systems do not produce as much torque as mass expulsion or reaction wheel systems, they do provide a viable option for satellite applications which do not require rapid attitude reorientations.

B. HISTORY

Initial use of passive magnetic control was implemented in 1960 with the Transit navigational satellite program. The methodology was to align one of the satellite axes along the direction of the Earth's magnetic field. A year later, the TRAAC satellite was launched with a system that had the capability of providing magnetic stabilization on command. [Ref. 3] Other spacecraft which have used magnetic control include the Nimbus, ERTS, ITOS, RAE and OAO satellites. On the Nimbus and ERTS spacecraft, the magnets were used to offset fixed imbalances and could be adjusted via ground commands. The ITOS system used magnetics for precession control, but the system was not autonomous and needed to be controlled from the ground. In contrast, a closed loop magnetic system has been used to regulate reaction wheel momentum on the OAO spacecraft. [Ref. 2] Finally, the HCCM satellite used a system which is similar to the one proposed for use here and the new Iridium system plans to use a momentum bias with magnetic control.

C. PURPOSE

The purpose of this thesis is to develop, and verify by simulation, the performance of an autonomous attitude control system which can serve the needs of the sun-watching satellite program. This system should be able to acquire the satellite after separation from the launch vehicle, reorient the spacecraft to a sun-pointing attitude via ground command, and then perform accurate sun-pointing attitude control throughout the mission life. Most attitude control applications that contained magnetic torque rods for control were used in an Earth-oriented configuration. This system must be able to perform in an

-Can past magnetic torque control laws be modified to operate in this new sun-oriented configuration?

-How small can Beta angle become before non-linear assumptions break down for the system during Earth to sun satellite reorientation? (Beta angle is defined in Chapter II, page 7)

-Can the desired pointing accuracies be achieved with this system?

-How long will it take to achieve initial capture and reorientation to the sun?

II. SPACECRAFT CONFIGURATION AND MISSION ASSUMPTIONS

The spacecraft bus configuration to be used is extracted from the NPS-STEDI project [Ref. 4] developed at the Naval Post Graduate School for the Advanced Spacecraft Design class (AA 4871). This provided a baseline for equipment selection, disturbance torque estimation and moments of inertia. The development of this thesis is not intended to be an extension of the NPS-STEDI project, but a general exploration of magnetic attitude control for sun-oriented operations. The NPS-STEDI spacecraft uses a momentum biased system to provide three-axis stabilization. Attitude information is provided by sun sensors and a single Earth sensor with magnetometer data as a coarse backup when Earth sensor data is unavailable. The selected Earth sensor is mounted on the momentum wheel, which provides a significant cost saving over using separate systems. The system to be developed here will use most of these design criteria, but the selection of Earth sensor location will be made after system performance at low Beta angles is analyzed. Beta angle is discussed later.

The type of configuration to be considered leaves the designer a great deal of options to explore. The first decision should be which direction to orient the momentum-bias vector. It could be oriented perpendicular to the solar ecliptic which means that the momentum vector does not need to be reoriented by one degree per day to follow the sun. In this configuration, wheel speed would be used to point the solar arrays and experiment toward the sun. Unfortunately, this configuration increases the number of earth sensors required for pitch angle error sensing as well as the number of communication antennae in use. Furthermore, there may be thermal cycling problems which arise in this configuration. Finally, the momentum vector would not necessarily keep the solar arrays in a sun-pointed direction during safe mode/shut down. Another approach would be to orient the momentum-bias vector toward or away from the sun. This gives the spacecraft gyroscopic stiffness which would keep the solar arrays and the

experiment aligned with the sun. This is ideal for safe mode/shut down operation as it would help to guarantee power to the satellite after a malfunction by keeping the solar arrays pointed in the direction of the sun. However, the momentum vector would have to be reoriented by 1 degree per day. Also, unless two Earth sensors are used, pitch angle sensing data may not be available throughout the entire orbit period for low Beta angle orbit configurations. If the Earth sensor could somehow be mounted on the sun-facing side of the satellite, then sensing data would be available during the critical period of eclipse (this configuration could cause problems with the mounting of the solar arrays). When pitch angle sensing data is lost, magnetometer data could be used to provide coarse pitch angle attitude sensing for control.

For this application, the fixed momentum bias vector is oriented along the negative pitch axis and is used to provide gyroscopic stiffness once the spacecraft is separated from the launch vehicle. In addition, the wheel's speed will be used to control pitch angle. The momentum wheel size is driven by the need to keep the momentum vector pointed within one half degree of the sun line throughout an assumed maximum eclipse period of 35 minutes. This maximum eclipse time is estimated for a low Beta angle, 1:30 am/pm orbit and will decrease as Beta angle increases.

The next thing to consider in this type of approach, is what type of torque source to use for momentum wheel desaturation and roll/yaw control. The two types of systems to consider are thrusters and magnetic torque rods. Thrusters will not be used because it was decided that no orbit control thruster system was required for this mission, and a thruster system would increase weight, complexity, space requirements and decrease the satellite's potential life-span. Magnetic torque rods will be used for momentum wheel desaturation and roll/yaw control (wheel speed will be maintained at 3000 RPM +/- 10%). Roll/yaw corrections will only be accomplished during sunlight periods. Error signals generated by sun sensors mounted on the negative Y face (sun pointing) will be fed back to the attitude control system to provide torque commands to the magnetic torque rods. The torque rods will be used to zero these error signals over the course of the sunlight

the sunlight periods, thus providing near-zero spacecraft pointing error at the beginning of the eclipse period. Individual aspects of this design are discussed below and additional assumptions are made.

A. ORBIT

The orbit selected was a circular, sun-synchronous orbit with an altitude of 550 kilometers. This leads to an orbit inclination angle of 97.58 degrees and an orbit period of 95.65 minutes. The driving force for this orbit in the NPS-STEDI project was the need for an ultraviolet sunrise on every orbit so that a complete atmospheric density profile could be measured by the all reflection Michelson interferometer [Ref. 4]. To achieve this, the initial longitude of the ascending node was selected to be 127.5 degrees which corresponds to a 2:30 a.m./p.m. orbit when right ascension of the sun in the ecliptic plane is 90 degrees (summer solstice). For this application, continuous sun coverage is desired (i.e. 6:00 orbit) but orbits ranging from 6:00 to 1:30 will be explored to test the validity of attitude dynamics assumptions at low Beta angles.

B. BETA ANGLE DEVELOPMENT

Before discussing orbital reference frames, the topic of Beta angle and its relationship to this problem needs to be discussed. Beta angle is defined as the angle between the orbit plane and the sun line, which is the line between the center of the Earth and the center of the sun. This angle can be seen in Figure 1 and is defined using Figures 2 and 3 as

$$\beta = \arcsin[SuSeCi + CuSiSw - SuCeSiCw] \tag{1}$$

where S is the sine of the angle, C is the cosine of the angle, i is the orbital inclination (97.58 degrees), e is the Earth spin axis tilt with respect to the ecliptic (23.442 degrees), u is the right ascension of the sun measured in the ecliptic plane and defined as

$$u=u0+udot*time \tag{2}$$

with udot=0.985648 degrees/mean solar day; and w is the right ascension of the line of nodes defined as

$$w=w0+wdot*time \quad (3)$$

where wdot is the nodal regression rate given by

$$wdot=[[-9.9639(R/(R+h))^{3/5}]Ci]/(1-Ecc^2)^2 \text{ (degrees/mean solar day)} \quad (4)$$

with Ecc being the eccentricity (zero for a circular orbit), h being the altitude of the satellite in orbit, i being the orbit inclination, and R being the radius of the Earth [Ref. 5]. The values for u0 and w0 are selected to vary Beta angle to test attitude dynamics assumptions for simulation runs. The reason for varying Beta angle is to generate different Earth to sun rotation angles which will be derived later. These rotation angles affect gravity gradient and aerodynamic disturbance torque inputs for the simulation.

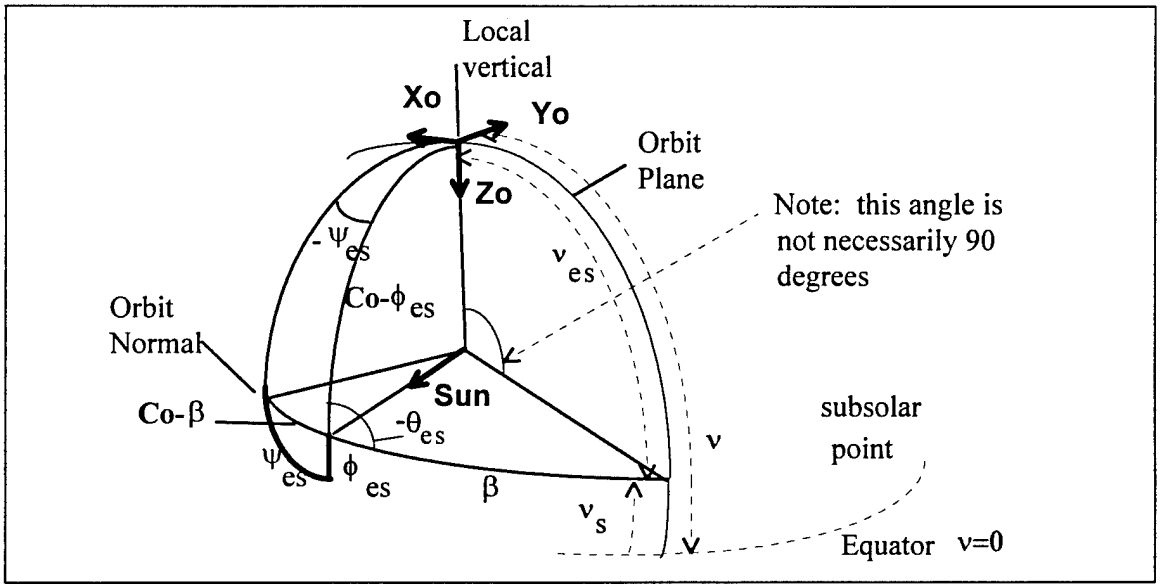

Figure 1. Beta angle spatial relationships with Earth to Sun rotation angles

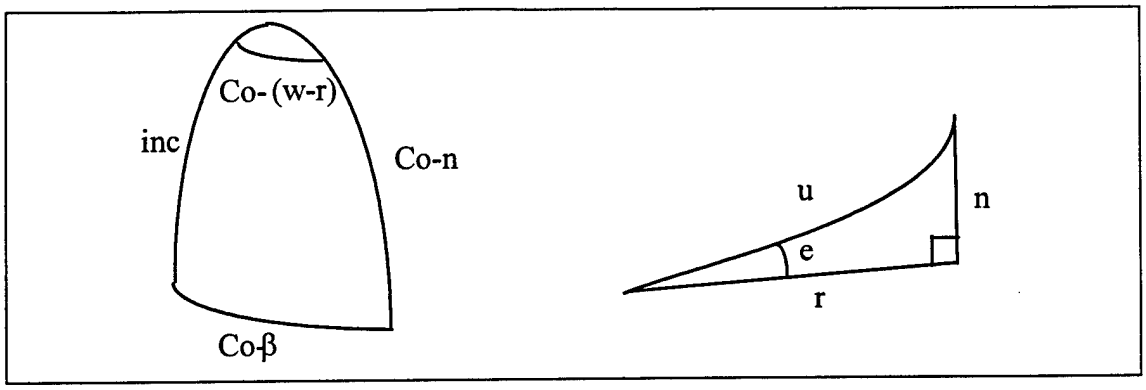

Figure 2. Napier's circle relationships used in Beta angle definition

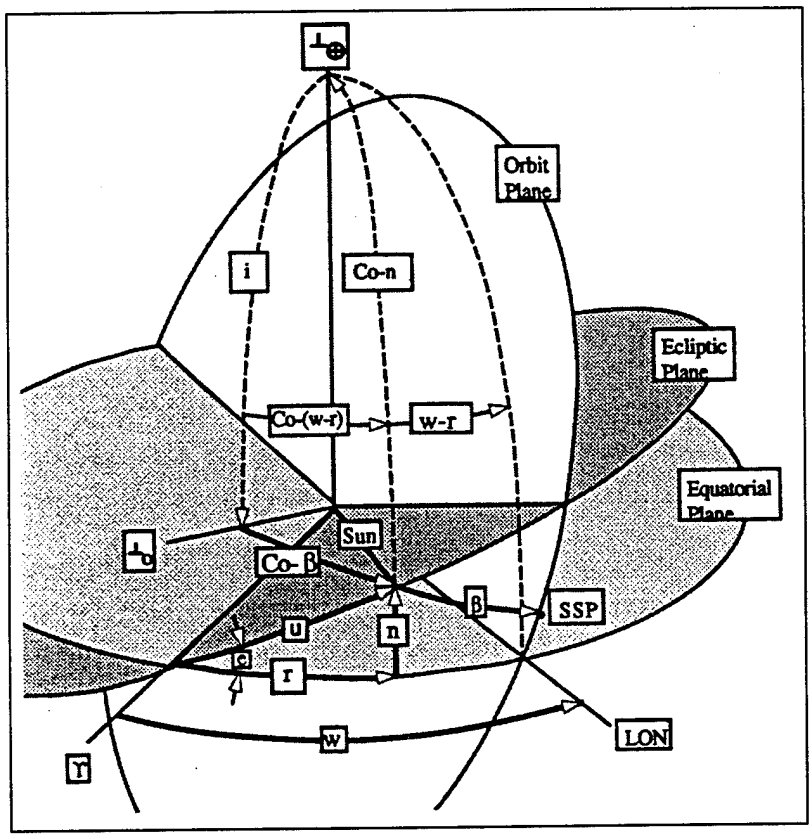

Figure 3. Beta angle spatial definition [Ref. 5]

The key to the topic of a beta angle is the fact that the angles ϕ_{es}, θ_{es}, and ψ_{es} in Figure 1 are dependent on beta angle and that these angles are vital to the coordinate transformation rotations needed to reference the Earth-oriented orbital frame to the

Sun-oriented reference frame as discussed below. Using Figures 1 and 4 along with Napier's Circle relationships, the Earth to sun angles can be calculated as

$$\phi_{es} = \arcsin[\cos\beta \cos\nu_{es}] \tag{5}$$

$$\theta_{es} = \arctan[\frac{\tan\nu_{es}}{\sin\beta}] \tag{6}$$

$$\psi_{es} = \arcsin[\cos\beta \sin\theta_{es}] \tag{7}$$

where β is defined as above and

$$\nu_{es} = \nu_s + \omega_o t \tag{8}$$

where ν_s is a spatial factor necessary to orient the subsolar point in Figure 1 to the true anomaly ν of the satellite. This is better seen by saying that the satellite starts its orbit at the equator (ν=0) and proceeds around the Earth with angular rate ω_o. This means that

$$\nu = \omega_o t \tag{9}$$

The quantity ν_{es} is also increasing at a rate equal to ω_o, but it starts ($\nu_{es} = 0$) at the subsolar point instead of the equator; thus the need for the offset ν_s. Since the value of ν_s is dependent on the position of the subsolar point, it must be a function of the Earth's position in its orbit about the sun. This relationship can be developed using Figure 3 and some spatial relationship variables p, q, and t. A spherical triangle showing a portion of Figure 3 is given in Figure 5. Napier's circle relationships are used to solve for the angle q as

$$q = \arccos[-\cos(180 - inc)\cos e + \sin(180 - inc)\sin e \cos w] \tag{10}$$

Now using spherical triangle relationships, p can be solved for as

$$p = \arcsin[\frac{\sin(180-inc)\sin w}{\sin q}] - u \qquad (11)$$

Using Equations (10) and (11) and the larger triangle of Figure 5, t can be solved for as

$$t = \arcsin[\frac{\sin e \sin w}{\sin q}] \qquad (12)$$

Now using the smaller triangle and Napier's circle relationships of Figure 5 and Equation (12), ν_s can be solved for as

$$\nu_s = t - \arcsin[\tan\beta \tan(90-q)] \qquad (13)$$

This offset becomes important later, because the Magnetic field model of the Earth is affected if this offset is not utilized.

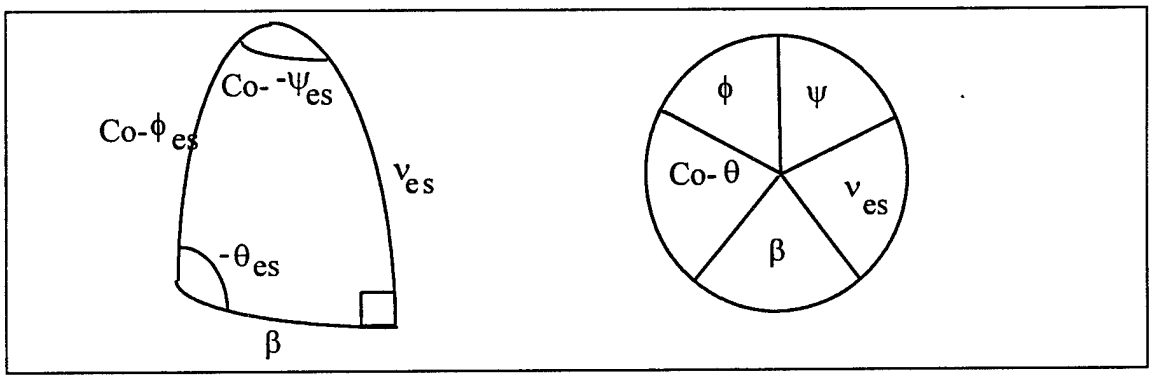

Figure 4. Napier's circle relationships for Earth to Sun rotation angle definition

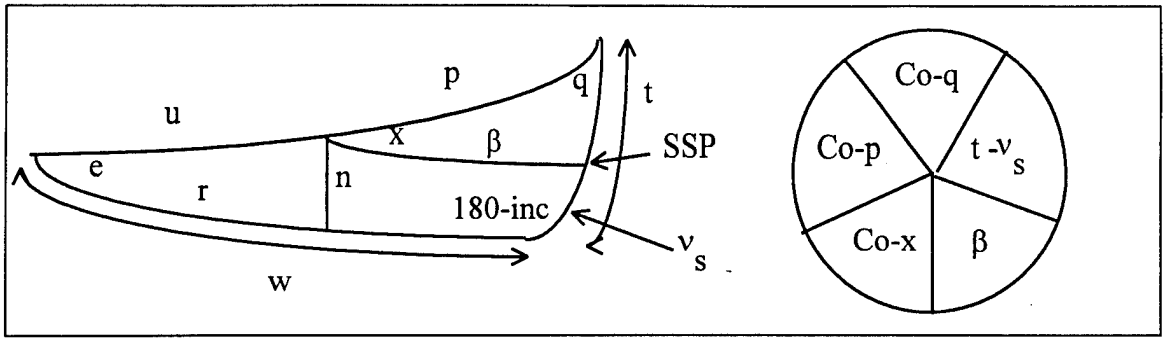

Figure 5. ν_s spatial relationship generation

C. REFERENCE FRAMES

1. Earth-oriented Orbital Reference Frame

This reference frame is the standard orbital coordinates reference frame that is used in most attitude dynamics publications. The positive X axis of the frame is oriented along the satellite's velocity vector with the positive Z axis located in the orbital plane in a nadir pointing direction (i.e. toward the center of the Earth). The positive Y axis is formed by taking the cross product of the Z and X axes. The Y axis is perpendicular to the orbital plane and along the negative orbit normal.

2. Sun-oriented Orbital Reference Frame

This reference frame is specially designed for this orbit application. In this reference frame, the negative Y axis is oriented in the direction of the sun and the plane formed by the Y and Z axes cuts through the center of the Earth. To orient the spacecraft in this reference frame, two axis rotations are performed from the Earth-oriented orbital reference frame using the Earth to Sun rotation angles discussed above. The first rotation is performed about the 3-axis or Z_o axis of Figure 1 using the angle ψ_{es}. This forms a new set of axes called x1, x2, and x3. It can be shown that the x1-z1 plane and the y1-z1 plane still cut through the center of the Earth since the z1 axis is still oriented toward the center of the Earth. Now a rotation about the x1 axis is performed using the angle ϕ_{es}. This rotation serves to now orient the negative Y axis in the direction of the Sun as in Figure 1. Now, since the x1 axis is perpendicular to the y1-z1 plane by definition, and

since the y1-z1 plane cuts through the center of the Earth before the rotation; it must still be cutting through the center of the Earth, which is the desired configuration.

3. Body-fixed Reference Frame

This reference frame is obtained by performing a standard 3-1-2 (Yaw-Roll-Pitch) Euler axis rotation in the Sun-oriented orbital reference frame. The rotations about all three axes will be small angles, so small angle approximations can be used in the definition of the equations of motion.

D. SPACECRAFT BUS DESCRIPTION

The spacecraft bus is shown in Figure 6. The main body of the bus has dimensions in inches of 19 x 19 x 30. There are three identical solar panels with the center panel mounted directly to the bus with the other two panels hinged to either side. All sun-monitoring equipment will be mounted on the top of the satellite. Figure 6 shows a rectangular box which will act as the equipment in this case for disturbance torque analysis. The momentum wheel and co-mounted Earth sensor are located at the back of the satellite toward the bottom. The Earth sensor assembly protrudes out the back of the satellite slightly.

Inertia and center of mass properties for the satellite were extracted from Reference 4 and are listed below. The reference point (0,0,0) for all calculations is located at the center of the base of the satellite (i.e. on the center of the positive Z face at the bottom of the satellite).

$$
\begin{aligned}
I_{xx} &= 8.363 \text{ kg-m}^2 \\
I_{yy} &= 9.284 \text{ kg-m}^2 \\
I_{zz} &= 4.012 \text{ kg-m}^2 \\
I_{xy} &= -0.111 \text{ kg-m}^2 \\
I_{xz} &= 0.013 \text{ kg-m}^2 \\
I_{yz} &= 0.048 \text{ kg-m}^2
\end{aligned}
\qquad (14)
$$

$$COM_x = .000254 \text{ m}$$
$$COM_y = -.005842 \text{ m} \quad (15)$$
$$COM_z = -.453136 \text{ m}$$

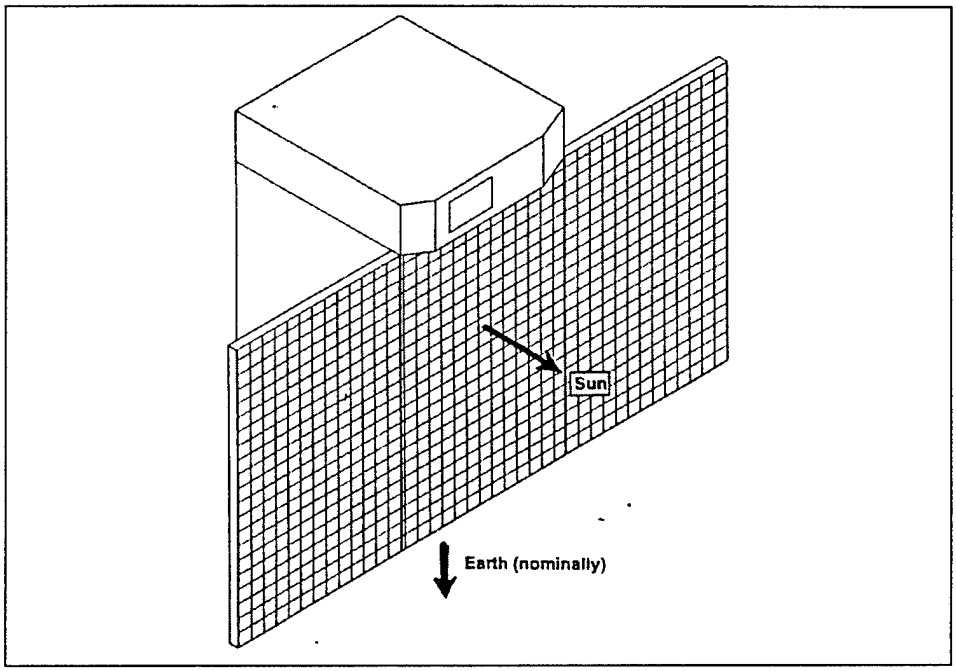

Figure 6. Spacecraft Bus [Ref. 4].

E. ATTITUDE DETERMINATION AND CONTROL COMPONENTS

Table 1 gives a listing of control system components selected for the design. Each component will be explained thoroughly below.

1. Sensors

a. Earth Sensor

Knowing the spacecraft attitude with respect to the Earth is of great importance in order to maintain constant communications with ground stations. Since the Earth appears to be rather large for near-Earth orbiting satellites, most sensors are designed to detect the Earth's horizon.

component	size	mass (kg)	power (watts)	comments
Momentum wheel	9.75 N-m-sec	5.8	5	3000 RPM +/- 10%
Magnetic Torque Rods	15 A-m^2	0.45 (x 3)	1.43 (x 3)	dual coil
Magnetometers	+/- 0.6 Gauss	0.25 (x 2)	0.04 (x 2)	2-axis
Earth Sensor		1.9	3.3	on momentum wheel initially
Sun Sensors		1.8	0.5	
		11.35	13.2	

Table 1. ADCS components

The smallest amount of horizon sensing ambiguity is achieved by using the spectral region in the infrared near the 15μm wavelength. Infrared detectors are not affected by night or the presence of a terminator. Furthermore, they are less susceptible to sunlight reflections off the surface of the spacecraft. However, visible light sensors have some advantages over infrared sensors including: lower cost, faster response time and higher signal to noise ratios due to increased visible radiated intensity. [Ref. 6]

The main purpose of the Earth sensor for this satellite is to provide pitch error data which will be used to control pitch angle and keep the communications antenna (located on the Earth-facing side) nominally Earth-pointed. This will be accomplished by keeping the pitch/yaw plane in such an orientation that it cuts a great circle arc on the Earth. This guarantees Earth sensor data to the maximum extent possible. Due to the orbit configuration and attitude control approach selected, Earth sensor data will not always be available. Using Figure 7, one can see the relationships between the Earth sensor scan line, which is canted at a 45 degree angle up from the local vertical, and the surface edge of the Earth. It is easy to determine that if the Earth to Sun roll rotation

angle (ϕ_{es}) is greater than 22 degrees in the negative direction, then the scan line of the sensor will not hit the Earth and sensing data will be unavailable. Current simulation results show that Earth sensor data will be unavailable for an increasing percentage of the orbit as Beta angle decreases. When Earth sensor data is unavailable, the magnetometers and an orbital elements model with a magnetic field model will be used to detect coarse pitch errors (magnetometer sensing error is approximately 5 degrees).

The Earth sensor is mounted on the momentum wheel and protrudes out the positive pitch axis surface of the spacecraft (anti-sun face). Consideration was given to mounting the Earth sensor on the sun-facing side of the spacecraft for increased sensing data during eclipse when roll/yaw error signals are unavailable from the sun sensors, but solar array development considerations and the cost of an Earth sensor mounted separately from the momentum wheel can make this option unattractive. The addition of this extra Earth sensor may become necessary to provide sensing data in eclipse for low Beta angle applications, which will be explored in the simulations.

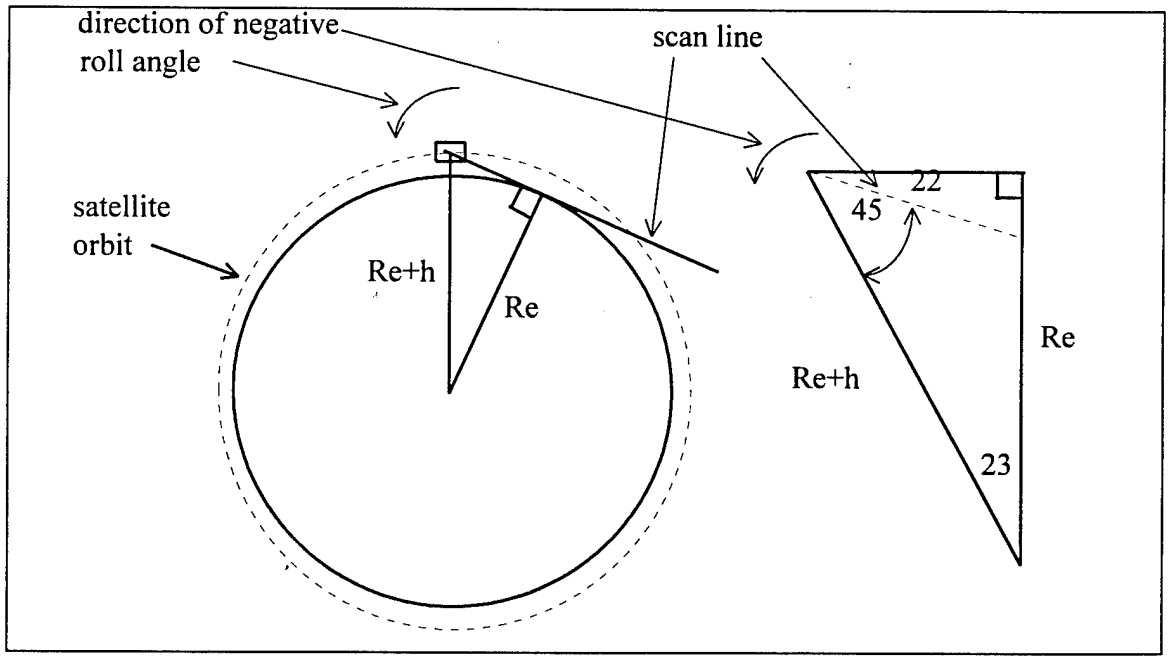

Figure 7. Earth sensor coverage relationships

b. Sun Sensors

Sun sensors have been used on nearly all spacecraft which have flown. Since the distance to the sun is rather large for Earth orbiting satellites, the angular radius of the sun is nearly independent of the type of orbit and for most applications, the sun can be treated as a point-source. Furthermore, the sun is bright enough to allow the use of simple equipment to discriminate among radiation sources with small power requirements. Generally, sun sensors are used for detecting sun presence, directing the solar arrays toward the sun and providing the relative sun vector for protection of sensitive equipment such as star trackers and other sensors. Sun sensors can have very narrow to very wide fields of view and resolutions from several degrees to less than one arc-second. The three basic types of sun sensors include: Analog sensors which provide a continuous output which is a function of sun angle; sun presence sensors which have a constant output when the sun is present; and digital sensors which provide a discrete output as a function of sun angle [Ref. 6].

High accuracy sun sensors will be used on the sun-facing side of the spacecraft to provide sun line roll/yaw error signals to the attitude control system for magnetic torque rod control. Coarse sun sensors will also be used on each face of the spacecraft in case a problem develops and the spacecraft's attitude with respect to the sun needs to be known for solar array pointing. These coarse sun sensors will also be needed to provide pointing control while reorienting the spacecraft from its Earth-oriented configuration during checkout to the sun pointing mode.

c. Magnetometers

Magnetometers are very popular attitude determination sensors and have been used widely on spacecraft. They are vector sensors because they provide both direction and magnitude of the ambient magnetic field. Furthermore, they are reliable, lightweight, and have low power requirements; they have no moving parts; and they can operate over a wide temperature range. Unfortunately, magnetometers are not very accurate inertial attitude sensors mainly due to the lack of an accurate model of the

Earth's magnetic field. Also, the Earth's magnetic field strength decreases as a function of the inverse cube of the satellite distance from the center of the Earth. This could result in residual spacecraft magnetic effects dominating the field strength, generally limiting the use of magnetometers to spacecraft below 1000 kilometers (note: missions have successfully used magnetometers above this altitude) [Ref. 6].

The magnetometer consists of a magnetic sensor and an electronics unit for transforming sensor measurements into a usable format. There are two main types of magnetometers: quantum magnetometers, which utilize atomic properties; and induction magnetometers, which are based on Faraday's Law of Magnetic Inductance. The latter group is more popular and will be discussed further here. [Ref. 6]

Faraday's law states that an electromotive force (EMF) is induced in a conducting coil when it is placed in a time-varying magnetic flux. There are two types of induction magnetometers called search-coil and fluxgate magnetometers. Search-coil magnetometers contain a solenoid coil of N turns surrounded by a ferromagnetic core with magnetic permeability μ, and cross-sectional area A. The EMF induced in the coil when placed in a magnetic field produces a voltage as a function of the time varying component of the magnetic field which is parallel to the solenoid. This type of magnetometer is mainly used on spin-stabilized spacecraft to provide precise phase information. The fluxgate magnetometer uses two coils and two saturable cores to detect the presence of any ambient magnetic field by measuring harmonic frequencies formed by the time-varying field.

A pair of two-axis magnetometers will be used to detect the ambient magnetic field the spacecraft is encountering. The data will be used primarily to calculate electrical currents needed to generate desired control torques with the magnetic torque rods and also in a backup roll to detect course attitude errors as discussed in the Earth sensor section above. The magnetometers will be mounted in such a way that each element detects a component of the magnetic field along each major body axis. These

signals will then be averaged to determine the magnetic field strength and direction. This configuration will provide some backup in case of failure in one of the components.

2. Actuators

a. Momentum Wheel

Angular momentum storage devices are used on spacecraft for several purposes including: the addition of stability to counter disturbance torques, to provide a variable momentum to allow operation at one revolution per orbit for Earth oriented missions, to absorb cyclic torques, and to transfer momentum to the spacecraft for slewing maneuvers. The principle of momentum for a spinning wheel is derived from the relationship

$$\mathbf{h} = I\omega \tag{16}$$

where I is the moment of inertia of the wheel and ω is the rotational velocity.

Momentum wheels are designed to provide a variable momentum 'bias' or nonzero momentum which can be used for storage capability about the rotational axis of the wheel which is generally fixed with respect to the spacecraft. The same momentum can be achieved with a large inertia, slowly rotating wheel and a small inertia, rapidly rotating wheel. Design tradeoffs usually favor the smaller wheel for the weight savings, but the increased wheel speed can lead to greater wear on the bearings which may shorten the wheel lifetime.

Torque motors using either direct or alternating current (DC or AC) are used to transfer momentum between the wheel and the spacecraft body. The DC motors are generally more efficient and provide high torques at low speed, but they do require the use of brushes which can wear out. AC motors do not have this drawback, but they do require gearing systems due to their high speed. Also, they are less efficient and provide a lower torque. Tachometers are used to measure wheel speed for attitude control purposes.

The main purpose of the momentum wheel on this spacecraft is to provide gyroscopic stiffness along the pitch axis once the spacecraft is operational. It also serves to control pitch angle by changing wheel speed to generate the necessary control torques. The amount of time that the momentum bias vector needs to keep pointing accuracy is assumed to be 35 minutes; the maximum eclipse time. Momentum wheel size is listed in Table 2 for several pointing accuracies over this maximum eclipse period assuming worst case disturbance torques are present throughout the eclipse. This assumption provides for some built in safety margin for the sizing.

accuracy after eclipse period (degrees)	momentum wheel size (N-m-sec)
0.1	25
0.2	12.5
0.5	4.8
1	2.4
2	1.2

Table 2. Momentum wheel size versus gyroscopic stiffness pointing accuracy

The amount of torque output required is driven by Iyy and pitch angular acceleration ($\ddot{\theta}$), which is a function of Beta angle. Equations for $\ddot{\theta}$ are developed in Reference 4 and are listed here as

$$\ddot{\theta}_{max} = \frac{\omega_o^2 K \sin\xi}{(1-\sigma\cos\xi)^2} \tag{17}$$

where

$$K = \frac{4\cos^2\beta\sin\beta}{(1+\sin^2\beta)^2} \tag{18}$$

$$\sigma = \frac{1-\sin^2\beta}{1+\sin^2\beta} \tag{19}$$

$$\xi = \arccos\left[\frac{\sqrt{1+8\sigma^2}-1}{2\sigma}\right] \tag{20}$$

The maximum momentum change required from the wheel is given by

$$\Delta H_{wheel} = (\dot{\theta}_{\max} - \dot{\theta}_{\min})I_{yy} = (\frac{1}{\sin\beta} - \sin\beta)\omega_o I_{yy} = \frac{\cos^2\beta}{\sin\beta}\omega_o I_{yy} \tag{21}$$

The maximum torque required from the wheel is then determined from

$$T_{\max} = I_{yy}\ddot{\theta}_{\max} \tag{22}$$

A wheel with a momentum of 9.75 N-m-sec at 3000 rpm with a torque rating of 0.025 N-m was selected. This provides a pointing deviation slightly less than 0.5 degrees over the maximum eclipse period assuming worst case disturbance torques are acting on the spacecraft throughout this period. Initial simulation results indicate that the maximum pitch angular acceleration can be shown to be approximately 2×10^{-6} rad/sec^2. This means there can be an extremely large Iyy before wheel torque becomes a concern.

b. Magnetic Torque Rods

Magnetic coils or electromagnets are used to generate torques necessary to control spacecraft attitude and momentum. This could include use for overcoming disturbance torques and compensating for residual magnetic effects. The magnetic moment generated by a loop of wire possessing N turns is given by

$$\mathbf{m} = NIA\mathbf{n} \tag{23}$$

where N is the number of turns, I is the current through the loop, A is the area enclosed by the loop and **n** is a unit vector normal to the plane of the loop. The positive sense of

the direction of the magnetic moment is determined by the right hand rule. The fingers of the right hand are curled around the turns of wire in the direction of the current and then the right thumb points in the direction of the magnetic moment.

The magnetic dipole moment depends on what type of material is enclosed within the turns of wire and is expressed by

$$\mathbf{M} = \mu\mathbf{m} \tag{24}$$

where μ is the permeability of the core material. The permeability of free space μ_o has the value $4\pi \times 10^{-7}$ N/A^2. Thus, it is clear that the values of core permeability, coil configuration, N and A, and the current values must be selected appropriately for the given application. Magnets on most satellites have used an "air" core. To generate magnetic control torques the following relationship is used

$$\mathbf{T}_{mag} = \mathbf{M} \times \mathbf{B} \tag{25}$$

where **M** is the magnetic dipole moment and **B** is the magnetic field expressed in body coordinates.

The magnetic torque rods will be used for momentum wheel desaturation and roll/yaw repositioning to zero out sun sensor error signals. The change in momentum required to reorient the momentum vector by 1 degree per day is approximately 0.122 N-m-s. This relates to a constant torque of 1.41×10^{-6} N-m throughout the day (or 2.82×10^{-6} N-m on a 50% duty cycle) . This value is much smaller than the maximum disturbance torque, so the latter will be used to size the magnetic torque rods. Assuming a worst case magnetic field strength of 1.5×10^{-5} tesla, the required torque rod moment is approximately 2.45 A-m^2 . Magnetometer sensing data will be used to provide control signals for electrical current generation which control the direction and amount of torque

output. The selected torque rods have two coils, which provides redundancy in the system, and have a magnetic moment of 15 A-m^2.

c. Thrusters

Since no orbit control is considered to be necessary, a thruster system was omitted due to a great increase in weight, complexity and cost.

F. SYSTEM PERFORMANCE

Once the injection vehicle has attained the proper orbit, the momentum wheel will be spun up with the injection vehicle providing torque to counter the increase in momentum. It will take approximately 7 minutes to spin up the wheel if injection vehicle control is available. In the event the launch vehicle cannot provide stabilization, the wheel will be spun up in accordance with the capture control section in Chapter IV. When the wheel has achieved speed, the separation system will activate (assuming injection vehicle control) and separate the satellite from the injection vehicle. Once clear, the solar arrays will deploy and operations will begin to establish a stable nadir-pointing attitude. Worst case tip off rate in pitch is expected to be approximately 5.5 degrees per second and worst case nutation angle (due to roll tip-off torque) is expected to be 5 degrees. The momentum wheel is designed with sufficient momentum storage to absorb the former and the magnetic torque rods will be used to damp out the latter.

When the satellite is stable in a nadir-pointing configuration, system checks will be performed. Next, ground commands will be used to initiate the reorientation of the momentum bias vector toward the sun with torque rod control. Following this, the attitude control system will maintain pointing accuracy of 0.5 degree in roll and yaw and 5.0 degrees in pitch.

The allowable speed region for the wheel will be 3000+/-300 RPM. Wheel desaturation will be performed as needed using the magnetic torque rods. Initial simulation results show that wheel speed takes several orbits to reach desaturation limits and that the magnetic control law is easily capable of accomplishing the desaturation. Other simulation results from MATLAB/SIMULINK also indicate that the momentum

bias vector is capable of limiting roll/yaw drift to .2 degrees throughout the maximum eclipse period (35 minutes) with no control inputs. If the proper alignment is achieved before eclipse entry, then the spacecraft should be oriented at visible sunrise so that the sun is within the field of view of the sun-monitoring instruments.

G. SIMULATION

An old SIMULINK program, developed by Professor Leonard at the Naval Post Graduate School, Monterey, California has been upgraded and tailored for this particular application. It includes simulation blocks for each disturbance torque (solar pressure, gravity gradient, and aerodynamic) and a simple simulation for the Earth sensor and sun sensors. From these inputs, spacecraft torques will be calculated and the spacecraft's dynamic properties will be simulated. A separate MATLAB program will be used to control the SIMULINK program and create output displays. SIMULINK and MATLAB block diagrams and control codes are listed in the appendix.

III. SPACE ENVIRONMENT AND ITS AFFECT ON THE SPACECRAFT

A. EARTH'S MAGNETIC FIELD DEVELOPMENT

The derivation of the Earth's magnetic field is very complex for both magnitude and direction. However, the field can be approximated by a large, tilted dipole located at the Earth's center with the 'south' end of the dipole located in the northern hemisphere. The location of the magnetic poles is constantly drifting at approximately .014 degrees per year [Ref. 6]. More accurate models of the field are available but they require vast computing resources to simulate; and they are not required for use in this feedback control application. Thus, the dipole approximation will be used.

The plane which is perpendicular to the dipole is called the magnetic equator and this is where the field is weakest in magnitude. Figure 8 shows how the magnetic field strength varies with altitude at the magnetic equator. It can be shown that the strength of the dipole field decreases as a function of the inverse cube of the distance from the dipole center (i.e. the center of the Earth) [Ref. 6].

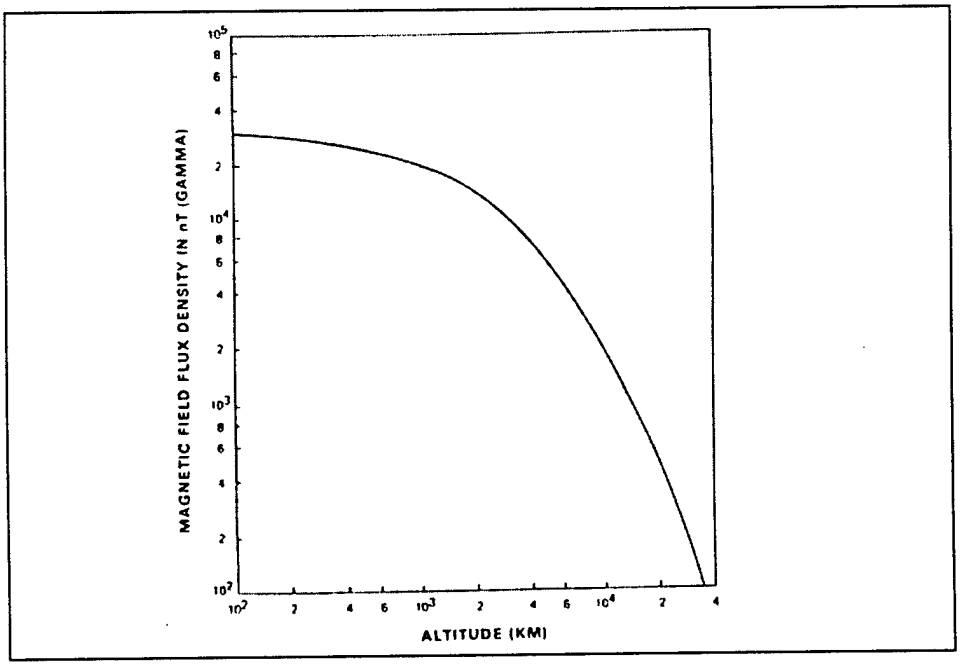

Figure 8. Magnetic Field Intensity at Equator in (nano-Tesla) [Ref. 6]

As magnetic latitude increases from zero to 90 degrees, the field strength at a given altitude doubles as shown in Figure 9.

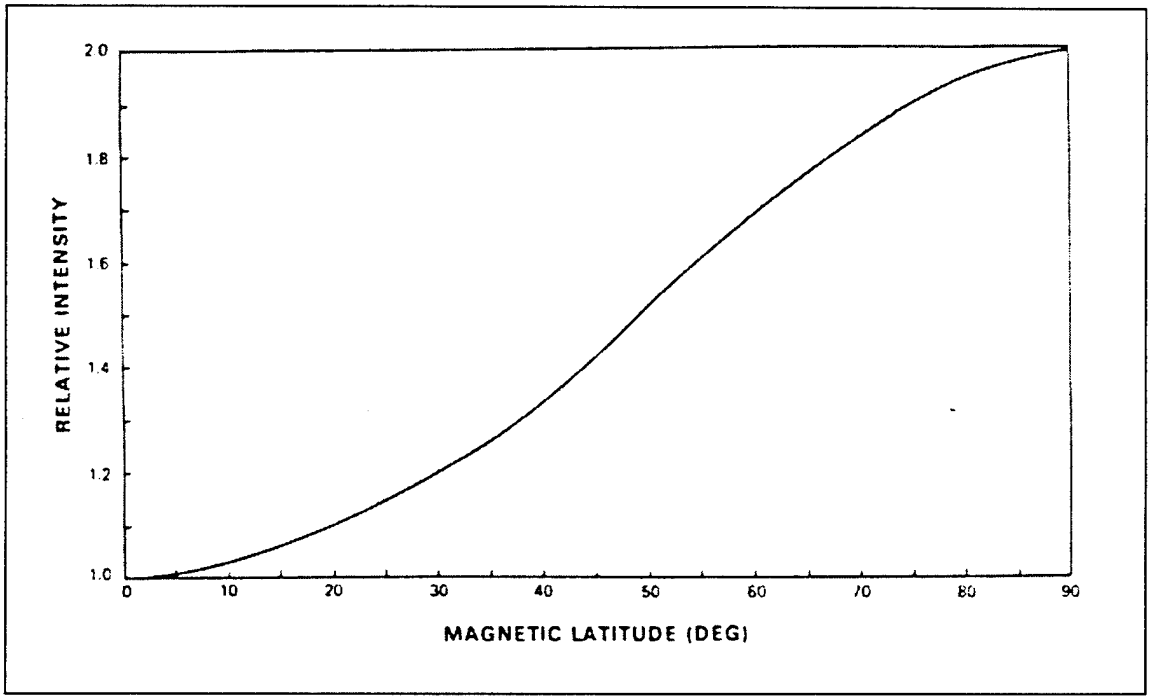

Figure 9. Relative Intensity of Magnetic Field as a Function of Latitude [Ref. 6]

For magnetic control, the Earth's magnetic field needs to be expressed in coordinates relative to the three primary body axes of the spacecraft. The magnetic field components expressed in the Earth oriented orbital reference frame are: [Ref. 7]

$$B_{xo} = \frac{M}{R^3}[C\varepsilon SiC\alpha - S\alpha S\mu S\varepsilon - CiC\alpha C\mu S\varepsilon] \tag{26}$$

$$B_{yo} = \frac{M}{R^3}[-C\varepsilon Ci - C\mu SiS\varepsilon] \tag{27}$$

$$B_{zo} = \frac{M}{R^3}[2C\varepsilon SiS\alpha + 2C\alpha S\mu S\varepsilon - 2CiS\alpha C\mu S\varepsilon] \tag{28}$$

Where C is the cosine of the angle, S is the sine of the angle, i is the orbit inclination, R is the radius of the satellite orbit, M is the Earth's Dipole strength (7.943×10^{15} Nm^2/Amp), ε is the dipole tilt with respect to the Earth's spin axis (11.7 degrees), μ is the Earth's rotation with respect to the ascending node (varies 360 degrees in one day), and α is the orbit angle with respect to the ascending node (i.e. the angular position of the satellite measured counterclockwise around the orbit from the ascending node).

To express these magnetic field components (B_{ox}, B_{oy}, and B_{oz}) in the spacecraft body axis reference frame, two coordinate transformations are needed. The first transforms the magnetic field from the Earth-oriented orbital reference frame to the sun-oriented orbital reference frame, while the second is a standard 3-1-2 Euler rotation which leads to the body-fixed reference frame orientation. Once the field components are represented in body-fixed coordinates, they can be used in the equations of motion for both disturbance torque analysis and magnetic control torque inputs.

B. TORQUES WHICH AFFECT THE SPACECRAFT

To be able to analyze the motion of the spacecraft on orbit one must be able to model all torques which act upon the spacecraft whether they are generated by the environment or by the spacecraft attitude control system. These torques can either be categorized as cyclic, varying sinusoidally over an orbit, or secular, accumulating with time and not averaged over an orbit. Numerical integration of Euler's equations requires that all torques be modeled as a function of time and the spacecraft's attitude. For this analysis, the major environmental disturbance torques to be considered are: aerodynamic drag, solar pressure, residual magnetic dipole and Earth's gravitational. These disturbance torques would quickly reorient the spacecraft if not resisted in some way by the attitude control system. The active control torques to be used are generated by the momentum wheel and magnetic coils.

1. Disturbance Torques

Before sizing the ADCS components, one must know the maximum possible disturbance torques that the spacecraft might experience throughout its lifetime. As

discussed above, the major categories of disturbance torques are: aerodynamic, solar pressure, residual magnetic dipole and Earth's gravitational. The type of torque which is the largest for this type of low altitude application is the aerodynamic torque. Also, since there are several techniques available to limit the effects of residual magnetic dipole disturbances, this category will be ignored for the purpose of simplicity in the simulation. Using References 6, 8 and 9, each disturbance torque is analyzed to determine its magnitude and which axes of the spacecraft it affects.

a. Aerodynamic

For lower altitude orbits, the interaction of the spacecraft with the Earth's upper atmosphere causes a disturbance torque about the spacecraft center of mass. The force due to the impact of atmospheric molecules on the spacecraft surface can be modeled as an elastic impact without reflection. The incident particle's energy is generally completely absorbed [Ref. 6]. The incremental force d**F** on a surface element area dA with outward normal **N** is given by

$$d\mathbf{F} = -\tfrac{1}{2} C_D \rho V^2 (\mathbf{N} \cdot \mathbf{V}) \mathbf{V} dA \tag{29}$$

where **V** is the unit vector along the translational velocity of the individual surface element relative to the incident stream of particles, C_D is the coefficient of drag (assumed to be 2.0 if no measured value is available) and ρ is the atmospheric density. To determine the total aerodynamic torque, the individual forces must be integrated as follows

$$\mathbf{T}_{aero} = \int \mathbf{R}_{cp-cg} \times d\mathbf{F} \tag{30}$$

where $\mathbf{R}_{cp\text{-}cg}$ is the vector measured from the center of mass of the spacecraft to the center of the individual incremental areas (i.e. the distance to the center of pressure for that individual area).

The aerodynamic disturbance torque is a fixed quantity for spacecraft which are oriented toward the Earth, but varies for those which are inertially referenced such as this spacecraft. The velocity vector for the spacecraft can be expressed in Earth-oriented coordinates as

$$\mathbf{V}_{sc} = I\mathbf{X}_o \tag{31}$$

To take the necessary cross products for determining the aerodynamic torque, this velocity vector must be expressed in body coordinates by performing the two required coordinate transformations using the Earth to sun angles and the sun to body Euler angles. Since the vector $\mathbf{r}_{cp\text{-}cg}$ for each individual piece of the satellite is known in body coordinates, it is easy to simulate the cross products and thus, the aerodynamic torques for each individual area of the spacecraft. These individual torques are then added to determine the overall aerodynamic torque.

From Reference 9, the worst case atmospheric density is approximately 2.0×10^{-12} kg/m^3. Using a coefficient of drag of 2.0, orbital velocity of 7585.1 m/sec and the effective surface area for each individual satellite panel the aerodynamic force on each face of the satellite can be calculated and the individual cross products can be determined. The individual, time varying computations are performed in the SIMULINK program and will not be listed here.

b. Solar Pressure

Radiation incident upon the body of the spacecraft produces a small disturbance torque about the center of mass of the spacecraft. The surface of the body is subjected to a radiation pressure (force per unit area) which is equal to the vector difference between the incident and reflected solar radiation energy. Since the intensity of the solar radiation is a function of distance from the sun, spacecraft altitude with respect to the Earth does not affect solar radiation pressure for Earth-orbiting spacecraft. The mean momentum flux acting on a surface normal is determined from

$$P = \frac{F_e}{c} \tag{32}$$

where F_e is the solar constant (1358 W/m^2) and c is the speed of light (3.0 x 10^8 m/sec). This flux value is constant except for a small periodic variation due to the eccentricity of the Earth's orbit about the sun [Ref. 6].

For most applications, the solar force can be modeled adequately by assuming the incident radiation is either absorbed, reflected specularly, reflected diffusely, or some combination of the above. Specular reflection means that the incident vector is reflected at the same angle as it came in to the surface, while diffuse reflection means that the incident vector is reflected in all directions. The differential force imparted by the particles which are totally absorbed is given by

$$d\mathbf{F}_{abs} = -PC_a \cos\theta \mathbf{S} dA \tag{33}$$

where C_a is the absorption coefficient, **S** is the unit vector from the spacecraft to the sun and θ is the angle between **S** and **N**, the unit vector normal to the differential surface. This last angle must be less than 90 degrees for a pressure force to exist on that area. The differential force for the specularly reflected radiation is given by

$$d\mathbf{F}_{spec} = PC_s[\mathbf{S} - 2(\cos\theta \mathbf{N}) - \cos\theta \mathbf{S}]dA \tag{34}$$

where C_s is the coefficient of specular reflection. For a surface which reflects diffusely, all reflection angles must be considered and integrated to form the total differential force for diffuse reflection as

$$d\mathbf{F}_{diff} = PC_d(-\frac{2}{3}\cos\theta \mathbf{S} - \cos\theta \mathbf{S})dA \tag{35}$$

where C_d is the coefficient of diffuse reflection. If all types of reflection play a part, then the total differential force is given by

$$d\mathbf{F}_{total} = -P\int[(1-C_s)\mathbf{S} + 2(C_s\cos\theta + \tfrac{1}{3}C_d)\mathbf{N}]\cos\theta dA \tag{36}$$

where $C_a + C_s + C_d = 1$ [Ref. 6].

The solar torque is then determined by taking the integral of all cross products between each differential solar force and its individual distance offset from the center of mass of the spacecraft [Ref. 6].

$$\mathbf{T}_{solar} = \int \mathbf{r}_{cp-cg} \times d\mathbf{F}_{total} \tag{37}$$

Since it is difficult to perform this integral, it is not unusual to break down the spacecraft to simple geometric elements and then estimate each of the individual torques for each element. This spacecraft will be treated in a similar manner. Since only the solar panel side of the spacecraft will be pointed at the sun during normal operations, we must consider that side only for solar pressure (i.e. the angle between **S** and **N** for the other sides is 90 degrees or the face is not illuminated). This means no solar torques about the Y axis will be generated. The surfaces on this side of the spacecraft include the solar panels and the sun-facing side of any monitoring instruments [Ref. 6].

For the solar arrays, the total surface area is 1.094 m^2 and it is assumed that $C_a = 0.8$, $C_s = 0.1$, and $C_d = 0.1$. The center of pressure for the array assembly is located at (x, y, z) = (0.0, -9.5, -14.9) inches or (0.0, -0.2413, -0.3785) meters using the body coordinate reference listed earlier. Utilizing Equations (15) and (37), this will cause a torque about the negative X and Z axes equal to

$$\begin{aligned} T_{spx} &= -4.31x10^{-7}\,N-m \\ T_{spz} &= -1.47x10^{-9}\,N-m \end{aligned} \tag{38}$$

The sun-monitoring equipment is assumed to have a surface area of 0.061 m^2 and it is assumed that $C_a = 0.05$, $C_s = 0.8$, and $C_d = 0.15$; with a center of pressure

located at (x, y, z) = (0.0, -9.5, -32.25) inches or (0.0, -0.2413, -0.8192) meters. This will cause a torque about the positive X axis and the negative Z axis equal to

$$T_{eqpmntx} = 1.92x10^{-7}\ N-m \qquad (39)$$
$$T_{eqpmntz} = -1.33x10^{-10}\ N-m$$

This yields a total solar torque for each axis of

$$T_{solarx} = -2.39x10^{-7}\ N-m \qquad (40)$$
$$T_{solarz} = -1.60x10^{-9}\ N-m$$

c. Gravity Gradient

Any non-symmetrical body in orbit will experience a gravitational torque because of the variation of the Earth's gravitational force over the object. This is due to the non-uniformity of the inverse square gravitational field. To develop the relationships for the gravity gradient torques it is assumed that the moments of inertia are known and that the spacecraft is orbiting a non-realistic, spherical Earth. Using Reference 8, the differential force acting on the spacecraft mass element dm located a distance R from the center of the Earth is given by

$$d\mathbf{F} = -\frac{\mu_e \mathbf{R} dm}{R^3} \qquad (41)$$

where μ_e is the Earth's gravitational constant and R is the distance from the center of the Earth to the individual incremental masses. Using Figure 10, **R** can be expressed as

$$\mathbf{R} = \mathbf{R}_o - \mathbf{r} \qquad (42)$$

where R_o is the distance from the center of the Earth to the center of mass of the spacecraft and r is the distance between the spacecraft center of mass and the individual

incremental masses. Substituting this relationship into the above equation and using the fact that $r / R_o << 1$ to expand R^{-3} in a Taylor series expansion yields

$$d\mathbf{F} \approx \frac{\mu_e(\mathbf{R}_o - \mathbf{r})dm}{R_o^3}\left(1 + 3\frac{\mathbf{r}\cdot\mathbf{R}_o}{R_o^2}\right) \tag{43}$$

The torque about the center of mass is obtained by integrating each of the individual incremental forces and noting that

$$\int \mathbf{r}\, dm = 0 \tag{44}$$

because **r** is a vector measured from the center of mass of the spacecraft.

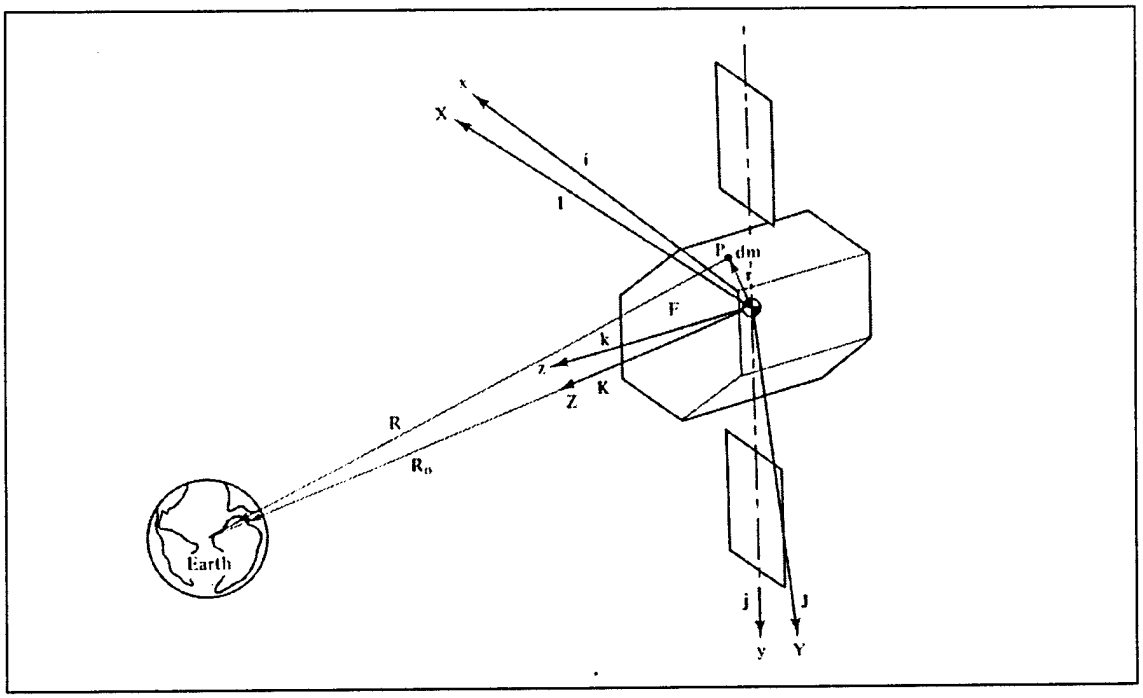

Figure 10. Gravity gradient spatial relationships [Ref. 8]

The final result is

$$\mathbf{T}_{gg} = \int \mathbf{r} \times d\mathbf{F} = \frac{3\mu_e}{R_o^5}\int (\mathbf{r}\times\mathbf{R}_o)(\mathbf{r}\cdot\mathbf{R}_o)dm \tag{45}$$

The vector $\mathbf{R}_o$, which is expressed in the Earth-oriented reference frame as R_o **K**, can be written in body coordinates by performing a coordinate transformation from the Earth-oriented to the body coordinate system. The result is

$$\mathbf{R}_o = R_o(A\hat{\mathbf{i}}_{body} + B\hat{\mathbf{j}}_{body} + C\hat{\mathbf{k}}_{body}) \tag{46}$$

where the expressions for A, B and C are given by

$$\begin{aligned} A &= S\phi_{es}[C\theta S\psi + S\phi S\theta C\psi] - C\phi_{es}[S\theta C\phi] \\ B &= S\phi_{es}[C\psi C\phi] + C\phi_{es}[S\phi] \\ C &= S\phi_{es}[S\theta S\psi - S\phi C\theta C\psi] + C\phi_{es}[C\theta C\phi] \end{aligned} \tag{47}$$

where C is the cosine of the angle and S is the sine of the angle. Substituting Equation (46) into Equation (45) and integrating yields the gravity gradient torques about each axis in body coordinates (ignoring cross-product terms) as

$$\begin{aligned} T_{ggx} &= \frac{3\mu_e}{R_o^3}(I_{zz} - I_{yy})\mathrm{BC} \\ T_{ggy} &= \frac{3\mu_e}{R_o^3}(I_{zz} - I_{xx})\mathrm{AC} \\ T_{ggz} &= \frac{3\mu_e}{R_o^3}(I_{xx} - I_{yy})\mathrm{AB} \end{aligned} \tag{48}$$

d. Residual Magnetic Torque

Through the use of non-ferrous materials and proper wiring configurations, the residual magnetic dipole of the spacecraft can be greatly reduced and, in most cases, neglected. There can be no specific determination of the residual magnetic

dipole until the spacecraft is actually built and tested. For simulation purposes, residual magnetic torques will be ignored in this application.

e. Total Torque

Initial simulation results show that the estimated worst case torques for each axis are expected to be approximately:

roll	2.0×10^{-5}	N-m	
pitch	9.0×10^{-6}	N-m	(49)
yaw	2.0×10^{-5}	N-m	

Since the yaw and roll torques are expected to be the largest, they will be used to size the ACS equipment.

IV. EQUATIONS OF MOTION AND ATTITUDE CONTROL LAWS

A. EQUATIONS OF MOTION

From Reference 8, the basic moment or torque equation is

$$\mathbf{T}_c = \dot{\mathbf{H}}_{crel} + \omega \times \mathbf{H}_c \tag{50}$$

where H_c is given for a system with a momentum storage wheel by the equation

$$\mathbf{H}_c = I\omega + \mathbf{h}_{wheel} \tag{51}$$

where I is the inertia matrix of the satellite and ω contains the body rotational rates of the satellite given by

$$\begin{aligned}
\omega_x &= C\theta\dot{\phi} - C\phi S\theta\dot{\psi} - \omega_{on}(C\theta S\psi + S\phi S\theta C\psi) \\
\omega_y &= \dot{\theta} - S\phi\dot{\psi} - \omega_{on} C\phi C\psi \\
\omega_z &= S\theta\dot{\phi} + C\phi C\theta\dot{\psi} - \omega_{on}(S\theta S\psi - S\phi C\theta C\psi)
\end{aligned} \tag{52}$$

where ϕ, θ and ψ are the angles used in the 3-1-2 Euler angle rotation from the sun-oriented orbital reference frame to the body reference frame. The term ω_{on} is the angular velocity of the sun-oriented reference frame. Assuming the time rate of change of Beta to be zero, it is given by

$$\omega_{on} = \dot{\theta}_{es} \approx \frac{\cos^2\theta\omega_o}{\cos^2\nu \sin\beta} \tag{53}$$

Equation (50) can be written in components as

$$T_x = \dot{H}_x + \omega_y H_z - \omega_z H_y$$

$$T_y = \dot{H}_y + \omega_z H_x - \omega_x H_z \qquad (54)$$

$$T_z = \dot{H}_z + \omega_x H_y - \omega_y H_x$$

A special case to consider occurs when the rotating axes x, y and z coincide with the principle inertia axes of the spacecraft. Then Equation (51) simplifies to

$$H_x = I_{xx}\omega_x + h_{wheelx}$$

$$H_y = I_{yy}\omega_y + h_{wheely} \qquad (55)$$

$$H_z = I_{zz}\omega_z + h_{wheelz}$$

These equations can be substituted back into Equation (54), noting that for this application there is only wheel momentum about the y axis, to form

$$T_x = I_{xx}\dot{\omega}_x + \omega_y\omega_z(I_{zz} - I_{yy}) - \omega_z h_{wheely}$$

$$T_y = I_{yy}\dot{\omega}_y + \omega_x\omega_z(I_{xx} - I_{zz}) + \dot{h}_{wheely} \qquad (56)$$

$$T_z = I_{zz}\dot{\omega}_z + \omega_x\omega_y(I_{yy} - I_{xx}) + \omega_x h_{wheely}$$

These equations can be manipulated, using substitutions from above and noting that the wheel momentum is oriented along the negative y axis, to form the linearized moment equations for each major axis

$$T_{cx} + T_{dx} = I_{xx}(\ddot{\phi} - \omega_{on}\dot{\psi} - \dot{\omega}_{on}\psi) + (I_{yy} - I_{zz})(\omega_{on}\dot{\psi} + \omega_{on}^2\phi) + h(\dot{\psi} + \omega_{on}\phi)$$

$$T_{cy} + T_{dy} = I_{yy}(\ddot{\theta} - \dot{\omega}_{on}) - \dot{h} \qquad (57)$$

$$T_{cz} + T_{dz} = I_{zz}(\ddot{\psi} + \dot{\omega}_{on}\phi + \omega_{on}\dot{\phi}) - (I_{yy} - I_{xx})(\omega_{on}\dot{\phi} - \omega_{on}^2\psi) - h(\dot{\phi} - \omega_{on}\psi)$$

where T_c constitutes the control torques and T_d constitutes the disturbance torques.

B. CONTROL FLOW

Figures 11 and 12 present the control flow for the spacecraft attitude control system and Earth sensor/Pitch control.

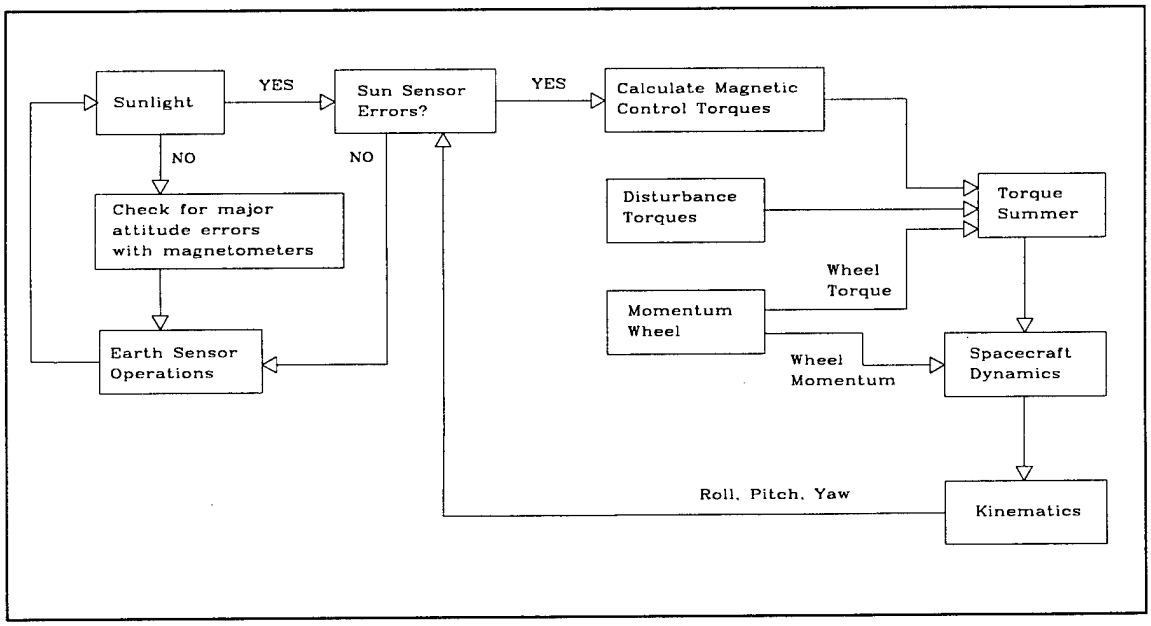

Figure 11. Spacecraft attitude control flow

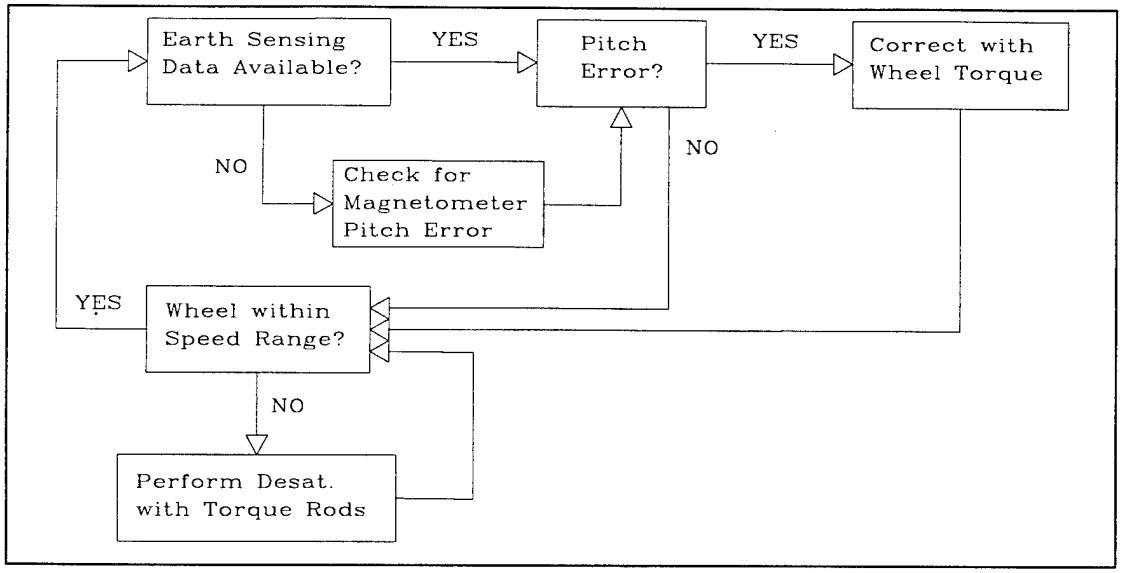

Figure 12. Wheel/Pitch control flow

C. ATTITUDE CONTROL LAWS

1. Satellite Capture After Booster Separation

Once the launch vehicle achieves the proper Earth-oriented configuration, the satellite will be separated. Two possible separation scenarios will be considered and simulated. In the first case, the momentum wheel will be spun up with the launch vehicle providing attitude stabilization until the wheel reaches optimum speed. Upon separation, only disturbance torques and torques generated by the separation mechanism will cause the satellite to tumble. For the second case, it is assumed that the launch vehicle cannot provide attitude stabilization. The satellite will be separated from the launch vehicle and the momentum wheel will be spun up at the maximum torque rating. This procedure, along with any torques generated by the separation system and disturbance torques, will cause the satellite to spin at an increasing angular rate about the pitch axis until the wheel is up to speed. It is assumed here that only one spring failure will occur among the four springs in the separation system. This single spring failure will cause the satellite to tumble if the wheel is not up to speed, and will cause nutation or pitch error if the wheel is up to speed. All tumbling motion needs to be removed so the satellite can be stabilized

in an Earth-oriented configuration for system check out and subsequent transition to the sun-oriented mode.

Reference 2 suggests the use of the following magnetic control moments

$$M_x = -K\dot{B}_x$$

$$M_y = -K\dot{B}_y \tag{58}$$

$$M_z = -K\dot{B}_z$$

where K is the control gain and the B_i components are the time derivatives of the magnetic field relative to the body axes of the satellite. These quantities can be generated by taking the derivative of the magnetometer outputs [Ref. 2].

This theory functions on the premise that the kinetic energy of a body, due to the rotation about its center of mass, can be reduced; which eliminates all angular motion between the satellite and the magnetic field. This results in a terminal motion where the satellite rotates twice per orbit about the pitch axis (once per orbit relative to the Earth-oriented orbital reference frame) [Ref. 2].

The time derivative of the rotational kinetic energy is given by

$$\frac{dKE}{dt} = \tau \cdot \omega \tag{59}$$

where τ is the external torque acting on the body and ω is the rotational velocity vector. A torque generated by the magnetic control torque rods is given by

$$\tau_{mag} = \mathbf{M} \times \mathbf{B} \tag{60}$$

Now the derivative of the magnetic field can be estimated by (assuming $\omega >> \omega_o$)

$$\dot{\mathbf{B}} \approx \mathbf{B} \times \omega \tag{61}$$

Combining the above equations, yields

$$\frac{dKE}{dt} = \dot{\mathbf{B}} \cdot \mathbf{M} \tag{62}$$

Implementing the magnetic moment equations in Equation (58) yields

$$\frac{dKE}{dt} = -K\dot{B}^2 = -K|\mathbf{B} \times \omega|^2 \tag{63}$$

This quantity is clearly less than or equal to zero which is desired to remove rotational energy. Equation (63) shows that this law cannot reduce the kinetic energy associated with the component of ω parallel to the magnetic field. Fortunately, the orbital motion of the satellite will ensure that the direction of the magnetic field relative to the body is continuously changing [Ref. 2].

Results are shown in Figures 13 through 15. A control gain of 1 x 10^9 (N-m-sec^2 /tesla^2) was used to maintain torque rod saturation throughout the capture procedure. Figure 13, shows the results of a simulation where the wheel has already been spun up and the initial pointing error between the orbit normal and the spin axis is 20 degrees. This was done to show that the system can remove the initial nutation due to the inertial body rotational velocities and also remove the pointing error between the orbit normal and spin axis. Visible is the initial chaotic reaction to the separation where the rapidly changing initial response is due to nutation. Once all body rotational rates have been neutralized, the system begins to remove the pointing error. This particular simulation took approximately 2 orbits to remove the pointing error between the orbit normal and the spin axis.

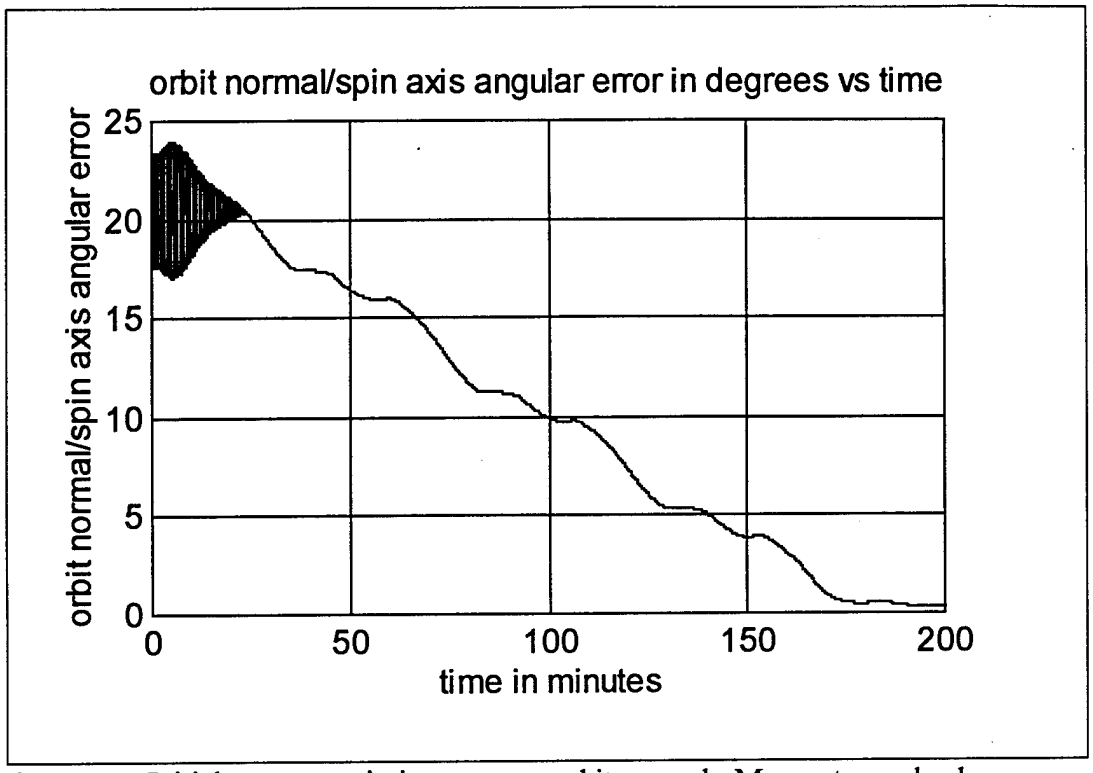

Figure 13. Initial capture pointing error to orbit normal. Momentum wheel spun up before separation

Figure 14, displays the simulation results for the case where the satellite momentum wheel has not been spun up and the satellite is ejected with initial rotational velocities about the x and y axes of approximately five degrees per second. As is clearly apparent, the satellite tumbles through several revolutions before the momentum bias overcomes the body angular momentum magnitude, which is being continuously decreased via the control law. This simulation shows that the satellite went through 30 complete rotations before it settled in the proper configuration. There is, however, an inherent problem with this approach to capture when the wheel is not up to speed at separation. The spin axis will always align itself with the orbit normal, but there is the possibility that the satellite will be turned about the yaw axis by 180 degrees (momentum vector pointed in opposite direction to that desired). In this case, ground command will be necessary to precess the momentum vector through that 180 degree swing to get into the proper configuration. Figure 15 is an expanded view of Figure 14.

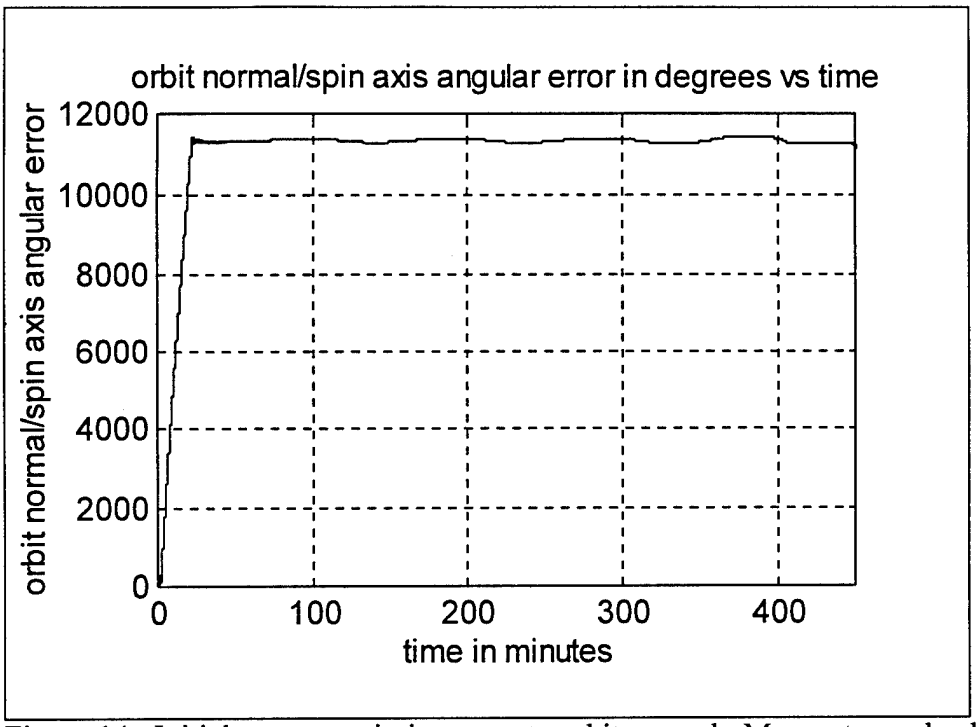

Figure 14. Initial capture pointing error to orbit normal. Momentum wheel spun up after separation.

2. Momentum Wheel Control

Wheel momentum will be controlled using the proportional/differential control law

$$\dot{h} = -K_\theta(\tau_\theta \dot{\theta} + \theta) \tag{64}$$

where θ is the pitch error signal provided by the Earth sensor or magnetometers and K_θ and τ_θ are control gains [Ref. 8]. Substituting Equation (64) into Equation (57) yields

$$T_{cy} + T_{dy} = I_{yy}\ddot{\theta} + K_\theta \tau_\theta \dot{\theta} + K_\theta \theta - I_{yy}\dot{\omega}_{on} \tag{65}$$

Ignoring the wheel desaturation control input T_c for now and considering the last term on the right hand side to be part of the disturbance torques (this term is on the order of 10^{-5} in magnitude or it can be canceled by feeding forward an estimate of the signal) yields

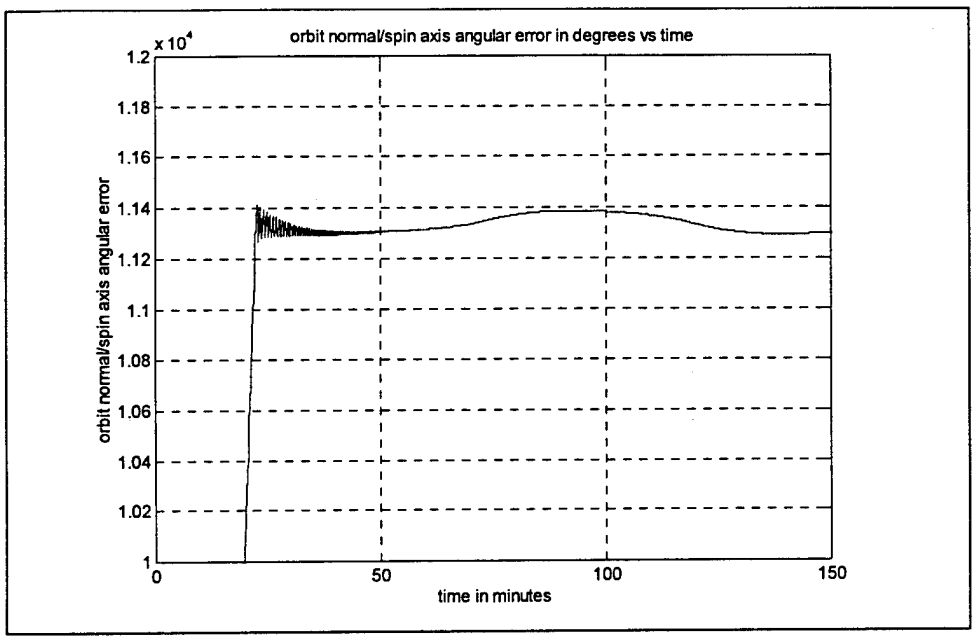

Figure 15. Exploded view of Figure 14 showing final pointing angle.

$$T_{dynew} = I_{yy}\ddot{\theta} + K_\theta \tau_\theta \dot{\theta} + K_\theta \theta \tag{66}$$

Transforming to the Laplace domain

$$\frac{\theta(s)}{T_{dynew}(s)} = \frac{1/I_{yy}}{s^2\theta(s) + K_\theta \tau_\theta / I_{yy} s\theta(s) + K_\theta / I_{yy}\theta(s)} \tag{67}$$

This is the transfer function for a second order damped oscillator with natural frequency

$$\omega_n = \sqrt{\frac{K_\theta}{I_{yy}}} \tag{68}$$

and damping ratio

$$\xi = \frac{\tau_\theta}{2}\sqrt{\frac{K_\theta}{I_{yy}}} \tag{69}$$

The design point is for a critically damped system where ξ=1 and then

$$\tau_\theta = 2\sqrt{\frac{I_{yy}}{K_\theta}} \tag{70}$$

If K_θ is selected as 0.36 kg-m^2/sec^2 and τ_θ is selected as 10 seconds, the natural frequency is 0.19 radians/second with a settling time of approximately 40 seconds, assuming settling time is defined as four times the time constant τ_θ.

System response to an initial pitch error of five degrees is shown in Figure 16. The system is reacting as a critically damped oscillator with a settling time of approximately 40 seconds, as designed.

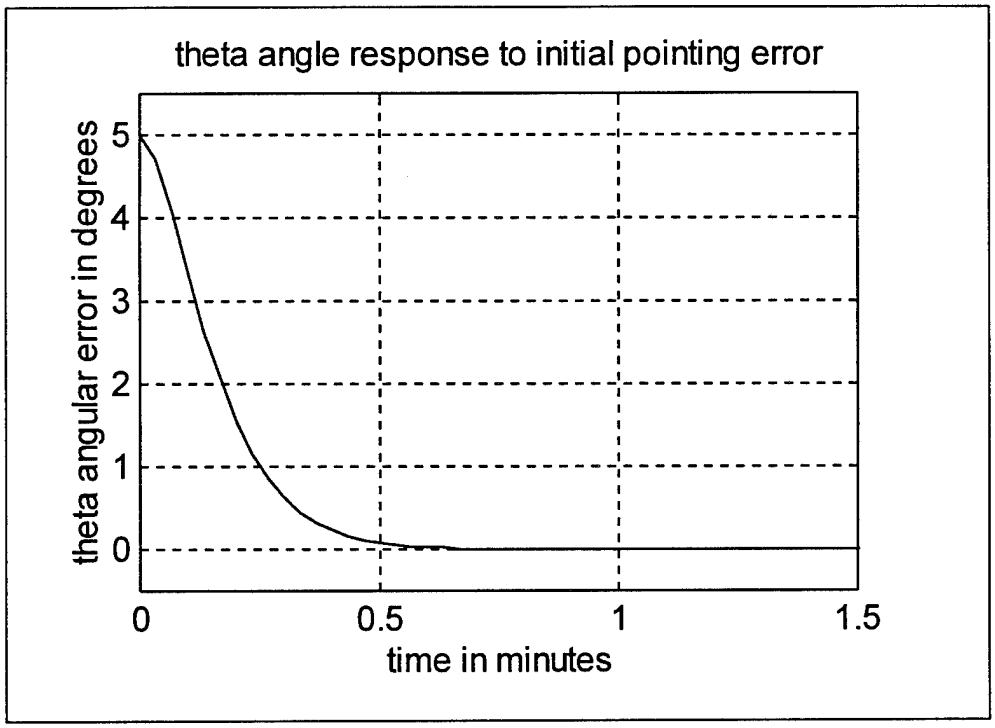

Figure 16. Momentum wheel control response to initial pitch error.

An interesting pitch response occurs when Earth sensor data is unavailable and only magnetometer pitch error is fed back for control. Since pitch rate is no longer available, Equation (67) becomes an undamped oscillator which will grow over time with

pitch disturbance torque input. Fortunately, Earth sensor data is unavailable for only a short period of time, so the pitch response does not grow too large as in Figure 17. If this oscillation becomes a problem for the overall system response, then some rough estimation of pitch rate will need to be generated to provide some damping.

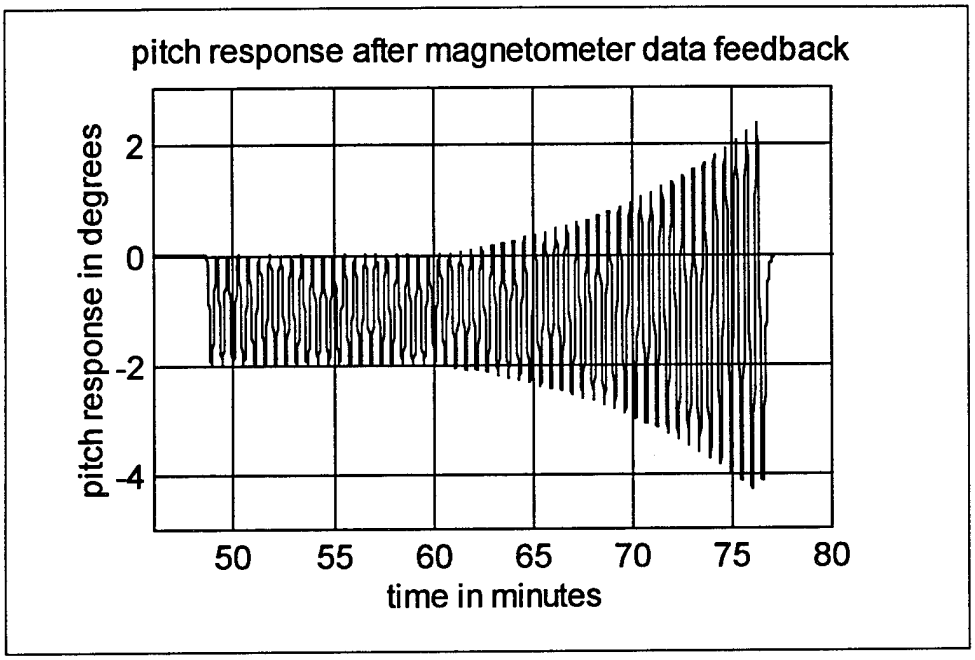

Figure 17. Pitch response with magnetometer pitch angle feedback only

3. Momentum Wheel Desaturation Control

If a secular disturbance torque is experienced about the pitch axis, momentum wheel speed will grow without bound to counteract the disturbance torque [Ref. 8]. Once the momentum wheel's speed has deviated far enough away from its nominal speed (3000 rpm), something must be done to return the wheel to the correct speed. That is the purpose of the momentum wheel desaturation control. The portions of the magnetic control moments for wheel desaturation are given by

$$M_x = -K_u B_z \Delta h$$

$$M_y = 0 \tag{71}$$

$$M_z = K_u B_x \Delta h$$

where Δh is the overall change in the wheel's momentum from its nominal value and K_u is the control gain for desaturation. After the cross product is taken with the magnetic field, the control torques are calculated to be

$$T_x = -K_u B_x B_y \Delta h$$

$$T_y = K_u (B_x^2 + B_z^2) \Delta h \tag{72}$$

$$T_z = -K_u B_y B_z \Delta h$$

Of note, this control law generates the required torque about the y axis for wheel desaturation, but it also creates disturbances about each of the other axes which must be accounted for. Also, the control gain, K_u, must be a negative number. This can be seen by the need for a negative y axis torque if Δh is a positive quantity and vice versa. The control gain K_u is sized to provide torque rod saturation when Δh is ten percent of nominal wheel momentum. This leads to a control gain of $-1.538 \times 10^6 (\text{sec}^{-1} - \text{tesla}^{-2})$.

Momentum wheel desaturation control will be shut off when sun sensor data is unavailable because the control law creates disturbances for the x and z axes which cannot be dissipated while there is no sun sensor data.

4. Control for Transition from Earth-oriented to Sun-oriented Attitude

The control law for sun-oriented control was developed first with the hope that it could be used without modification to accomplish the transition from Earth-oriented/ checkout operations to sun-oriented operations. The orbit configuration will be adjusted in order to vary the Earth to sun angles ϕ_{es} and ψ_{es} and test the control law at several

values of Beta angle. It was not known whether the sun-oriented control law could handle such large angular errors since the control law was based on small angle assumptions).

Reorientation simulations were only performed for a 1:30 orbit and a 3:00 orbit. It was assumed that if the reorientation worked for these initial conditions, then it would work for the 4:30 and 6:00 orbit because the transition angles will be smaller and disturbance torques will be smaller due to the lower Earth to sun angular values.

Figure 18 displays the results of a reorientation simulation from an initial sun pointing error of approximately 72 degrees. This constitutes a reorientation for a 1:30 am/pm orbit with average Beta angle of 18 degrees. It takes several orbits to perform the reorientation as expected. Figure 19 shows a reorientation simulation for a 3:00 am/pm orbit. The raised dotted lines at the bottom of the plots represent the time periods when the satellite is not in eclipse. If the value of the dotted line is one, then roll/yaw attitude sensing data is available. The eclipse control also serves to cut off momentum wheel dumping control when the satellite is in eclipse.

5. Sun-oriented Attitude Control

The pitch axis control torque will be generated as discussed in the momentum wheel and wheel desaturation control sections. The magnetic moment equations are given as

$$M_x = -K_u B_z \Delta h$$

$$M_y = K_1 B_x \phi + K_2 (B_z \dot{\phi} - B_x \dot{\psi}) + K_3 B_z \psi \qquad (73)$$

$$M_z = K_u B_x \Delta h$$

where K_1 and K_3 are used for precession control, while K_2 is used to control nutation. Reference 10 used the control law

$$M_y = K_1 B_x \phi + K_2 \dot{B}_y \tag{74}$$

For small angles, since no measurement for yaw existed; $\dot{B}_y$ can be approximated by

$$\dot{B}_y = (B_z \dot{\phi} - B_x \dot{\psi}) - \omega_o (\frac{\psi B_z}{2} + 2\phi B_x) \tag{75}$$

In the orbital reference frame, B_y is constant for an Earth-pointing satellite. For a sun-pointing satellite, it is not constant, so the control law from Reference 10 should not be used. Instead, the y axis torque rod control moment is selected as the second equation of Equation (73), which is quite similar to Reference 10. The additional $K_3 B_x \psi$ term has been added because there is a yaw error measurement which is not available when using a horizon sensor, which is the standard sensor for Earth-pointing satellites.

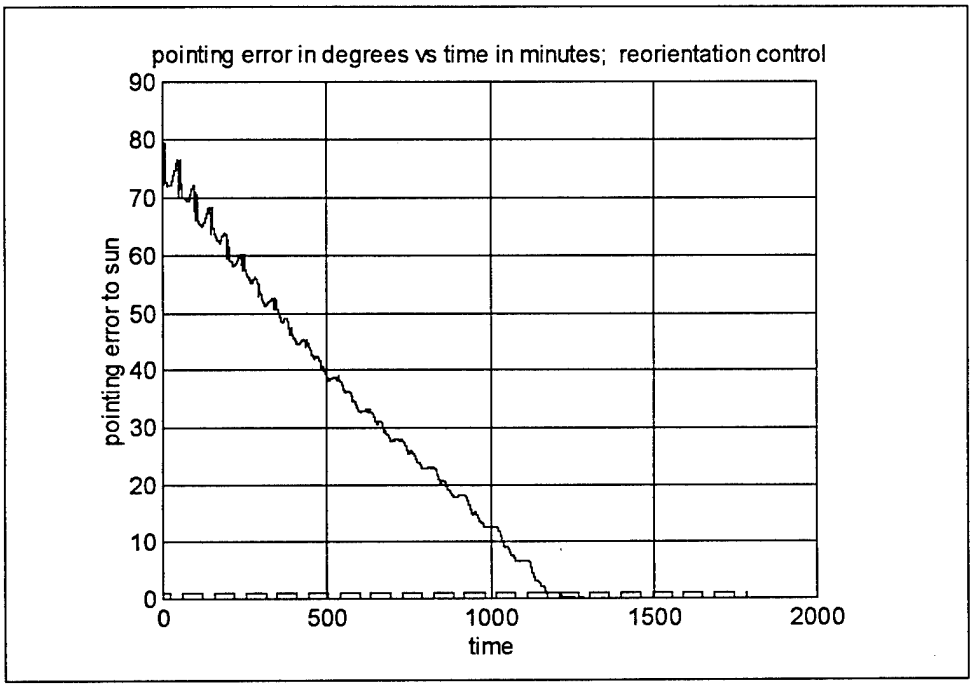

Figure 18. Earth to sun reorientation (1:30 orbit)

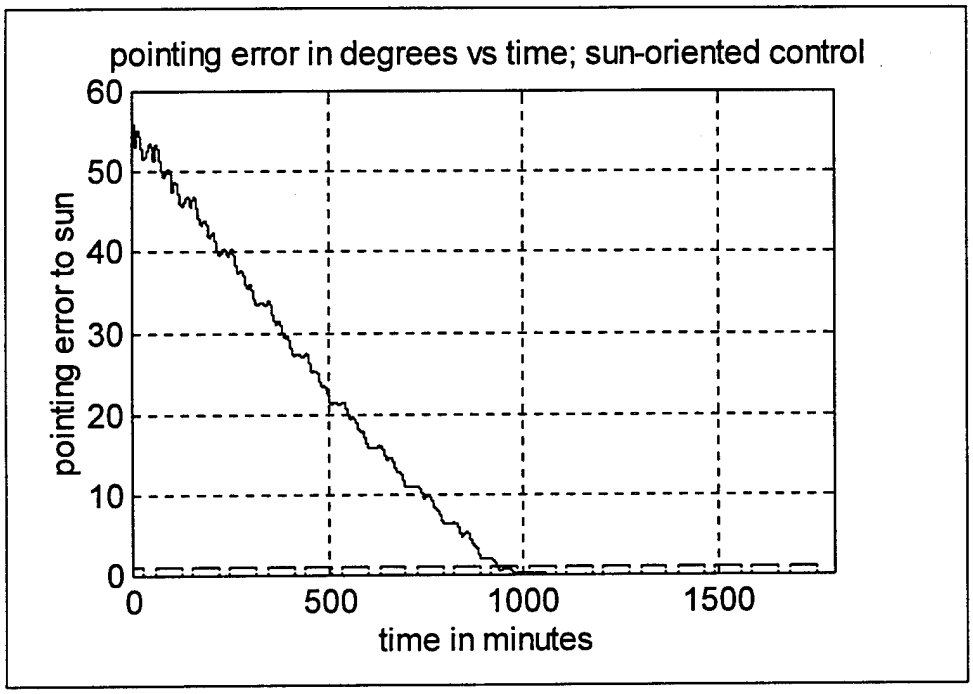

Figure 19. Earth to sun reorientation (3:00 orbit)

When the **M** x **B** cross product is performed the following control torques are generated

$$T_x = K_1 B_x B_z \phi + K_2 (B_z^2 \dot{\phi} - B_x B_z \dot{\psi}) + K_3 B_z^2 \psi - K_u B_x B_y \Delta h$$

$$T_y = K_u (B_x^2 + B_z^2) \Delta h \tag{76}$$

$$T_z = -K_1 B_x^2 \phi - K_2 (B_x B_z \dot{\phi} - B_x^2 \dot{\psi}) - K_3 B_x B_z \psi - K_u B_y B_z \Delta h$$

When these control torques are substituted into Equation (57) above, the total torque equations become

$$\begin{aligned} T_{dx} = I_{xx} \ddot{\phi} - K_2 B_z^2 \dot{\phi} - [(I_{xx} - I_{yy} + I_{zz}) \omega_{on} + h - K_2 B_x B_z] \dot{\psi} + K_u B_x B_z \Delta h \\ + [(I_{yy} - I_{zz}) \omega_{on}^2 + h \omega_{on} - K_1 B_x B_z] \phi - [I_{xx} \dot{\omega}_{on} + K_3 B_z^2] \psi \end{aligned}$$

$$T_{dy} = I_{yy} \ddot{\theta} + K_\theta \tau_\theta \dot{\theta} + K_\theta \theta - K_u (B_x^2 + B_z^2) \Delta h - I_{yy} \dot{\omega}_{on} \tag{77}$$

$$T_{dz} = I_{zz}\ddot{\psi} + [(I_{zz} - I_{yy} + I_{xx})\omega_{on} - h + K_2 B_x B_z]\dot{\phi} - K_2 B_x^2 \dot{\psi} + K_u B_y B_z \Delta h$$
$$+[I_{zz}\dot{\omega}_{on} + K_1 B_x^2]\phi + [(I_{yy} - I_{xx})\omega_{on}^2 + h\omega_{on} + K_3 B_x B_z]\psi$$

Figures 20 and 21 show the reason for selecting the control laws as listed. In Figure 20, a positive ϕ error is shown which requires a change in momentum in the positive z direction. This can be generated by the ($-K_1 B_x^2\ \phi$) portion of the z axis magnetic torque in Equation (76). If K_1 is selected as a negative number, this generates a positive torque as required to achieve the desired change in momentum. Figure 21 shows what happens when there is a negative ψ error. This error requires a change in momentum in the positive x direction which is generated by the ($K_3 B_z^2\ \psi$) portion of the x axis control law in Equation (76). Of note, the portions of the x and z axes control laws which contain $B_x B_z$ create disturbance torques about their respective axis. However, over the course of one orbit, these disturbances should average out to zero. This averaging could be precluded by the effects of eclipse which would cut off attitude data for a portion of the orbit.

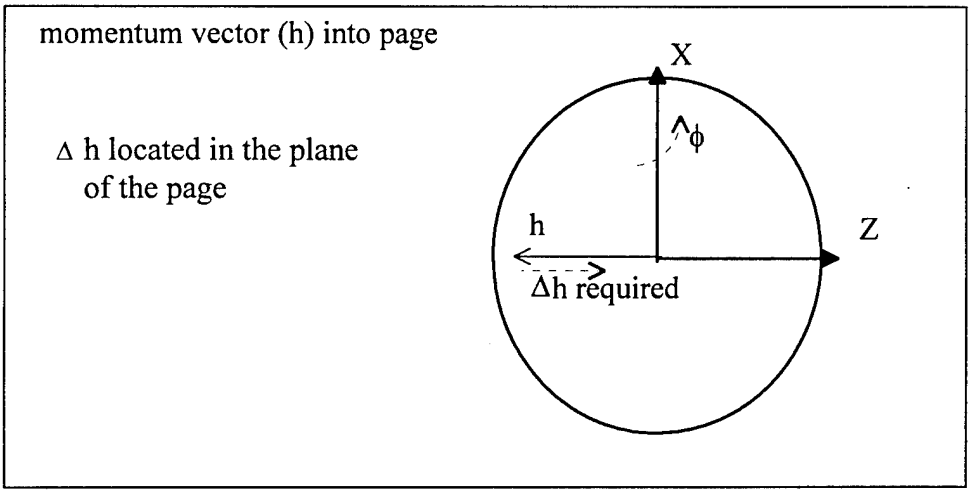

Figure 20. Generation of required control torques; z axis

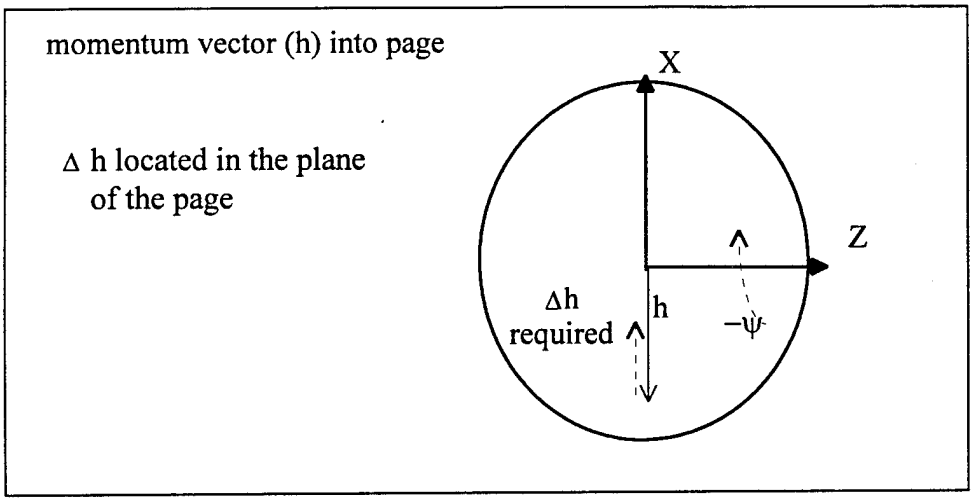

Figure 21. Generation of required control torques; x axis

The roll and yaw equations can be expressed in matrix form as

$$\begin{bmatrix} T_{dx} - K_u B_x B_z \Delta h \\ T_{dz} - K_u B_y B_z \Delta h \end{bmatrix} = \begin{bmatrix} A & C \\ B & D \end{bmatrix} \begin{bmatrix} \phi(s) \\ \psi(s) \end{bmatrix} \tag{78}$$

where

$$A = I_{xx}s^2 - K_2 B_z^2 s + [(I_{yy} - I_{zz})\omega_{on}^2 + h\omega_{on} - K_1 B_x B_z]$$

$$B = [(I_{zz} - I_{yy} + I_{xx})\omega_{on} - h + K_2 B_x B_z]s + [I_{zz}\dot{\omega}_{on} + K_1 B_x^2] \tag{79}$$

$$C = -[(I_{xx} - I_{yy} + I_{zz})\omega_{on} + h - K_2 B_x B_z]s - [I_{xx}\dot{\omega}_{on} + K_3 B_z^2]$$

$$D = I_{zz}s^2 - K_2 B_x^2 s + [(I_{yy} - I_{xx})\omega_{on}^2 + h\omega_{on} + K_3 B_x B_z]$$

Using methods introduced in Reference 10, the nutation and orbital time constants of the system can be estimated by

$$\tau_n = \frac{4hI_{xx}I_{zz}}{B_o^2[(4I_{xx}+I_{zz})hK_2 - I_{xx}I_{zz}(4K_3+K_1)]}$$

$$\tau_{01} = \frac{4h\omega_0}{\pi B_o^2(K_1+10K_3)} \qquad (80)$$

$$\tau_{02} = \frac{4h\omega_0}{3\pi B_o^2(K_1+2K_3)}$$

where B_o is M/R^3 of Equation (26) and the time constants are expressed in orbits. The values of K_1 and K_3 were selected to saturate the torque rods for an angular error of one degree. This leads to a selection of the control gains as

$$\begin{aligned} K_1 &= -9.555 \times 10^7 \text{ Amp-m}^2\text{/Tesla} \\ K_2 &= -4.777 \times 10^8 \text{ Amp-m}^2\text{-sec/Tesla} \\ K_3 &= -2.389 \times 10^7 \text{ Amp-m}^2\text{/Tesla} \end{aligned} \qquad (81)$$

which results in time constant values of

$$\begin{aligned} \tau_n &= 13.711 \text{ seconds} \\ \tau_1 &= 6.848 \text{ minutes} \\ \tau_2 &= 5.326 \text{ minutes} \end{aligned} \qquad (82)$$

These time constants only apply under conditions of no torque rod saturation and continuous control (i.e. no eclipse shut off of attitude sensing data). Since the gains are sized to create torque rod saturation above one degree pointing error, the simulated time constants will be slightly longer. Of note, K_1 AND K_3 are destabilizing for nutation. This can be managed by ensuring that the following relationship is satisfied

$$(4K_3+K_1) < [(4I_{xx}+I_{zz})hK_2]/I_{xx}I_{zz} \qquad (83)$$

Figures 22 and 23 show simulation results which can be used to estimate system time constants. Figure 22 shows nutation and Figure 23 shows the orbital time constants.

Using these figures to estimate the time constants yields a nutation time constant of approximately 21 seconds, and an orbital time constant of approximately 6.5 minutes. These estimations are close to the calculated values.

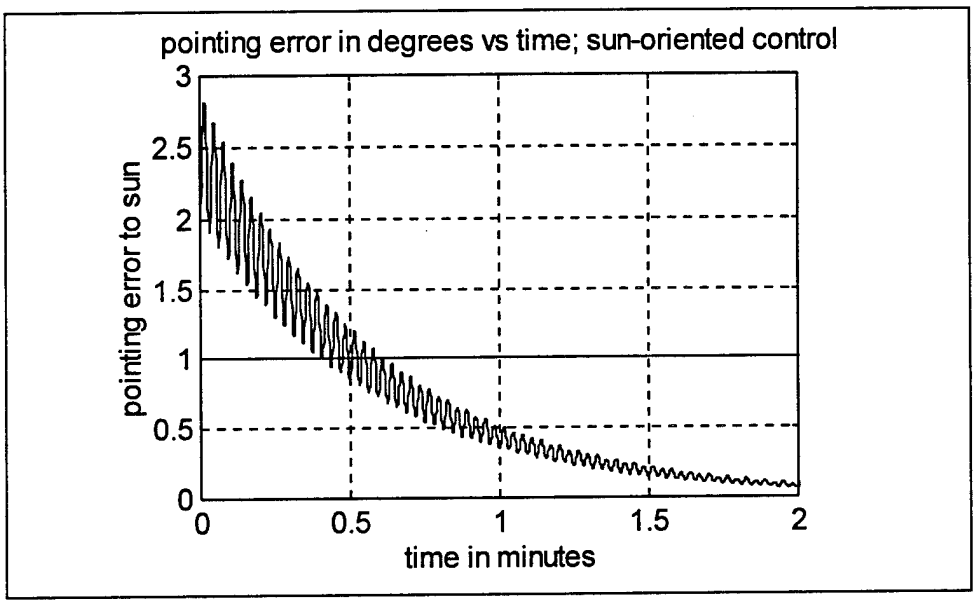

Figure 22. Nutation time constant response

Figures 24 through 34 show simulation results for sun-oriented control in different orbit configurations (1:30, 3:00, 4:30 and 6:00 orbits). Figures 24 through 27 do not include sensor noise inputs or cross product of inertia effects. Figures 28 through 31 do include these effects with a sensor noise gain of 0.07 degrees which is much higher than those typically found in commercial sensors. Figure 28 and Figures 32 through 34 include results for a 1:30 orbit with noise and cross product of inertias at different Earth positions around the sun. Figure 28 simulates Summer Solstice, Figure 32 simulates Vernal Equinox, Figure 33 simulates Autumnal Equinox, and Figure 34 simulates Winter Solstice. All eleven simulations use the following initial conditions

ϕ_0 = 1 degree	$\omega_{x0} = 0.00075$	radians / second	
θ_0 = 2 degree	$\omega_{y0} = \omega_{on0}$	radians / second	(see Equation (53))
$\psi_0 = -0.5$ degree	$\omega_{z0} = -0.00003$	radians / second	

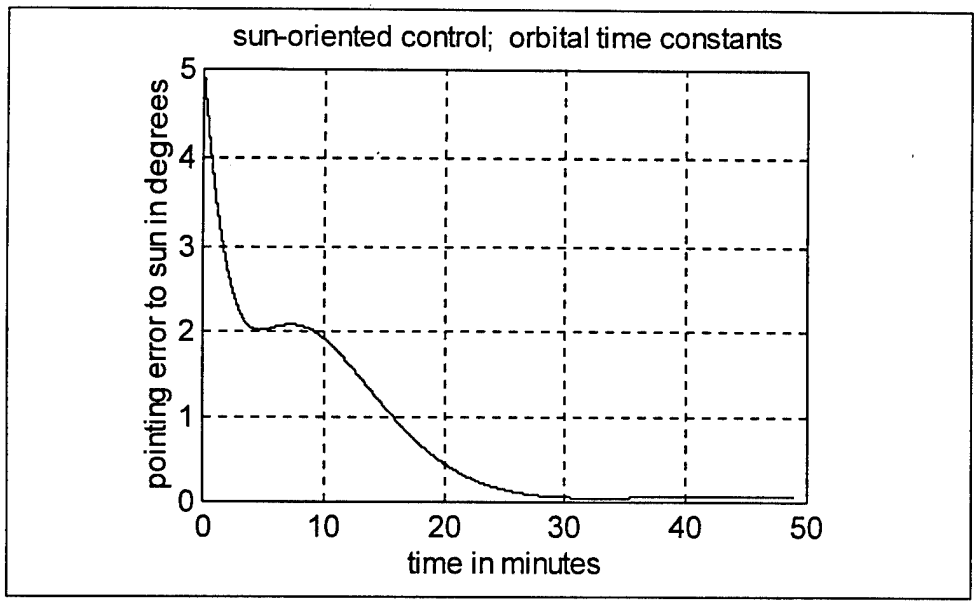

Figure 23. Orbital time constant response

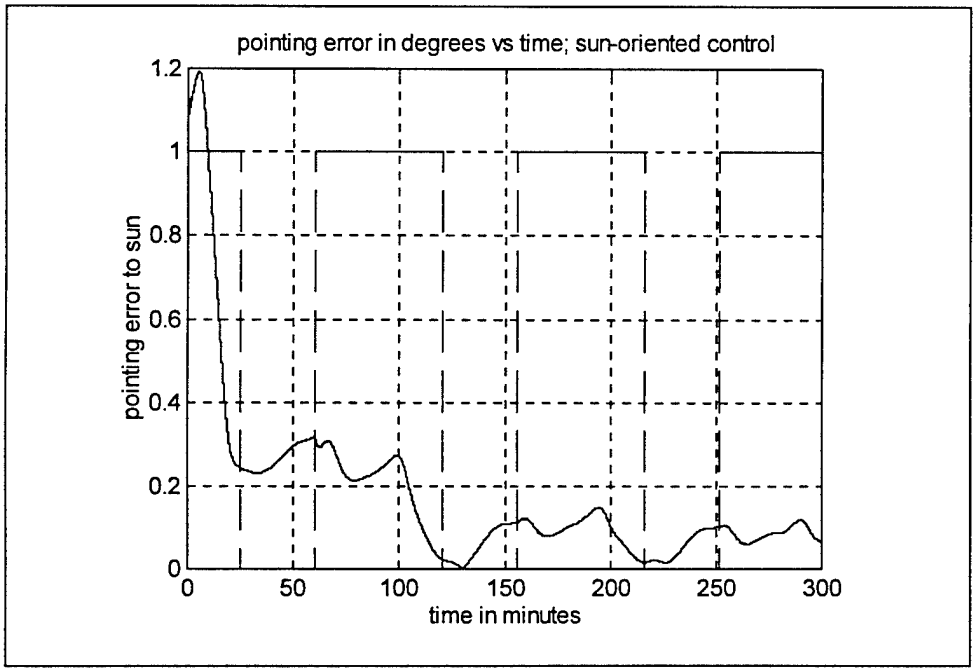

Figure 24. Sun oriented control; 1:30 orbit; no noise input

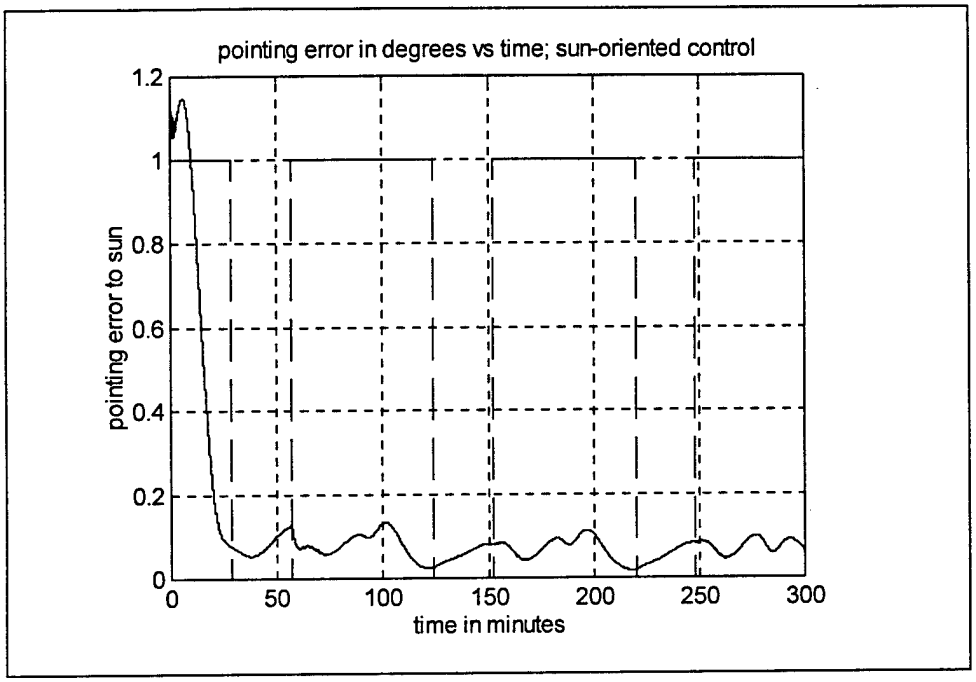

Figure 25. Sun oriented control; 3:00 orbit; no noise input

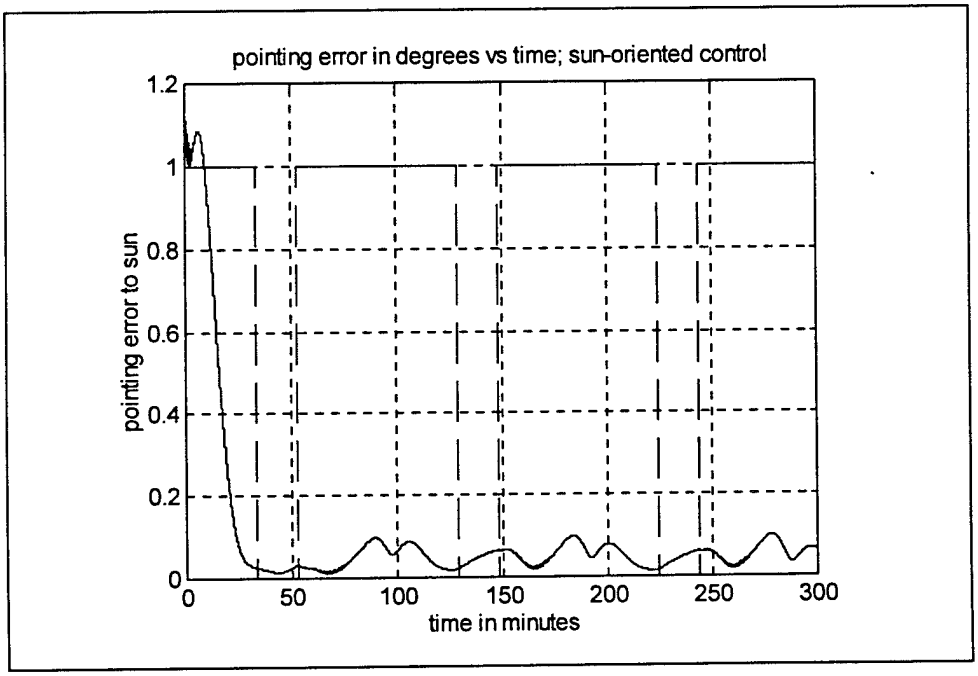

Figure 26. Sun oriented control; 4:30 orbit; no noise input

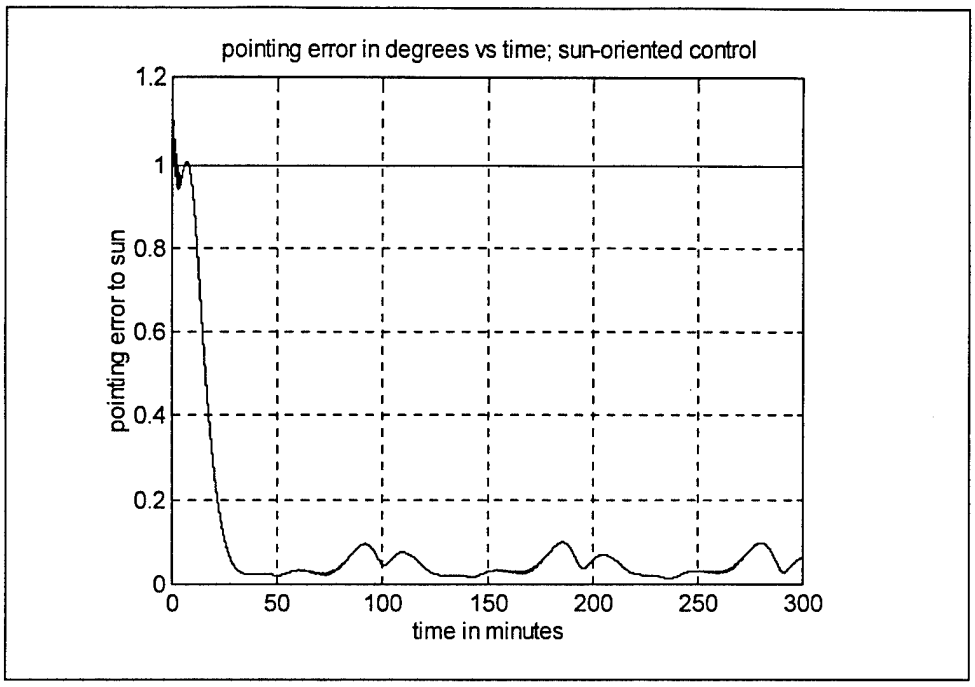

Figure 27. Sun oriented control; 6:00 orbit; no noise input

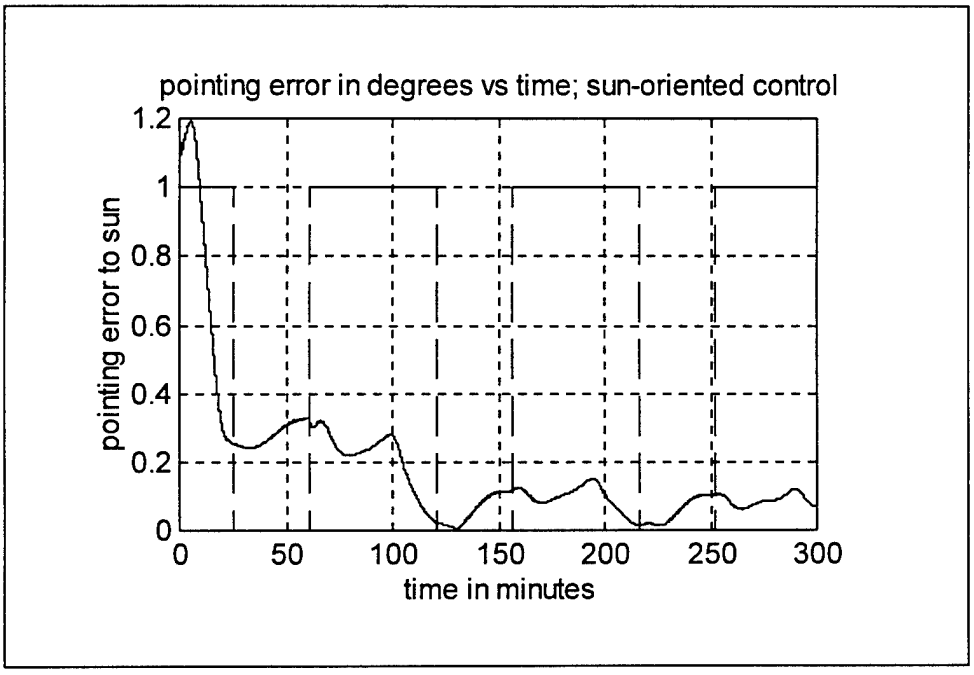

Figure 28. Sun oriented control; 1:30 orbit; with noise input

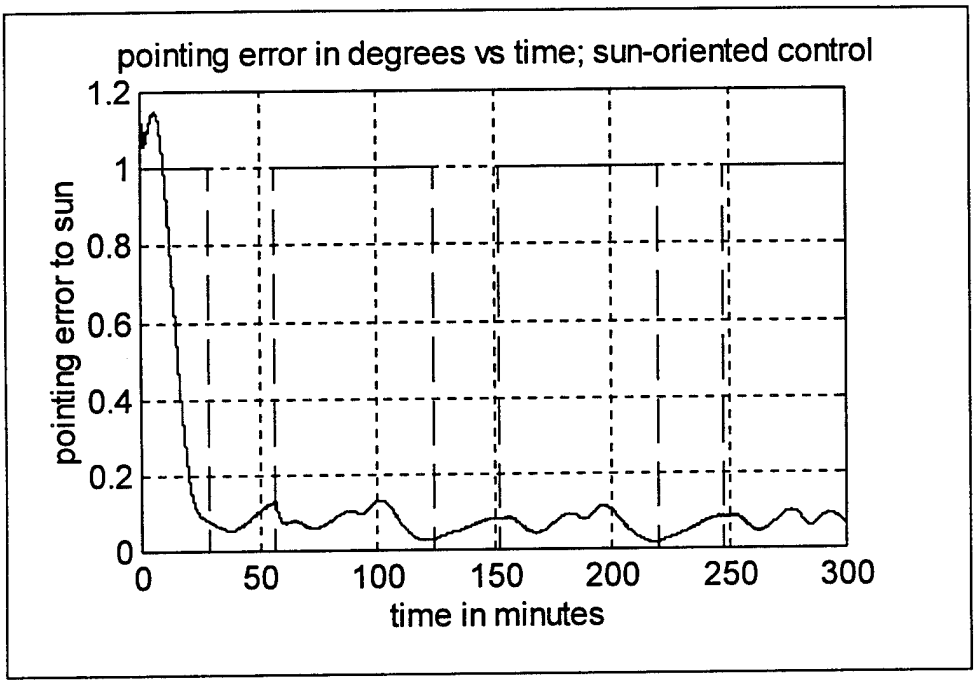

Figure 29. Sun oriented control; 3:00 orbit; with noise input

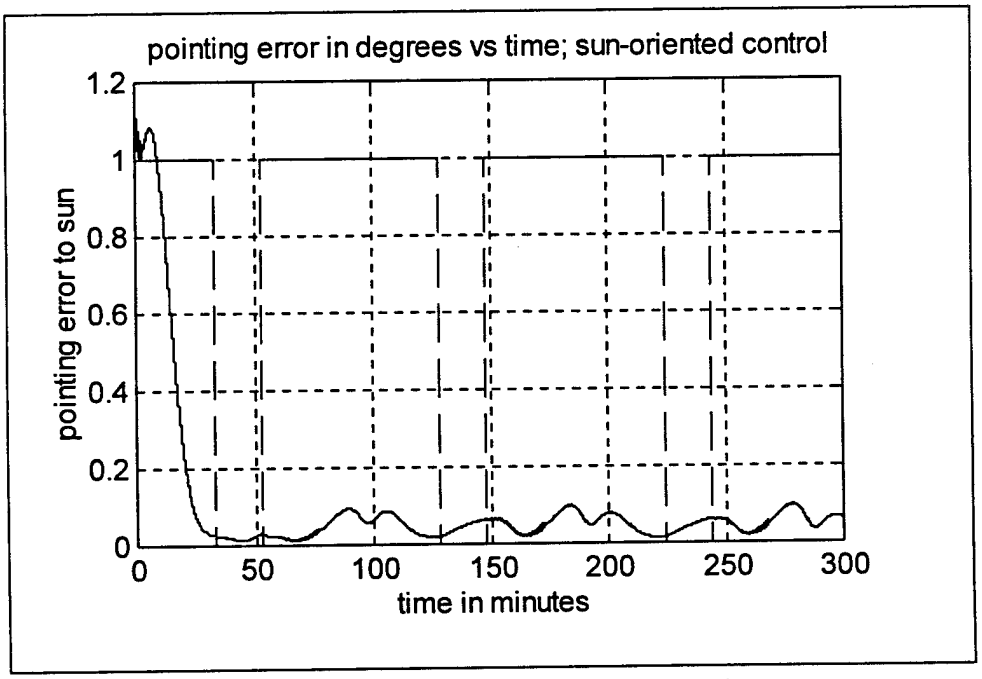

Figure 30. Sun oriented control; 4:30 orbit; with noise input

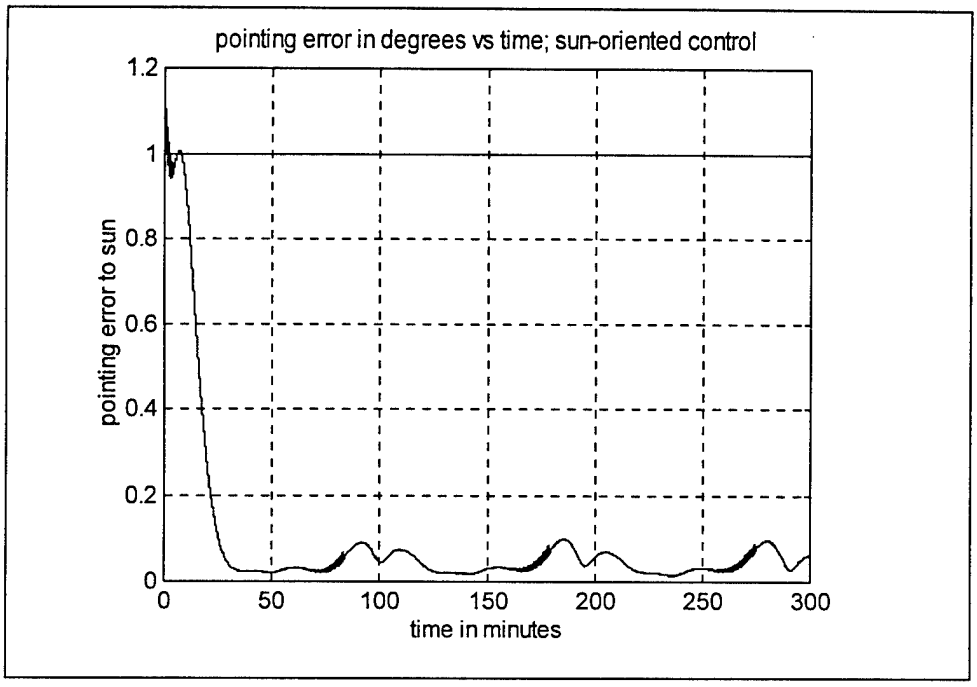

Figure 31. Sun oriented control; 6:00 orbit; with noise input

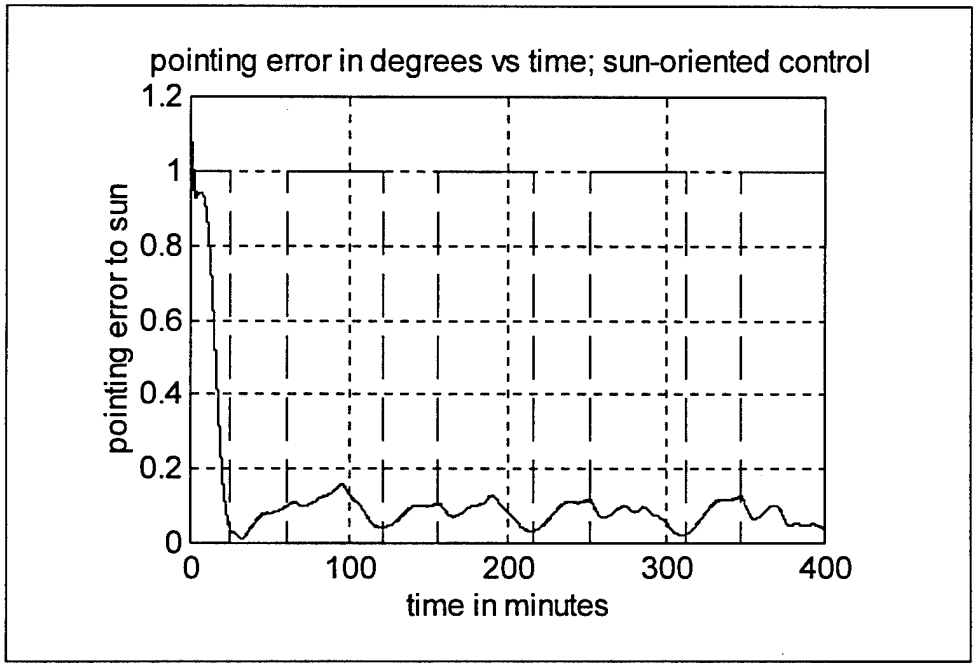

Figure 32. Sun oriented control; with noise input. Vernal Equinox

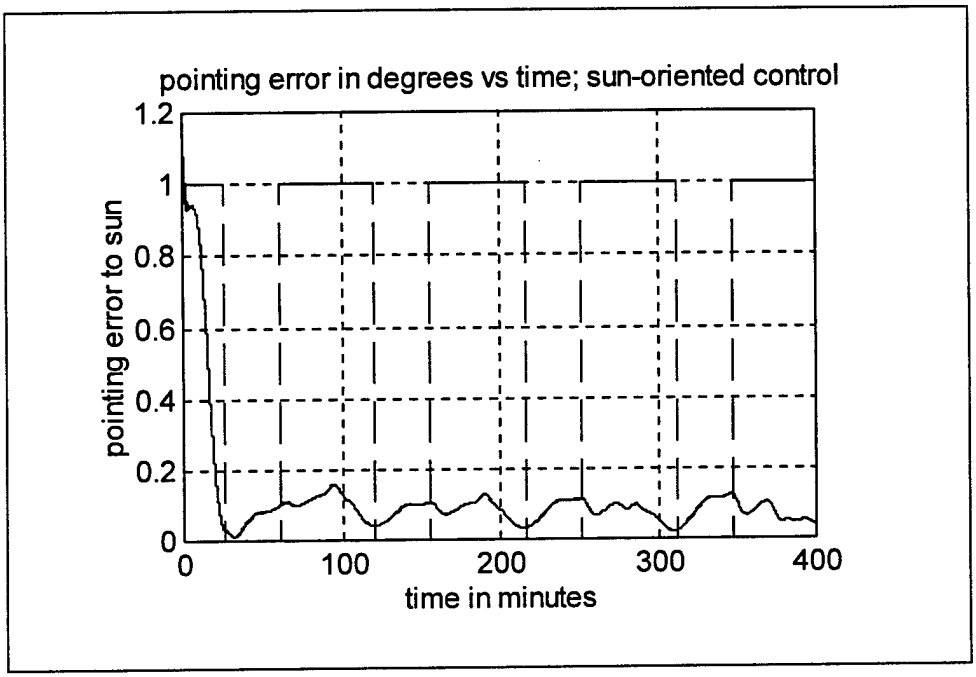

Figure 33. Sun oriented control; with noise input. Autumnal Equinox

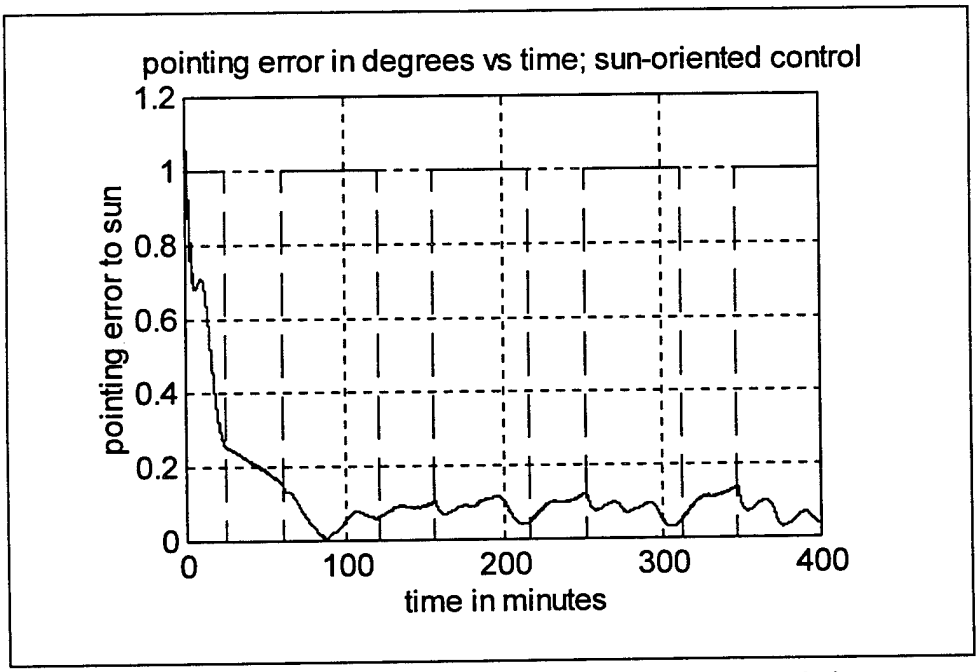

Figure 34. Sun oriented control; with noise input. Winter Solstice

V. CONCLUSIONS AND RECOMMENDATIONS

A. CONCLUSIONS

Equations of motion for a sun-oriented inertial reference frame were developed. Transformation to a body-oriented reference frame was accomplished using a 3-1-2 Euler axis rotation sequence with small angle approximations.

Magnetic attitude control laws for roll and yaw control were developed by modifying control laws which have been used in the past for Earth-oriented operation. Pitch control was accomplished by varying momentum wheel speed using a proportional / derivative feedback controller. The Earth-orientation control laws work well for this sun-oriented control application.

Simulations were performed to test capture control of the satellite once it is separated from the launch vehicle. The satellite was separated wtih and without the momentum wheel being spun up to nominal operating speed to test system performance. The control law is capable of removing all rotational kinetic energy and aligning the momentum vector along the orbit normal. The possibility exists for the momentum vector to be aligned away from the sun (180 degree misdirection) when the satellite is separated before the momentum wheel is spun up.

Reorientation from Earth-oriented / system check-out operations to a sun-oriented mode was performed using the same magnetic attitude control law as used for the sun-oriented roll and yaw control. The control law does not break down for low Beta angle orbit applications.

Sun-oriented control maintains a pointing accuracy better than 0.2 degrees for the worst case, 1:30 orbit configuration. Given this, momentum wheel size could probably be cut in half to maintain the desired pointing accuracy within 0.5 degrees. This would reduce weight and cost while also reducing reorientation times from the Earth-oriented to the sun-oriented mode. A second Earth sensor is not required to maintain pointing accuracy during eclipse in the current configuration.

Noise and cross product of inertia inputs do not have a noticeable affect on pointing accuracy output.

B. RECOMMENDATIONS

Future study could be done which implements a Kalman Filter for noise attenuation in the sensors. The filter could also be used to estimate pitch rate from magnetometer data when Earth sensor data is unavailable. This would avoid the undamped oscillations experienced without pitch rate feedback.

Study could be performed using a 6:00 orbit (continuous sun sensor input) without a momentum bias to test the ability of the torque rods to control the spacecraft by themselves. Torque rod size could also be modified to see how small the torque rods can be before they are unable to control the satellite.

The current SIMULINK program could be modified in order to speed up simulation times by removing several of the function blocks and constructing "hard wired" representations.

APPENDIX: SIMULATION BLOCKS AND MATLAB CODE

MATLAB/SIMULINK block diagrams are included here for the program used to simulate all satellite control sequences. Computer code for MATLAB control programs are also listed. The main SIMULINK program block is shown in Figure A1. The beta angle and Earth to Sun angle gernorater block creates beta angle and Earth to sun angles in accordance with Chapter II equations. The B-field block generates the Earth's magnetic dipole field in Earth-oriented orbital coordinates. This field is then transformed to body coordinates by performing the two coordinate transformations; 3-axis orbit to sun frame and 3-axis sun to body frame. The magnetometer block acts as the magnetic field sensor and time derivative estimator for the rate of change of the magnetic field with respect to the spacecraft body. These outputs are then fed to the Magnetic torque rod control along with change in wheel momentum (Δh), spacecraft attitude and spacecraft attitude rate. Magnetic moments are then created and fed to the torque rod block where saturation limiting is performed. The saturation limited magnetic moments are then used by the cross product block M x B to calculate magnetic control torque which is the cross product between the magnetic moments and the magnetic field expressed in body coordinates. These torques along with the disturbance torques are sent to a torque summer which feeds the overall external torque input to the spacecraft dynamics block where the body rotational rates (body rates) are calculated. The momentum from the momentum wheel is also input here to satisfy the equations of Chapter IV. The body rates are then input to the kinematics section to calculate the Euler angle rates which are integrated to form the Euler angles ϕ, θ and ψ. The attitude sensor block passes through attitude information with sensor noise input when sensor data is available. At all other times, is passes an error signal of zero to simulate the loss of attitude sensing information. Individual output blocks for each variable to be plotted are included to pass data to the MALAB workspace for subsequent processing. Each individual block is displayed on the following pages.

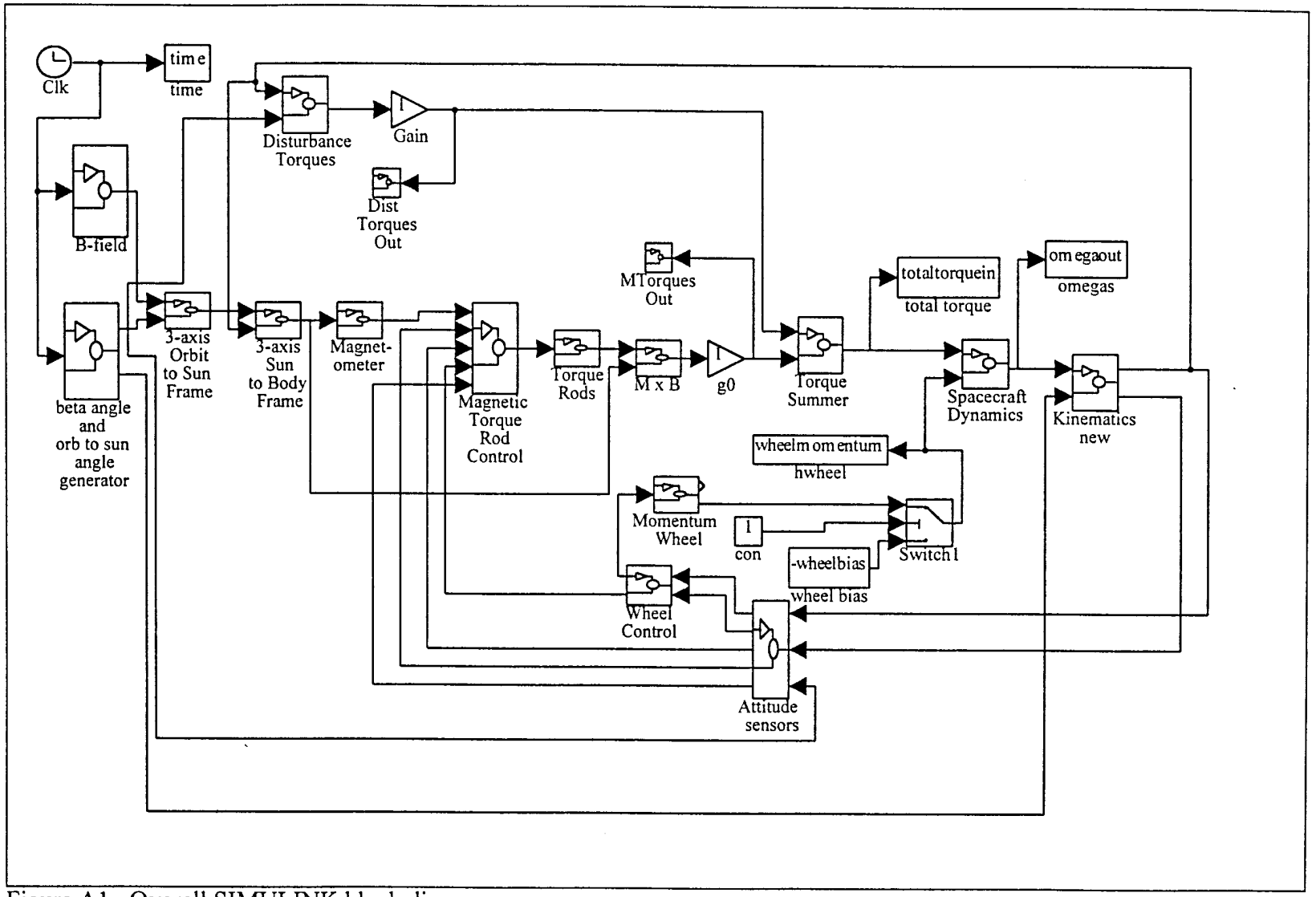

Figure A1. Overall SIMULINK block diagram

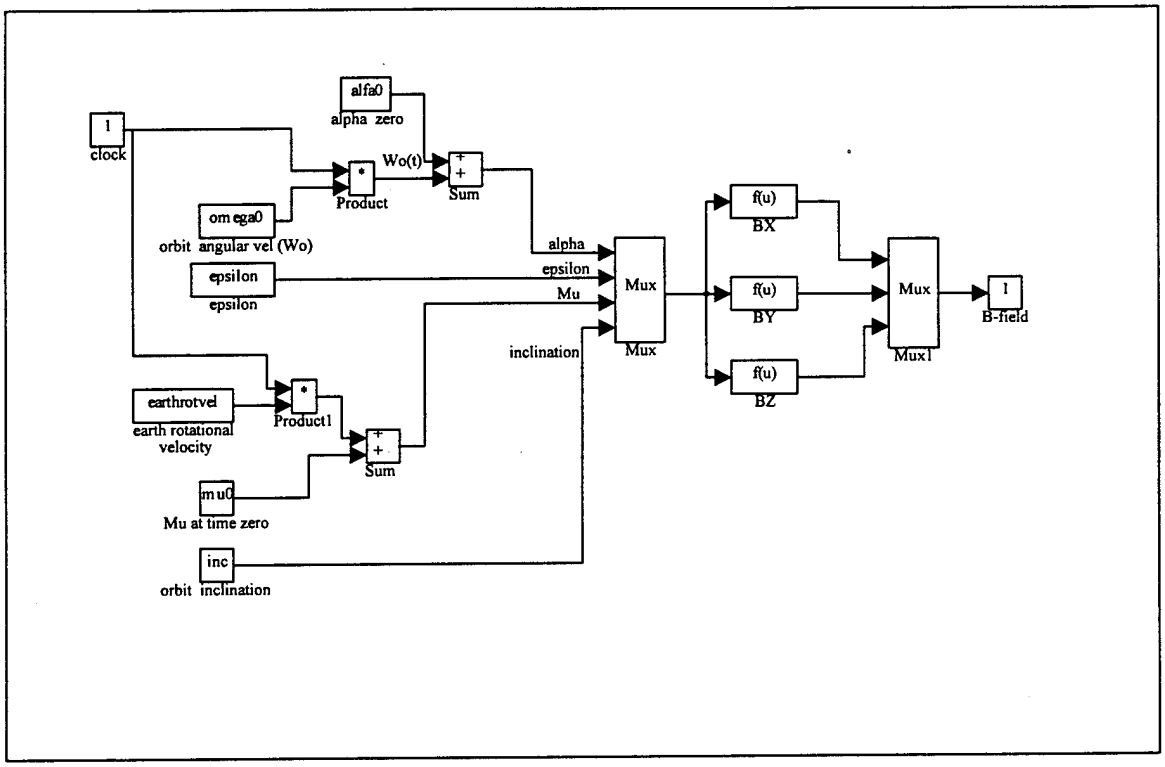

Figure A2. Earth's magnetic field in Earth-oriented coordinates

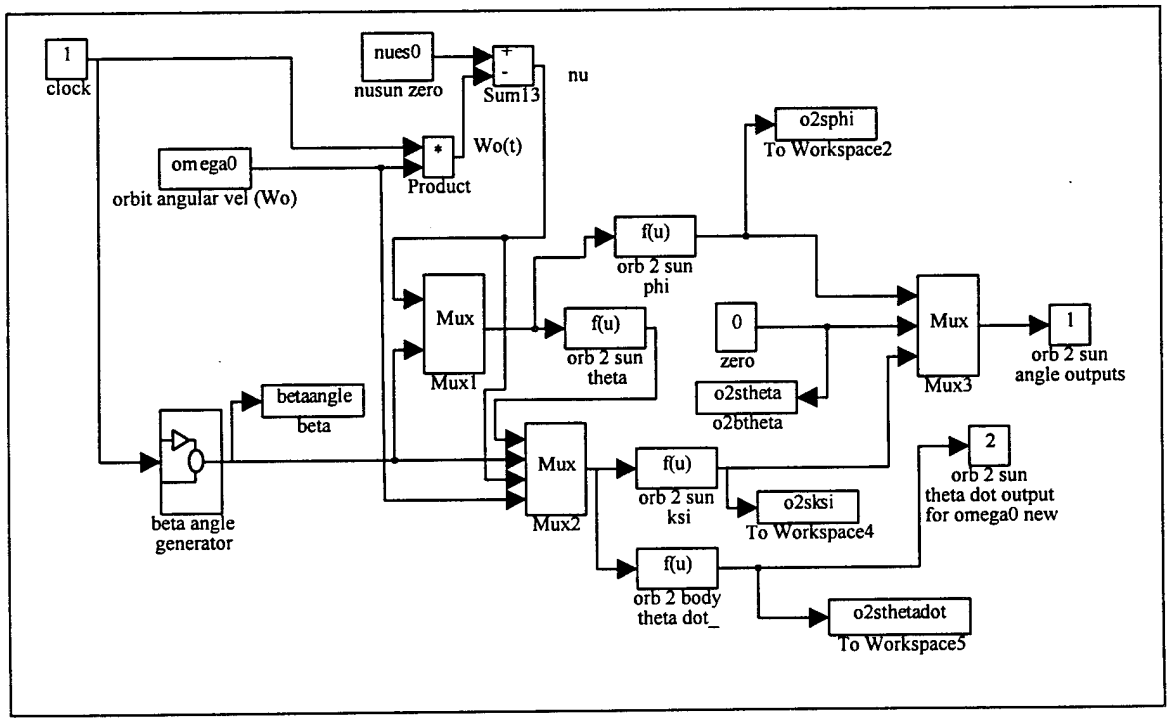

Figure A3. Beta and Earth to sun angle generation

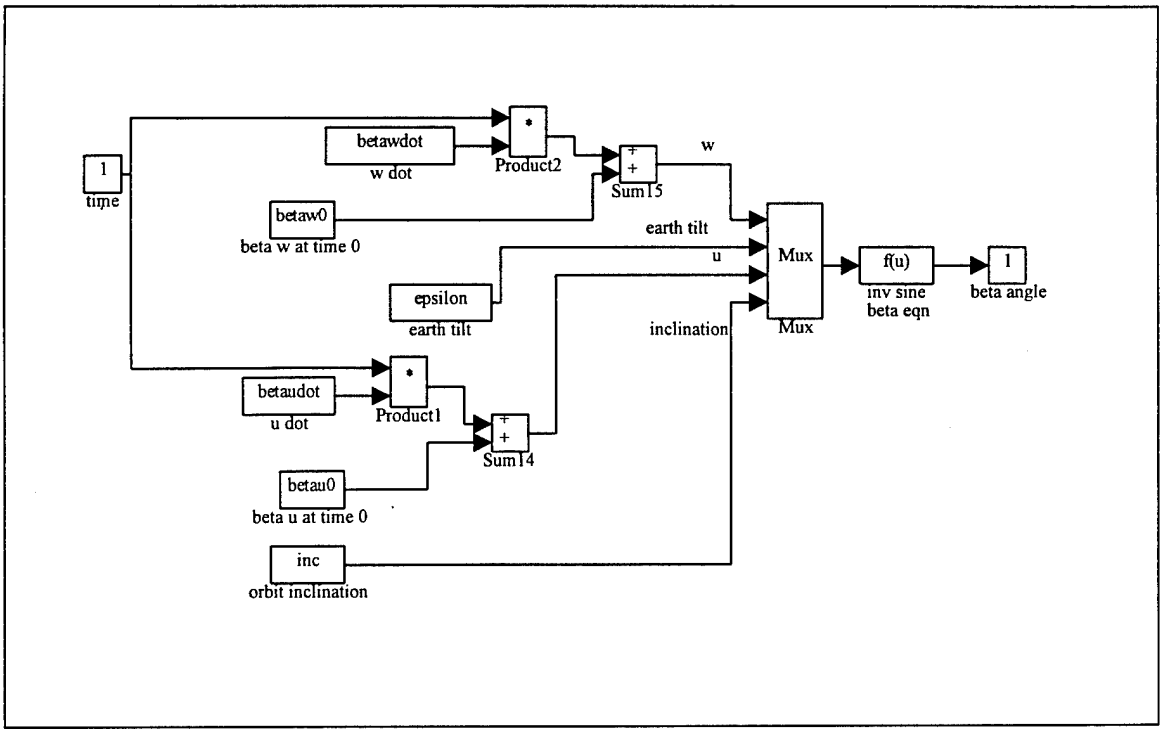

Figure A4. Beta angle generation

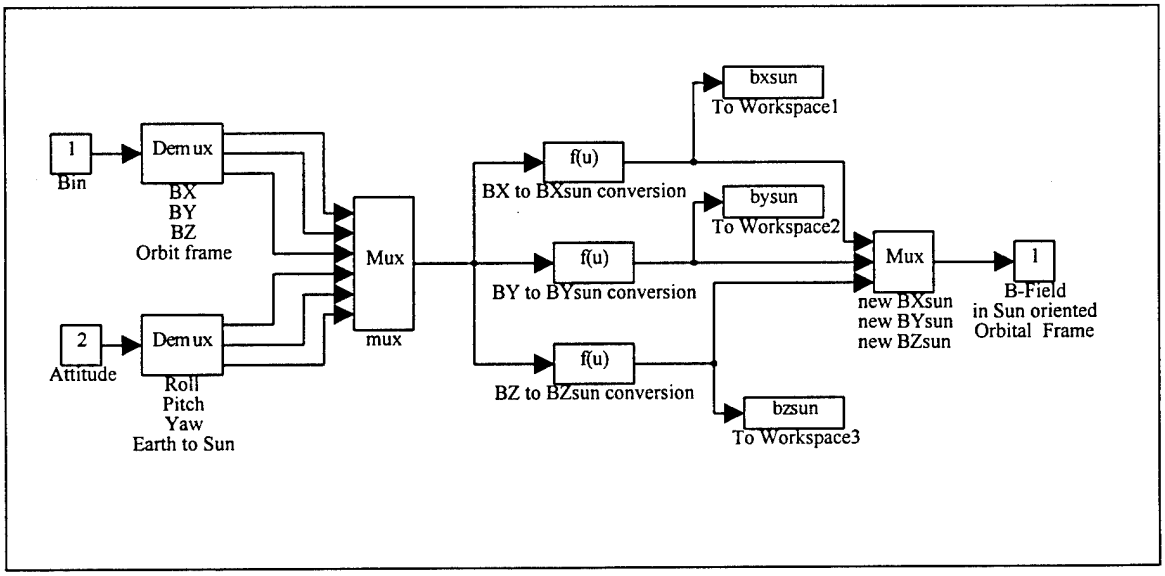

Figure A5. Coordinate transformation from Earth orientation to Sun orientation

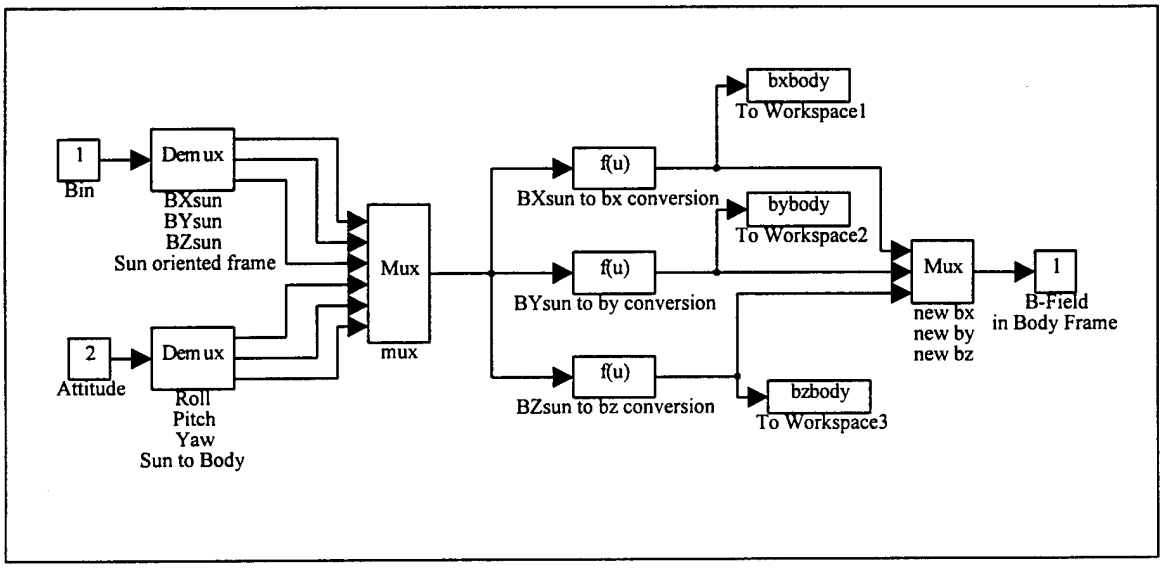

Figure A6. Coordinate transformation from Sun orientation to body orientation

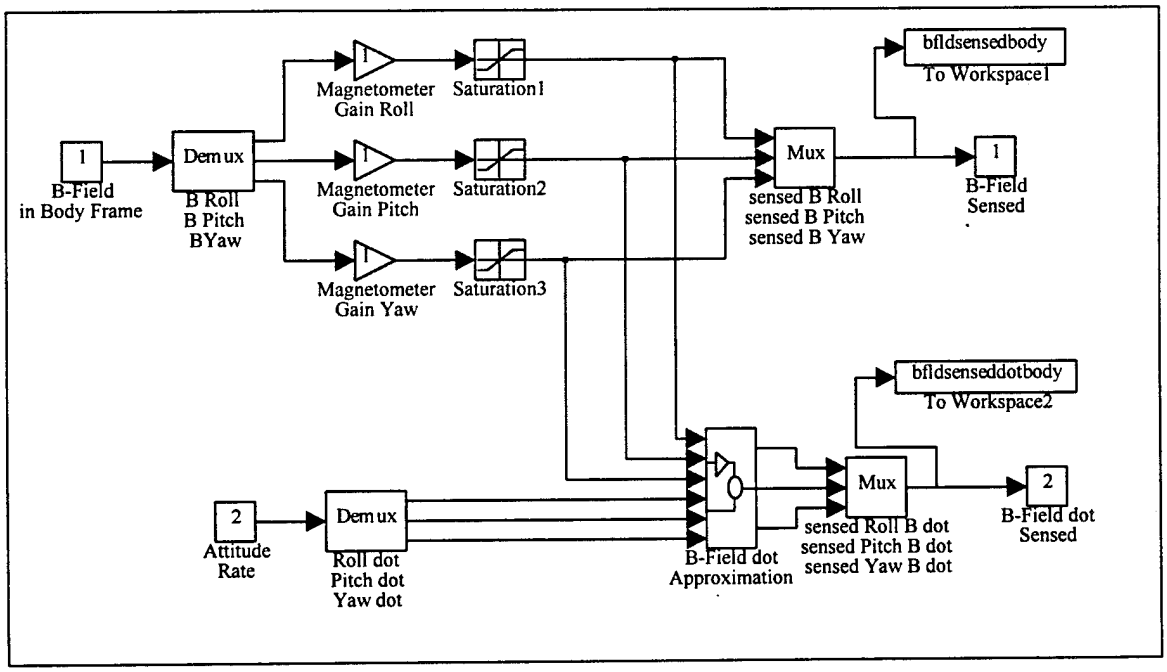

Figure A7. Magnetometer sensor

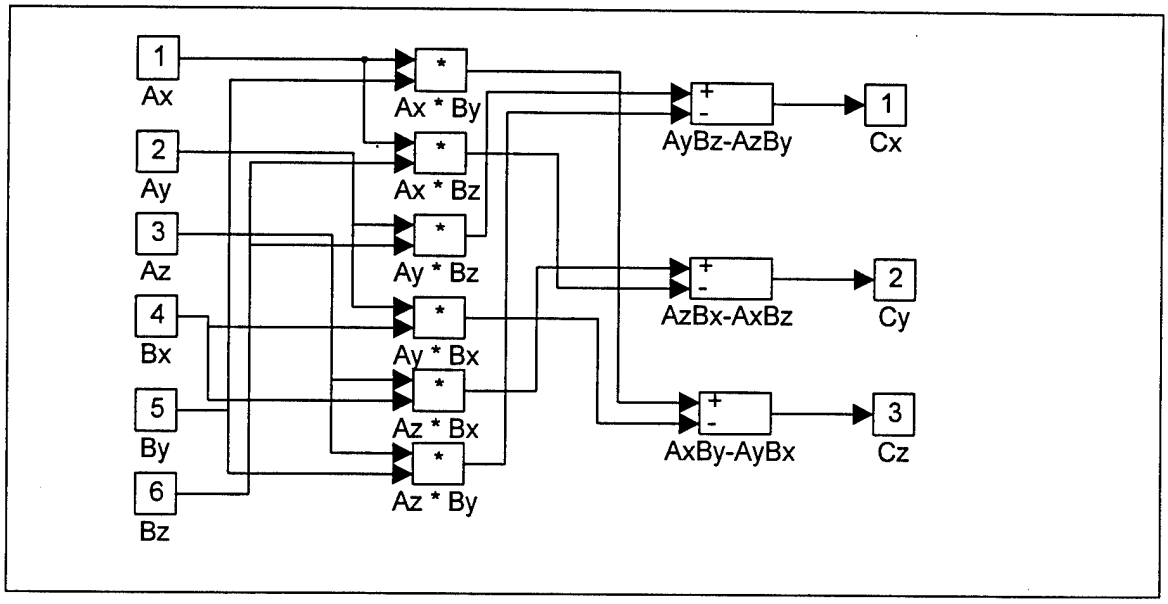

Figure A8. Magnetic field derivative approximation by cross product with Euler rates

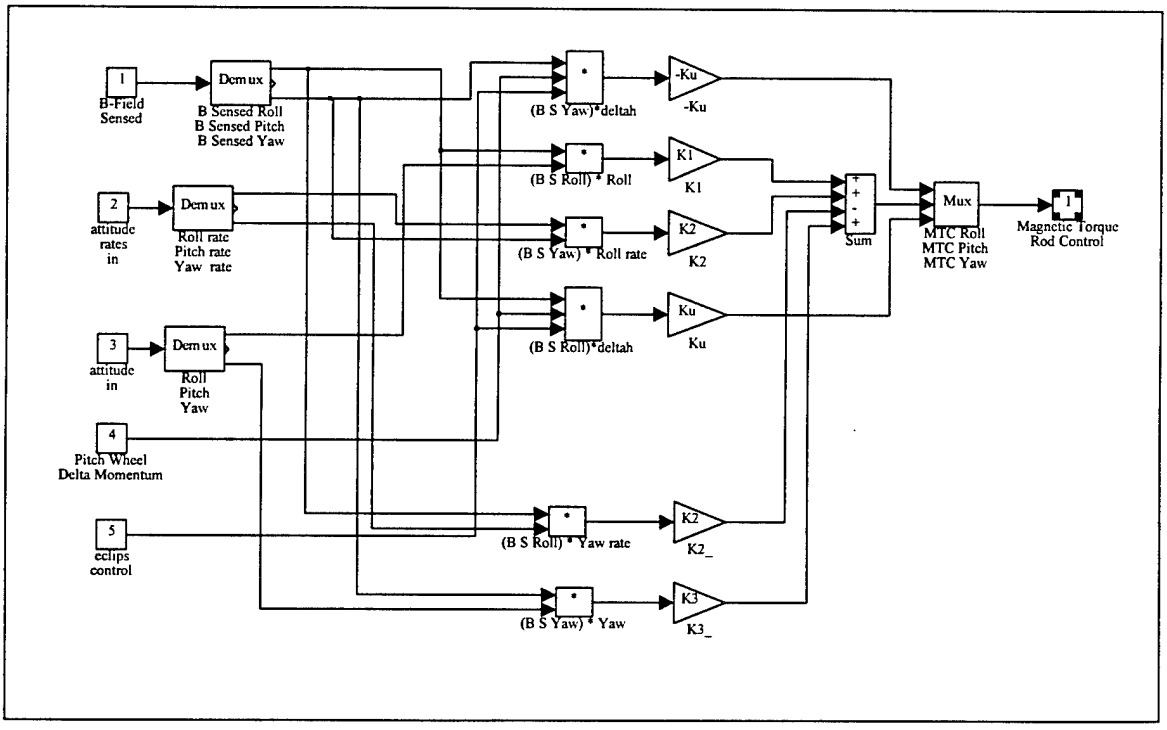

Figure A9. Sun-oriented magnetic torque rod control

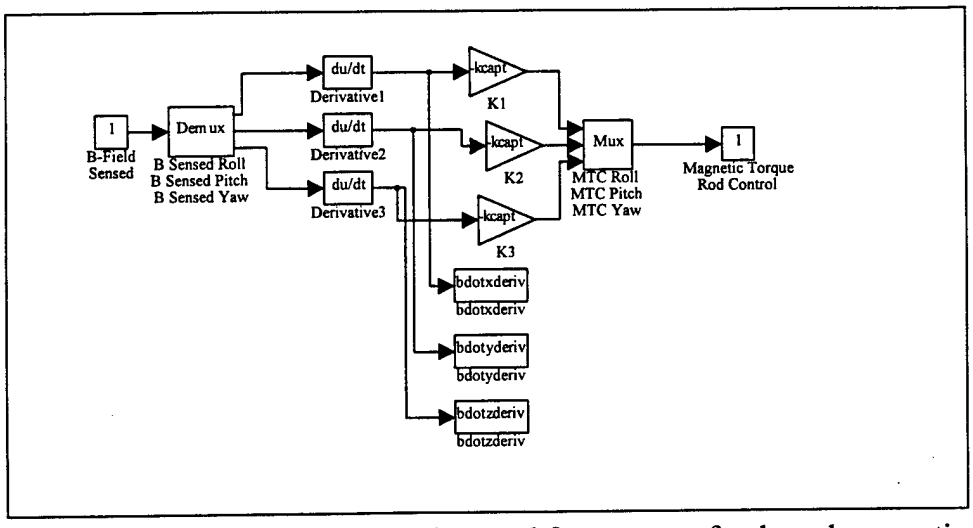

Figure A10. Magnetic torque rod control for capture after launch separation

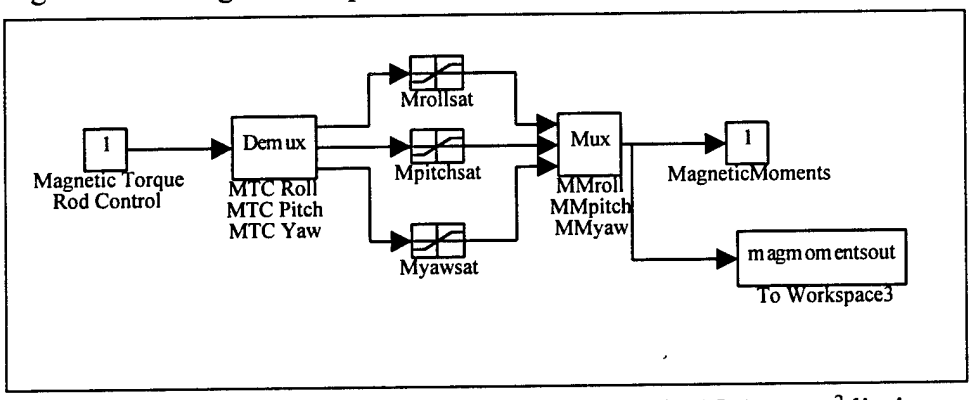

Figure A11. Magnetic torque rod saturation control. 15 Amp-m^2 limit.

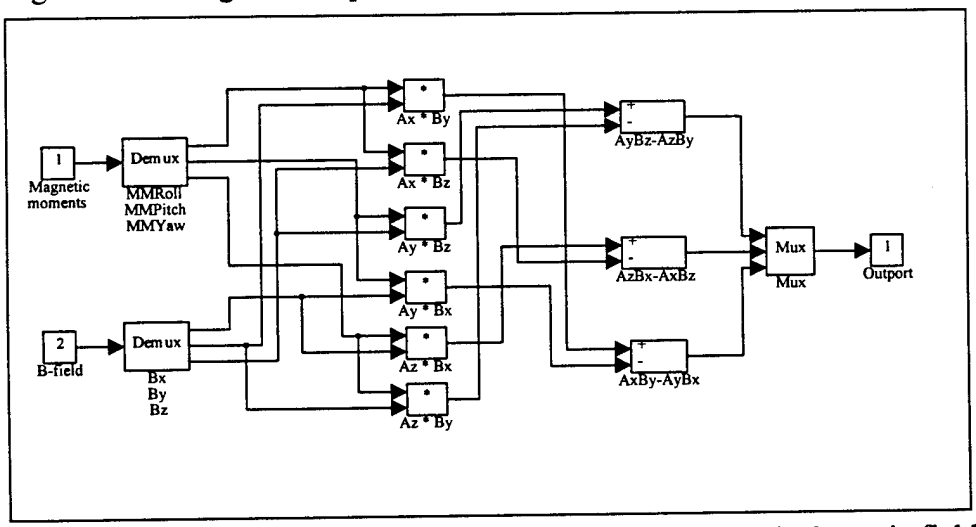

Figure A12. Cross product between Magnetic moments and Magnetic field

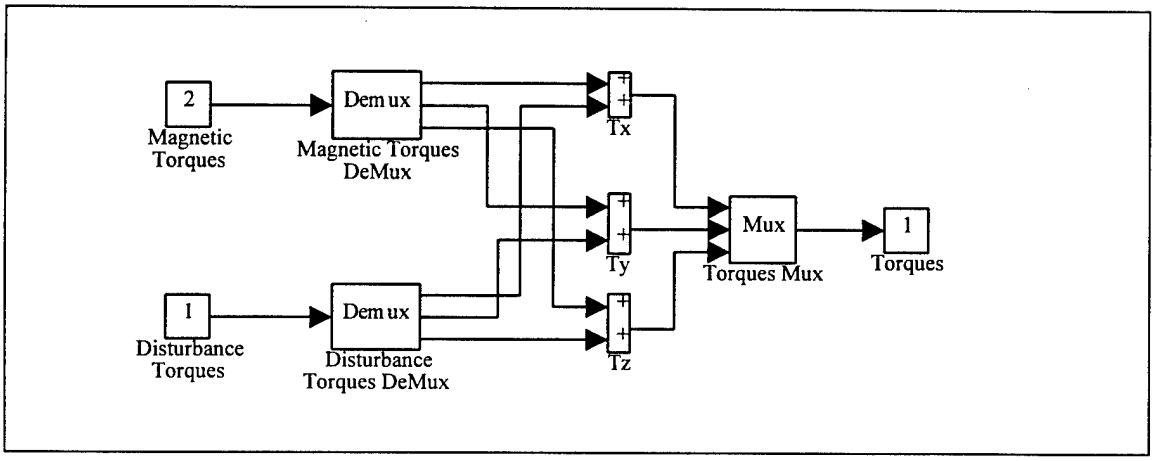

Figure A13. Torque summer

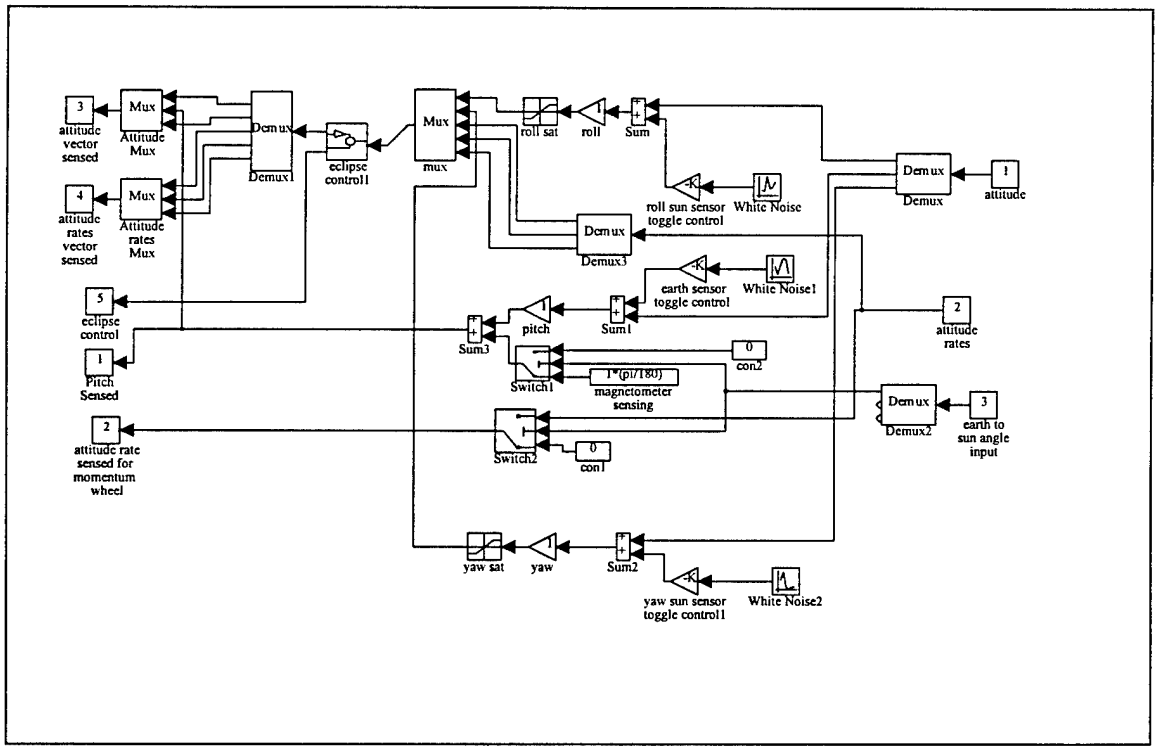

Figure A14. Attitude sensors. Earth and Sun sensors with noise input

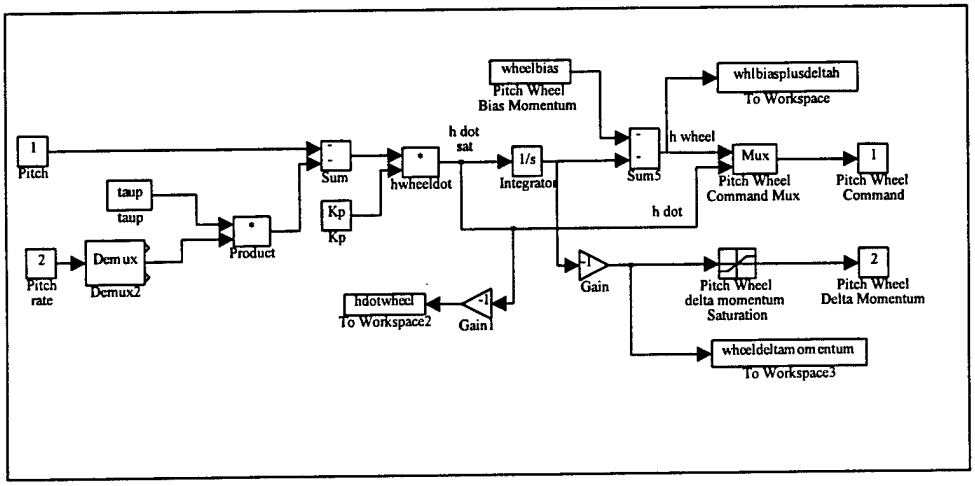

Figure A15. Momentum wheel control

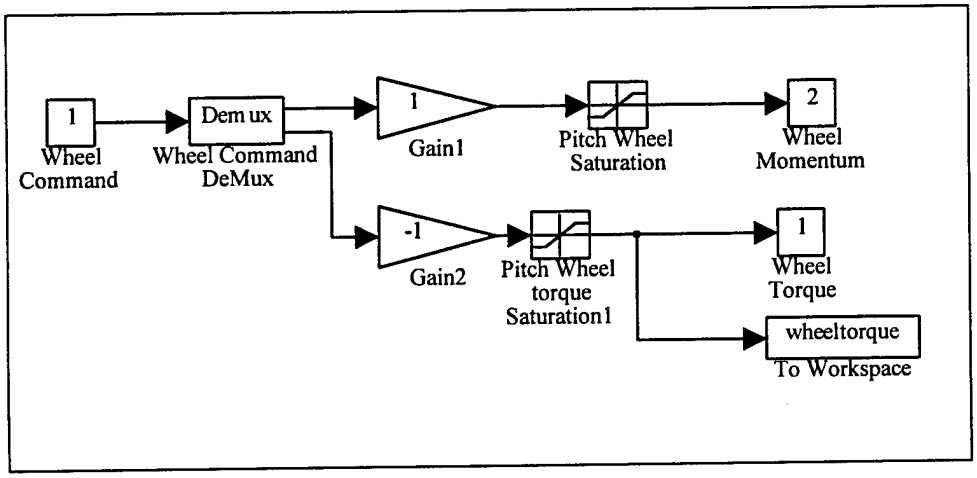

Figure A16. Momentum wheel saturation controls

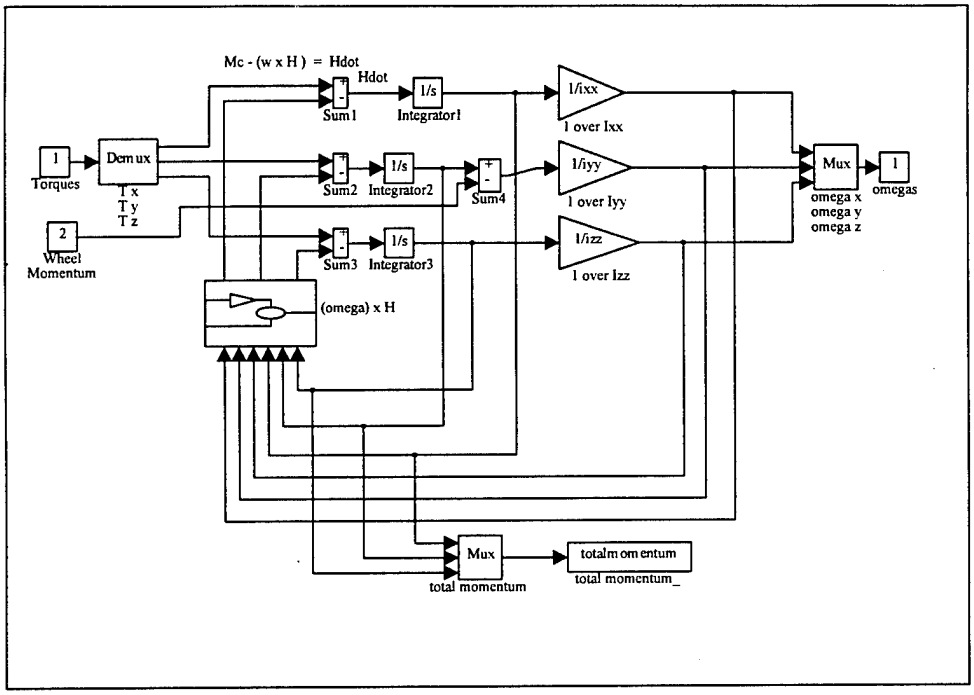

Figure A17. Spacecraft Dynamics

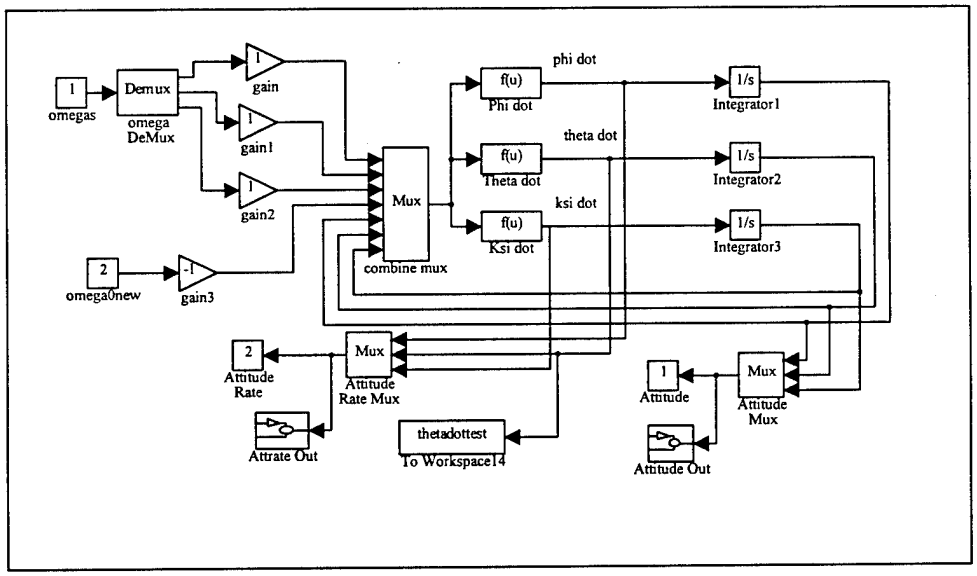

Figure A18. Spacecraft Kinematics

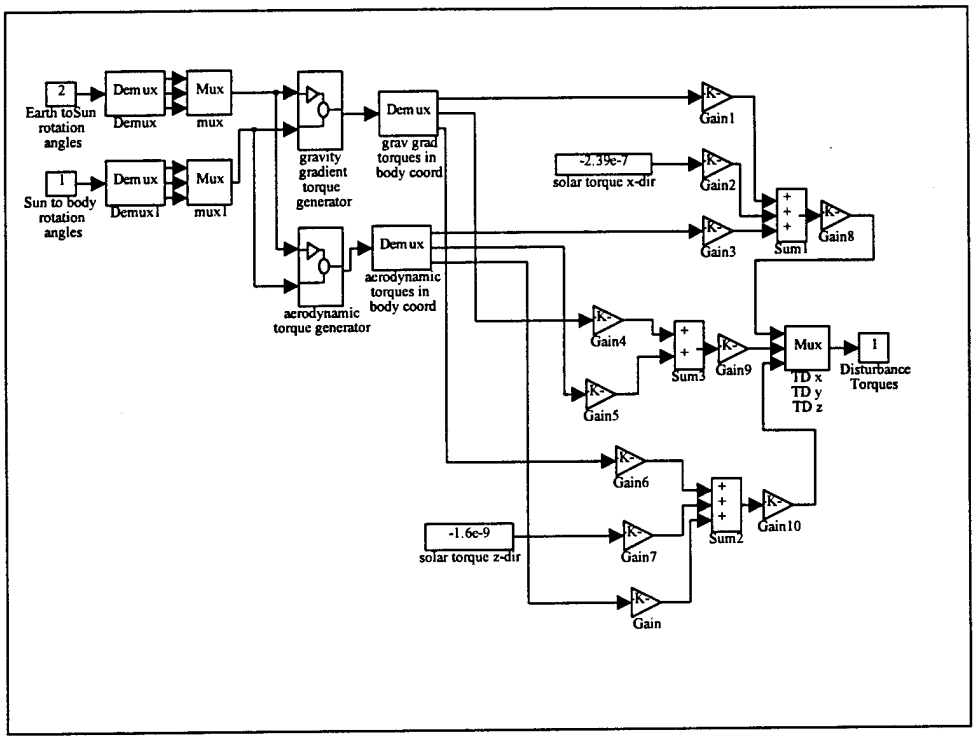

Figure A19. Disturbance torque generation

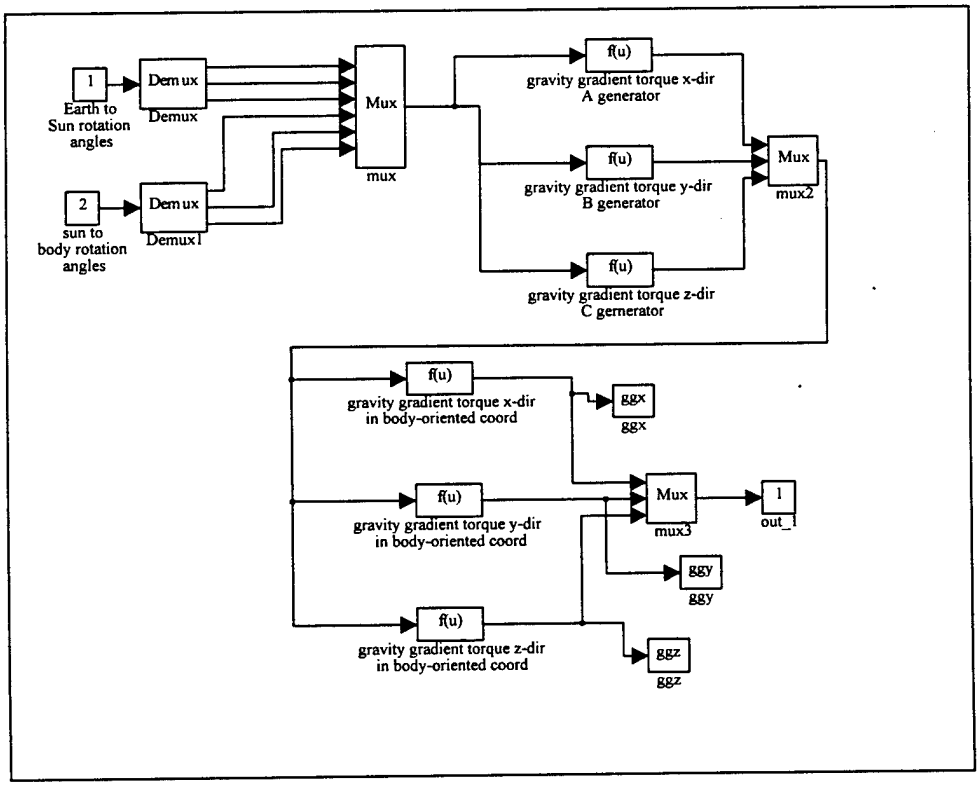

Figure A20. Gravity gradient torque generator

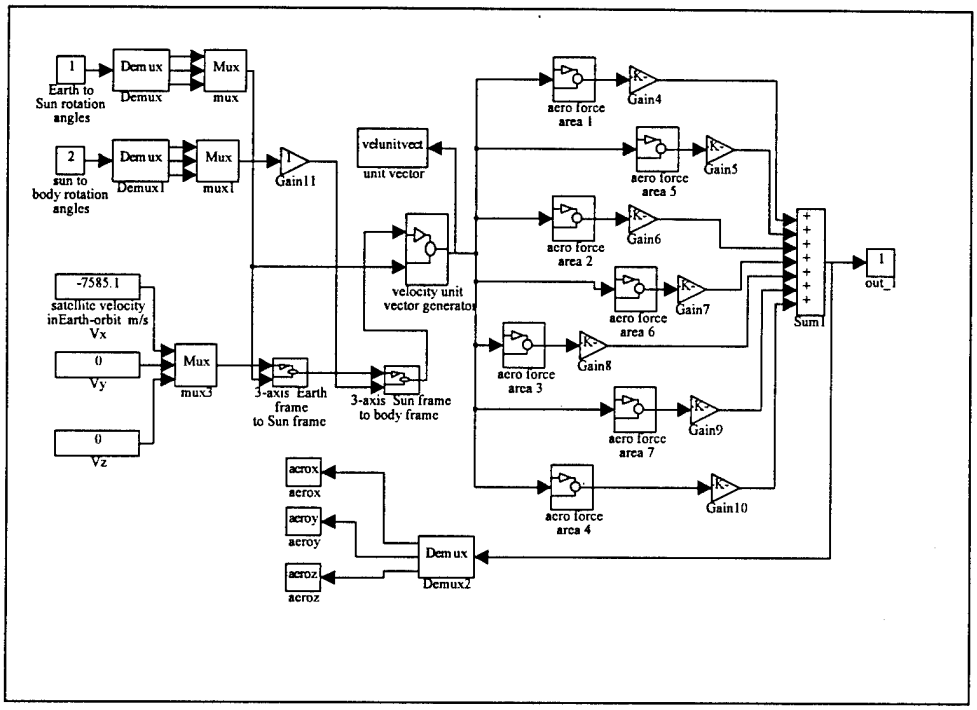

Figure A21. Aerodynamic disturbance torque generator

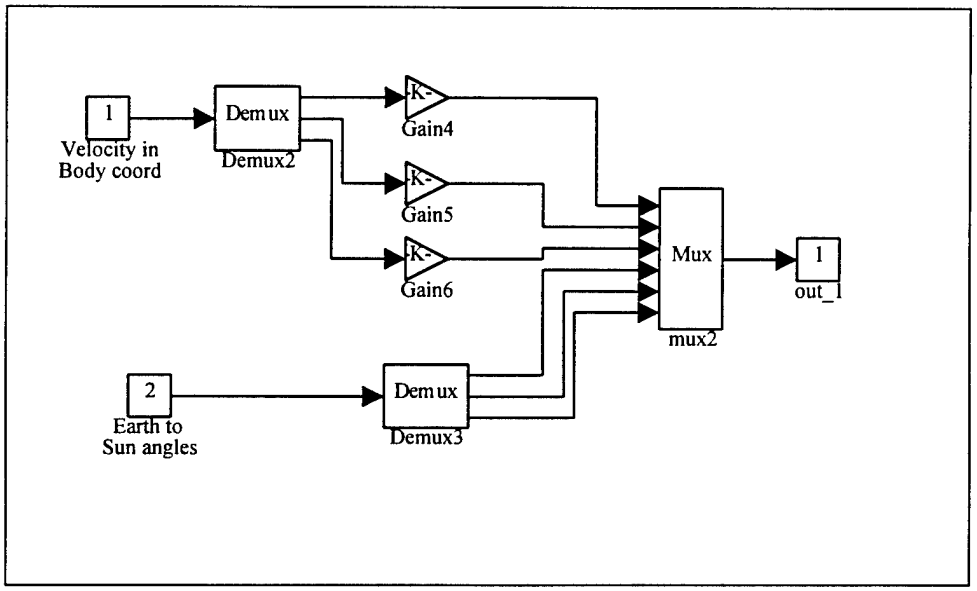

Figure A22. Generation of satellite velocity unit vector in body coordinates

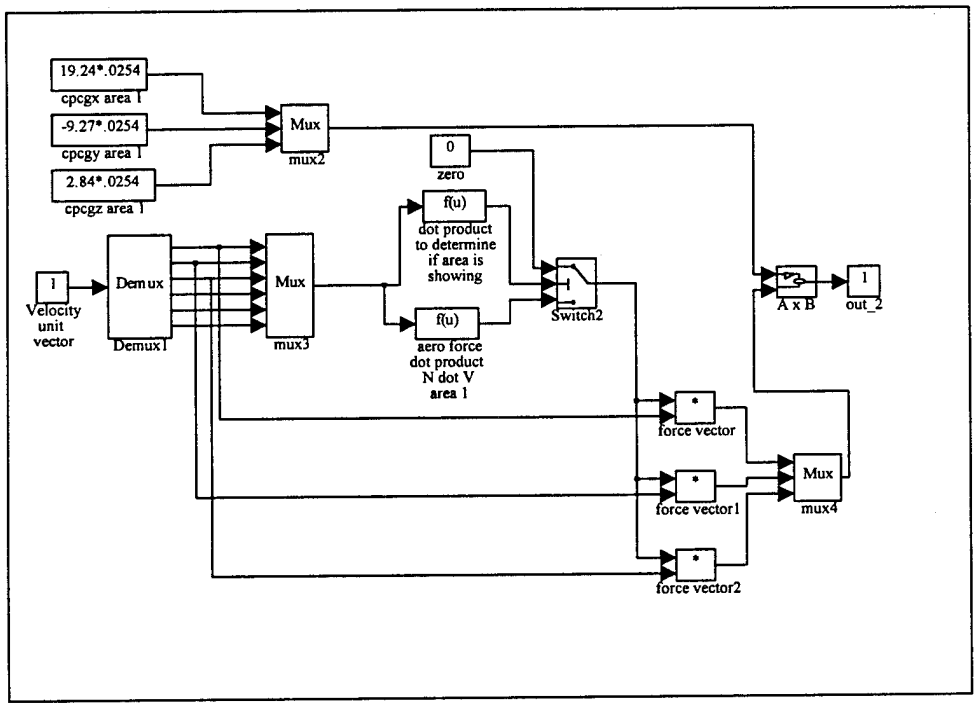

Figure A23. Computation for Aero disturbance torque for each area

MATLAB CODE

```
%this program is the controller for a simulink file projcon3 which will simulate
%the equations of the attitude determination and control system
%The program will set up several variables and initial conditions and will
%also control data display
%%%%%%%%%%%%%%%%%%%%%%%%%%%%%%%%%%%%%%%%%%%%%%%%%%%%%%%%%%%%%%%%%%%%%%%%%%%%%%%%%%%%%%
printcon=0;
control=1;                                  %set to 1 to call simulink program
mode=0;
lawcontrol=1;
if control==1,
clear
control=1;
lawcontrol=1;
mode=0;
printcon=0;
end
orient tall
%%%%%%%%%%%%%%%%%%%%%%%%%%%%%%%%%%%%%%%%%%%%%%%%%%%%%%%%
%variable, constants and initial conditions
maxrows=[80000,8];                          %sets max # of data points
```

```
stepsizemin=.09;                          %set step size for simulation
stepsizemax=.09;
starttime=0;
stoptime=10*5760;
eclipsecon=0;                             %1 means no eclipse
rearth=6378.135;                          %radius of Earth in km
alt=550;                                  %satellite altitude in km
earthrotvel=(360/24)*(1/3600)*(pi/180);   %spin rate of earth in rad/sec
wo=sqrt(398601.2/(rearth+alt)^3);         %orbital rotational velocity in
rad/sec
omega0=wo;
inc=97.59306*pi/180;                      %orbit inclination in degrees
nu0=wo*starttime*pi/180;                  %angle around orbit from ascending
node
epsilon=23.442*pi/180;                    %earth tilt wrt ecliptic
%
%moments of inertia
ixx=8.363;                                %kg-m^2
iyy=9.284;
izz=4.012;
ixy=-.111;
```

```
ixz=.013;
iyz=.048;
ii=[ixx -ixy -ixz;-ixy iyy -iyz;-ixz -iyz izz];
invI=inv(ii);                                   %inverse of inertia matrix for dyn
%
%beta angle generation
uoffset=88;                                     %set inital Earth position around sun
betaw0=(uoffset+22.5)*pi/180;
betawdot=-9.9639*cos(inc)*(1/24)*(1/3600)*(pi/180)*(rearth/(rearth+alt))^3.5;
betau0=(uoffset+0)*pi/180;
betaudot=(360/365.242)*(1/24)*(1/3600)*(pi/180);
beta0=asin(cos(inc)*sin(betau0)*sin(epsilon)+sin(inc)*sin(betaw0)*cos(betau0)...
        -cos(epsilon)*cos(betaw0)*sin(betau0)*sin(inc));
%
%solve for nusun for earth to sun angle computations
A=acos(-cos(pi-inc)*cos(epsilon)+sin(pi-inc)*sin(epsilon)*cos(betaw0));
phro=asin(sin(pi-inc)*sin(betaw0)/(sin(A)+.0000000001))-betau0;
B=asin(sin(epsilon)*sin(betaw0)/(sin(A)+.00000000001));
bbb=tan(beta0);
ccc=tan((pi/2)-A);
eee=asin(bbb*ccc);
```

```
nusun=B-(eee);

nues0=nu0+nusun;

%

%solve for theta earth to sun at time 0

thetaes0=atan2(tan(nues0),sin(beta0));

%%%%%%%%%%%%%%%%%%%%%%%%%%%%%%%%%%%%%%%%%%%%%%%%%%%%%%%%%%%%%%%%

%disturbance torques

%center of mass listings in meters

cgx=.01*.0254;

cgy=-.23*.0254;

cgz=-17.84*.0254;

%

%disturbance torque control

%aero cutoffs

ka1=1;

ka2=1;

ka3=1;

ka4=1;

ka5=1;

ka6=1;

ka7=1;
```

```
%axis cutoff by type of disturbance torque
ggxcon=1;
solarxcon=1;
aeroxcon=1;
ggycon=1;
solarycon=1;
aeroycon=1;
ggzcon=1;
solarzcon=1;
aerozcon=1;
%
%axis torque cutoff
distxcon=1;
distycon=1;
distzcon=1;
%%%%%%%%%%%%%%%%%%%%%%%%%%%%%%%%%%%%%%%%%%%%%
%sensor noise
earthsenscon=0*(.07*pi/180);                    %set nonzero for noise input
rollsunsenscon=0*(.07*pi/180);
yawsunsenscon=0*(.07*pi/180);
%
```

```
%b-field generation initial conditions
alfa0=nu0;
mu0=0;
%
%wheel control gains and momentum bias
taup=10;
Kp=3.6e-1;
wheelbias=9.75;                              %wheel inertia is .0310352 kg-m^2
wheelh0=0;
%
%torque rod control
K1=(-5*1.911e7);
K2=-5*9.554e7;
K3=(K1)/4;
Ku=-1*(1.538e6);
%%%%%%%%%%%%%%%%%%%%%%%%%%%%%%%%%%%%%%%%%%%%%%%%%%%%%%%%
%kinematics initial conditions
phi0=(1*pi/180);
theta0=(2*pi/180);
ksi0=(-.5*pi/180);
%%%%%%%%%%%%%%%%%%%%%%%%%%%%%%%%%%%%%%%%%%%%%
```

```
%spacecraft dynamics initial conditions

wx0=0;

wy0=((cos(thetaes0)^2)*(-wo)/((cos(nues0)^2)*sin(beta0)));

wz0=0;

%

Hx0=ixx*wx0;

Hy0=iyy*wy0-9.75;

Hz0=izz*wz0;

%%%%%%%%%%%%%%%%%%%%%%%%%%%%%%%%%%%%%%%%%%%%%i

if control==1,

%

%call simulink program

finalpr3

pause

end

%

wheelspeed=wheelmomentum*60/(2*pi*.0310352);

%percentspeed=100*abs(abs(wheelspeed)-3000)/300;

%percentwheeltorque=100*abs(hdotwheel)/.025;

%percentdeltamomentum=100*abs(wheeldeltamomentum/.9749996);

%
```

```
%phisqrd=phi.*phi;
%thetasqrd=theta.*theta;
%ksisqrd=ksi.*ksi;
pointerror=sqrt((phi.*phi)+(ksi.*ksi));
%%%%%%%%%%%%%%%%%%%%%%%%%%%%%%%%%%%%%%%%%%%
%plot results
clg
if control==101,
subplot(311),plot(time/60,bxorb)
title('bfild in Earth-oriented frame')
xlabel('time in minutes')
ylabel('bfield strength x in Earth-orbit frame')
grid
subplot(312),plot(time/60,byorb)
xlabel('time in minutes')
ylabel('bfield strength y in Earth-orbit frame')
grid
subplot(313),plot(time/60,bzorb)
xlabel('time in minutes')
ylabel('bfield strength z in Earth-orbit frame')
grid
```

```
pause
if printcon==1,
print
end
%
subplot(311),plot(time/60,bxsun)
title('bfield in Sun-oriented frame')
xlabel('time in minutes')
ylabel('bfield strength x in sun-oriented frame')
grid
subplot(312),plot(time/60,bysun)
xlabel('time in minutes')
ylabel('bfield strength y in sun-oriented frame')
grid
subplot(313),plot(time/60,bzsun)
xlabel('time in minutes')
ylabel('bfield strength z in sun-oriented frame')
grid
pause
if printcon==1,
print
```

```
end
%
subplot(311),plot(time/60,bxbody)
title('bfield in body frame')
xlabel('time in minutes')
ylabel('bfield strength x in body frame')
grid
subplot(312),plot(time/60,bybody)
xlabel('time in minutes')
ylabel('bfield strength y in body frame')
grid
subplot(313),plot(time/60,bzbody)
xlabel('time in minutes')
ylabel('bfield strength z in body frame')
grid
pause
if printcon==1,
print
end
end
```

```
%%%%%%%%%%%%%%%%%%%%%%%%%%%%%%%%%%%%%%%%%%%%%%%%%%%%%%%%%%%
subplot(311),plot(time/60,o2sphi*180/pi)
title('orb to sun angles  vs  time')
xlabel('time in minutes')
ylabel('o2s phi')
grid
subplot(312),plot(time/60,o2stheta*180/pi)
xlabel('time in minutes')
ylabel('o2s theta')
grid
subplot(313),plot(time/60,o2sksi*180/pi)
xlabel('time in minutes')
ylabel('o2s ksi')
grid
pause
if printcon==1,
print
end
%
clg
subplot(311),plot(time/60,o2sthetadot)
```

```
xlabel('time in minutes')
ylabel('o2s thetadot')
grid
subplot(312),plot(time/60,betaangle*180/pi)
xlabel('time in minutes')
ylabel('betaangle')
grid
subplot(313),plot(time/60,woddotfunct)
xlabel('time in minutes')
ylabel('omega0new dot rad/sec^2')
grid
pause
if printcon==1,
print
end
clg
%
if control==101
subplot(311),plot(time/60,velunitvect(:,1))
title('velocity unit vector components in body frame')
xlabel('time in minutes')
```

```
ylabel('velocity in x body')
grid
subplot(312),plot(time/60,velunitvect(:,2))
xlabel('time in minutes')
ylabel('velocity in y body')
grid
subplot(313),plot(time/60,velunitvect(:,3))
xlabel('time in minutes')
ylabel('velocity in z body')
grid
pause
if printcon==1,
print
end
end
%%%%%%%%%%%%%%%%%%%%%%%%%%%%%%%%%%%%%%%%%%%%%%%%%
subplot(311),plot(time/60,phi*180/pi)
title('euler angle in degrees')
xlabel('time in minutes')
ylabel('roll angle in degrees')
grid
```

```
subplot(312),plot(time/60,theta*180/pi)
xlabel('time in minutes')
ylabel('pitch angle in degrees')
grid
subplot(313),plot(time/60,ksi*180/pi)
xlabel('time in minutes')
ylabel('yaw angle in degrees')
grid
pause
if printcon==1,
print
end
%
subplot(311),plot(time/60,phidot*180/pi)
title('euler angle rates in degrees per second')
xlabel('time in minutes')
ylabel('roll angle rate in deg/sec')
grid
subplot(312),plot(time/60,thetadot*180/pi)
xlabel('time in minutes')
ylabel('pitch angle rate in degrees')
```

```
grid
subplot(313),plot(time/60,ksidot*180/pi)
xlabel('time in minutes')
ylabel('yaw angle rate in degrees')
grid
pause
if printcon==1,
print
end
%
if control==101,
subplot(311),plot(time/60,ggx)
title('grav grad torques  vs  time')
xlabel('time in minutes')
ylabel('grav grad x')
grid
subplot(312),plot(time/60,ggy)
xlabel('time in minutes')
ylabel('grav grad y')
grid
subplot(313),plot(time/60,ggz)
```

```
xlabel('time in minutes')
ylabel('grav grad z')
grid
pause
if printcon==1,
print
end
%
subplot(311),plot(time/60,aerox)
title('aero torques  vs  time')
xlabel('time in minutes')
ylabel('aero x')
grid
subplot(312),plot(time/60,aeroy)
xlabel('time in minutes')
ylabel('aero y')
grid
subplot(313),plot(time/60,aeroz)
xlabel('time in minutes')
ylabel('aero z')
grid
```

```
pause
if printcon==1,
print
end
end
%
clg
subplot(411),plot(time/60,wheelmomentum)
title('momentum wheel characteristics  vs  time')
xlabel('time in minutes')
ylabel('wheel momentum')
grid
subplot(412),plot(time/60,hdotwheel)
xlabel('time in minutes')
ylabel('h dot[wheel torque]')
grid
subplot(413),plot(time/60,wheeldeltamomentum)
xlabel('time in minutes')
ylabel('delta momentum')
grid
subplot(414),plot(time/60,wheelspeed)
```

```
xlabel('time in minutes')
ylabel('wheel speed in rpm')
grid
pause
if printcon==1,
print
end
%
clg
subplot(311),plot(time/60,magmomentsout(:,1))
title('magnetic torque rod moments  vs  time')
xlabel('time in minutes')
ylabel('actual mag moment x')
grid
subplot(312),plot(time/60,magmomentsout(:,2))
xlabel('time in minutes')
ylabel('actual mag moment y')
grid
subplot(313),plot(time/60,magmomentsout(:,3))
xlabel('time in minutes')
ylabel('actual mag moment z')
```

```
grid
pause
if printcon==1,
print
end
%
subplot(311),plot(time/60,magtorquex)
title('magnetic torque rod torques  vs  time')
xlabel('time in minutes')
ylabel('mag torque x')
grid
subplot(312),plot(time/60,magtorquey)
xlabel('time in minutes')
ylabel('mag torque y')
grid
subplot(313),plot(time/60,magtorquez)
xlabel('time in minutes')
ylabel('mag torque z')
grid
pause
if printcon==1,
```

```
print
end
%
subplot(311),plot(time/60,totaltorquein(:,1))
title('total torques each axis  vs  time')
xlabel('time in minutes')
ylabel('total torque x in  N-m')
grid
subplot(312),plot(time/60,totaltorquein(:,2))
xlabel('time in minutes')
ylabel('total torque y in  N-m')
grid
subplot(313),plot(time/60,totaltorquein(:,3))
xlabel('time in minutes')
ylabel('total torque z in  N-m')
grid
pause
if printcon==1,
print
end
%
```

```
subplot(311),plot(time/60,disttorquex)
title('dist torques each axis  vs  time')
xlabel('time in minutes')
ylabel('dist torque x in  N-m')
grid
subplot(312),plot(time/60,disttorquey)
xlabel('time in minutes')
ylabel('dist torque y in  N-m')
grid
subplot(313),plot(time/60,disttorquez)
xlabel('time in minutes')
ylabel('dist torque z in  N-m')
grid
pause
if printcon==1,
print
end
%
subplot(311),plot(time/60,bfldsensedbody(:,1))
title('sensed b-field  vs  time')
xlabel('time in minutes')
```

```
ylabel('sensed b-field x dir')
grid
subplot(312),plot(time/60,bfldsensedbody(:,2))
xlabel('time in minutes')
ylabel('sensed b-field y dir')
grid
subplot(313),plot(time/60,bfldsensedbody(:,3))
xlabel('time in minutes')
ylabel('sensed b-field z dir')
grid
pause
if printcon==1,
print
end
%
%end
%
clg
subplot(311),plot(time/60,omegaout(:,1))
title('body rates')
xlabel('time in minutes')
```

```
ylabel('omega x')
grid
subplot(312),plot(time/60,omegaout(:,2))
xlabel('time in minutes')
ylabel('omega y')
grid
subplot(313),plot(time/60,omegaout(:,3))
xlabel('time in minutes')
ylabel('omega z')
grid
pause
if printcon==1,
print
end
%
clg
subplot(311),plot(time/60,totalmomentum(:,1))
title('total momentum')
xlabel('time in minutes')
ylabel('total momentum x')
grid
```

```
subplot(312),plot(time/60,totalmomentum(:,2))
xlabel('time in minutes')
ylabel('total momentum y')
grid
subplot(313),plot(time/60,totalmomentum(:,3))
xlabel('time in minutes')
ylabel('total momentum z')
grid
pause
if printcon==1,
print
end
%
clg
plot(time/60,pointerror*180/pi,'b')
title('pointing error in degrees vs time; sun-oriented control')
xlabel('time in minutes')
ylabel('pointing error to sun')
grid
hold
plot(time/60,switchout,'b--')
```

```
pause

if printcon==1,

print

end
```

REFERENCES

1. David, Leonard, "Sun-watching Satellites Recommended for Climate Research," *Space News*, vol. 5, no. 38, p.18, Springfield, VA, October, 1994.

2. Stickler, Craig A. and Alfriend, K. T., "An Elementary Magnetic Attitude Control System," *AIAA Journal of Spacecraft and Rockets, Vol. 13, No. 5,* pp. 282-287 May, 1975.

3. Fischell, Robert E., "Passive Magnetic Attitude Control for Earth Satellites," Attitude Control Paper; notes in possession of Terry Alfriend, TENCAP Chairman, Naval Postgraduate School, Monterey, CA.

4. NPS-STEDI Project Proposal, Naval Postgraduate School, Monterey, CA July, 1994.

5. Leonard, B. S., Class notes from AA 4871 Satellite Design Class, August, 1994.

6. Wertz, James R., *Spacecraft Attitude Determination and Control,* D. Reidel Publishing Company, Hingham, MA, 1978.

7. Wheeler, P. C., NASA paper CR-313, pp. 175-179, July, 1971.

8. Agrawal, Brij N., *Design of Geosynchronous Spacecraft, Prentice-Hall,* Inc., Englewood Cliffs, NJ, 1986.

9. Larson, Wiley J. and Wertz, James R., *Space Mission Analysis and Design,* Microcosm Inc., Torrance, CA and Kluwer Academic Publishers, Netherlands, 1992.

10. Alfriend, K. T., "Magnetic Attitude Control System for Dual-Spin Satellites, "AIAA *Journal*, Vol. 13, No. 6, June, 1975.

INITIAL DISTRIBUTION LIST

1.	Defense Technical Information Center Cameron Station Alexandria, VA 22304-6145	2
2.	Library, Code 52 Naval Postgraduate School Monterey, CA 93943-5101	2
3.	Chairman, Code EC Department of Electrical and Computer Engineering Naval Postgraduate School Monterey, CA 93943-5121	1
4.	Chairman, Code AA Department of Aeronautics and Astronautics Naval Postgraduate School Monterey, CA 93943-5106	1
5.	Chairman, Code SP Space Systems Academic Group Naval Postgraduate School Monterey, CA 93943-5110	1
6.	Professor Harold A. Titus, Code EC/Ts Department of Electrical and Computer Engineering Naval Postgraduate School Monterey, CA 93943-5121	1
7.	Professor Terry Alfriend, Code SP/Al Space Systems Academic Group Naval Postgraduate School Monterey, CA 93943-5110	1
8.	Professor B. S. Leonard, Code AA/Ln Department of Aeronautics and Astronautics Naval Postgraduate School Monterey, CA 93943-5106	1

9.	Captain Thompson Office of the Chief of Naval Operations Code N63, Room 4E679 The Pentagon Washington, DC 20350-2000	1
10.	Commander, Naval Space Command ATTN: N112 5280 4th Street Dahlgren, VA 22448-5300	1
11.	Mr. Marv Levinson Code 8230 Naval Research Laboratory Washington, DC 20375	1
12.	Mr. Vern Weyers NASA/GSFC Mail Code 400 Greenbelt, MD 20771	1
13.	LT Scott M. Wolfe 531 Green St. N. Catasauqua, PA 18032	2